SMHI

REPORTS OCEANOGRAPHY NO. 45, 2013

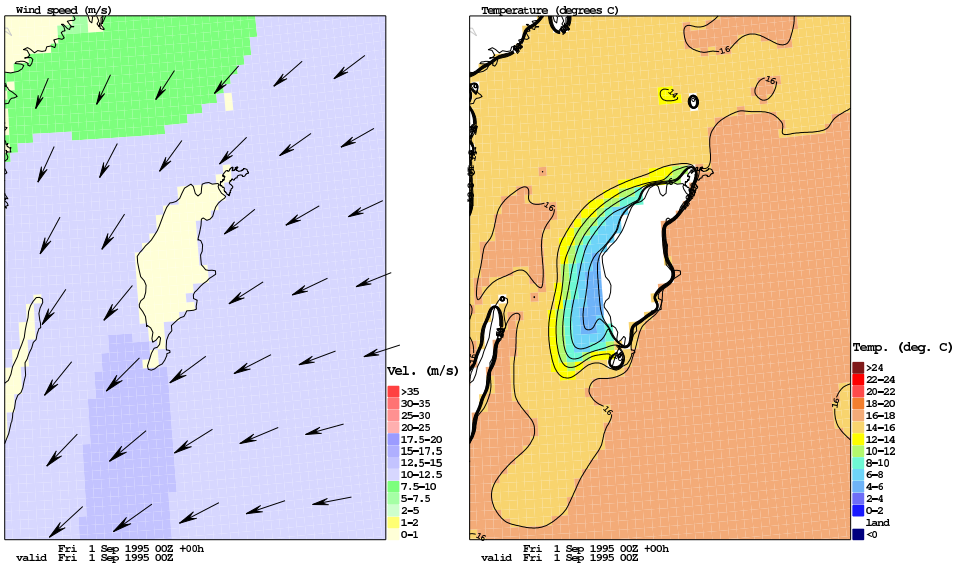

BSRA-15: A Baltic Sea Reanalysis 1990–2004

Lars Axell

Cover picture:

An upwelling event on the west coast of Gotland, on the last day of the 1st BALTEX conference in Visby, Gotland (September 1, 1995). The wind field at 00 UTC is shown to the left and the sea surface temperature to the right. The data were extracted from the BSRA-15 reanalysis data set. The author travelled together with colleagues from SMHI in a sailing boat on this day from Visby to the Swedish main land in the north west, and can confirm this very strong upwelling event.

ISSN: 0283-1112

Abstract

Oceanographic observations are often of high quality but are available only with low resolution in time and space. On the other hand, model fields have high resolution in time and space but are not necessarily in agreement with observations. To bridge the gap between these very different kinds of data sets, a reanalysis can be made, which means that fixed versions of the numerical model and the data assimilation system are used to analyse a period of several years. This report describes an oceanographic reanalysis covering the period 1990 to 2004 (15 whole years). The horizontal resolution is 3 nautical miles in the Baltic Sea and 12 nautical miles in the North Sea, and the vertical resolution varies between 4 meters near the surface to 60 meters in the deepest part (up to 24 vertical layers). The time resolution of the reanalysis product is 6 hours. The numerical ocean model used is HIROMB (High-Resolution Operational Model for the Baltic), version 3.0. The data assimilation method used in this reanalysis is the Successive Corrections Method (SCM) for salinity and temperature, whereas ice observations in terms of ice charts were simply interpolated. The result looks good in terms of sea levels, ice fields, and salinity and temperature structure, whereas currents have not been validated. This oceanographic reanalysis was probably the first one ever for the Baltic Sea (when it was done in 2005) and may serve as a starting point before longer, more advanced reanalyses are produced.

Contents

1 Introduction

The Baltic Sea is a huge estuary in northern Europe with only limited exchange through the Danish Straits (Öresund and the Greater and Lesser Belt Sea). The mean depth of the Baltic Sea is about 56 m and the maximum depth is 459 m in the Landsort Deep about 100 km south of Stockholm. The estuary has a positive water balance, which means that the freshwater input (rivers plus precipitation) exceeds evaporation from the sea surface. It also means that saline water originating outside the Baltic Sea enters the estuary as dense bottom currents. Because of the narrow constriction in the Danish Straits, the saline bottom water in the Baltic Sea is exchanged only intermittently depending on the weather. Another factor controlling the Baltic salinity is the freshwater supply from rivers and precipitation. These factors lead to a large variability of the mean salinity of the Baltic Sea depending on the weather. For instance, a decline in mean salinity took place during the 1980s and 1990s [e.g. Winsor et al., 2001, 2003; Omstedt and Nohr, 2004; Omstedt and Hansson, 2006].

The mean temperature of the Baltic Sea is also controlled by the weather, and displays a large interannual variability [Omstedt and Nohr, 2004; Omstedt and Hansson, 2006]. Curiously, according to the model studies by these authors, there seems to be no trend over the last four to five decades. To more fully understand, and possibly support, these results, a multi-decade Baltic reanalysis could be used.

In a reanalysis, a state-of-the-art three-dimensional, fully baroclinic model should be used in combination with a data assimilation method to ascertain that the model output is consistent with available oceanographic observations. Using such an integrated system, it is possible to make a reanalysis of the Baltic Sea, where the model and the data assimilation method are used to fill in all the gaps between the rather sparse observational data. This is in contrast with so-called hindcast simulations, forced by atmospheric data, which not necessarily yield results close to observations. A reanalysis gives a consistent and continuous picture of a large number of environmental variables for the Baltic Sea during the analysed period (within the resolution limits of the system). A long reanalysis thus yields an indispensable data set for use in e.g. climate change detection.

The circulation model currently used operationally at SMHI is HIROMB (High-Resolution Operational Model for the Baltic). It is an off-spring from the circulation model used at BSH (Bundesamt für Seeschiffahrt und Hydrographie) in the mid 1990s. Version 1.0 of HIROMB was launched in 1995 and had two nested grids, with an increasing horizontal resolution of 12 nm (nautical miles) and 3 nm going from the North Sea in to the Baltic. A validation study of this first version was made by Funkquist and Ljungemyr [1997].

In version 2.0 of HIROMB, launched in early 2002, the code had been parallellized by Wilhelmsson [2002]. This made it possible to introduce a third nested grid and run the model with 1 nm resolution in the Baltic Sea in addition to the 12 and 3 nm grids. This version of HIROMB was described in detail by Funkquist and Kleine [2007].

It was not until version 3.0 of HIROMB, made available in November 2005, that data assimilation was introduced to improve initial conditions before each forecast. This version also introduced an extended ice model including ridging parameters [Axell, 2006] and a state-of-the-art turbulence model (the k-ω model; see evaluation by Fransson [2005]), and was consequently the version used in the reanalysis described in this report.

The operational HIROMB fields have often been used for various projects, as they represent a huge amount of information in terms of sea levels, currents etc. However, due to a poor turbulence model and the lack of data assimilation, ice, salinity and temperature fields were not reliable before the release of version 3.0. At that time (2005), an idea emerged to make a reanalysis of the past years, using the latest version of HIROMB including the data assimilation system used at the time (Successive Corrections). The anticipated result was a large data set consistent with both available observations and the latest version of HIROMB. Since the start of the project in 2005, many experiments have been carried out using a slightly more advanced univariate OI (Optimal Interpolation) method in the data assimilation, as well as ensemble-based methods recently. However, these methods were not implemented until long after the production of the present reanalysis fields had ended.

Due to lack of funding, the present reanalysis project had to be limited in scope. E.g., there was no time to excavate the archives for all possible observations, only to use those readily available. In addition, as in many reanalysis projects, there had to be a trade-off in terms of e.g. horizontal

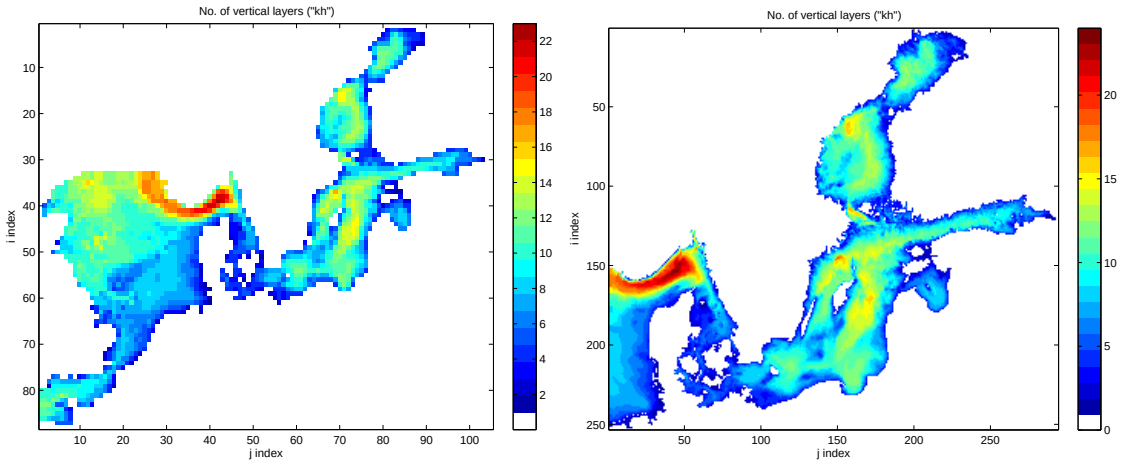

(a) (b)

Figure 1: HIROMB's (a) 12 nautical mile grid "NS12" and (b) 3 nautical mile grid "NB03". The figures show the number of vertical layers, which approximately reflects the bathymetry.

resolution. Thus, the 1 nm grid was considered too expensive to run. As a consequence, the highest resolution was 3 nm in the Baltic Sea and 12 nm in the North Sea.

This (probably) first-ever multi-year reanalysis of the Baltic Sea may be considered an experiment and covers only a limited period, 1990–2004. The last analysed year, 2004, was determined by the availability of observations of salinity and temperature at the time of this project (2005). Accordingly, the 15-year data set will be referred to as "BSRA-15", meaning a 15-year Baltic Sea Reanalysis. The intention of the project was to gain experience in oceanographic reanalyses and pave the way for future reanalyses, using more state-of-the-art data assimilation systems. Of course, it was also hoped that the produced reanalysis fields would be useful. Although the present reanalysis data set has been available since 2005, the work behind it has not been described until now. Hence, the purpose of this report is to describe both the reanalysis system used and the data set itself.

2 Model description

2.1 Model domain and lateral boundary conditions

The HIROMB ocean forecasting system incorporates a hierarchy of models with increasing resolution as the Baltic Sea is approached. First there is a storm surge model called NOAMOD, covering the north eastern Atlantic including the North Sea. The western and eastern longitude limits are about 21°W and 13°E, respectively, and the southern and northern latitude limits are about 48°N and 66°N, respectively. The horizontal resolution is 24 nautical miles in the north-south direction and 24 minutes in the east-west direction. This implies a grid of 52 by 46 grid cells.

The sea levels from NOAMOD are used as boundary conditions at the western open boundary for HIROMB's 12 nm grid, which has its western boundary around 4°W in the English Channel and a northern boundary along a section from Scotland to Norway; see Figure 1(a). In addition to the weather-forced sea levels from NOAMOD, tidal contributions are added at the open boundary. HIROMB also requires boundary conditions in terms of salinity and temperature profiles as well as ice variables, which are all supplied using climatology.

HIROMB's 3 nautical mile grid also has an open boundary in the west, near 6°E. The lateral boundary conditions here in terms of sea level and salinity and temperature profiles are supplied by the coarser 12 nautical mile grid; see Figure 1(b).

Table 1: Values of coefficients used in the turbulence model.

Notation	Description	Value	Unit
c_{LC}	coefficient in Eq. (8)	0.15	–
c_μ^0	coefficient in Eq. (6)	0.5562	–
$c_{\omega 1}$	coefficient in Eq. (2)	0.500	–
$c_{\omega 2}$	coefficient in Eq. (2)	0.833	–
$c_{\omega 3}$	coefficient in Eq. (2)	-1.25 / -3.33 / +1.0 (see text)	–
c_s	coefficient in Eq. (9)	0.016	–
c_1	coefficient in Eq. (16)	0.108	–
c_2	coefficient in Eq. (16)	0.308	–
c_3	coefficient in Eq. (16)	0.00837	–
c_4	coefficient in Eq. (17)	0.277	–
g	acceleration of gravity [Eq. (5)]	9.81	m s^{-2}
ρ_0	reference density of seawater [Eq. (5)]	1000	kg m^{-3}
σ_k^ω	coefficient in Eq. (1)	1.3	–
σ_ω	coefficient in Eq. (2)	1.552	–

2.2 Turbulence model

The turbulence model implemented in HIROMB is based on the buoyancy-extended k-ω model of Umlauf et al. [2003]. Thus, two separate transport equations are solved, one for k, the Turbulent Kinetic Energy (TKE), and one for ω, the inverse time scale of the turbulence:

$$\frac{\partial k}{\partial t} = \frac{\partial}{\partial z}\left(\frac{\nu_t}{\sigma_k^\omega}\frac{\partial k}{\partial z}\right) + P_s + P_b - \varepsilon, \tag{1}$$

$$\frac{\partial \omega}{\partial t} = \frac{\partial}{\partial z}\left(\frac{\nu_t}{\sigma_\omega}\frac{\partial \omega}{\partial z}\right) + \frac{\omega}{k}\left(c_{\omega 1}P_s + c_{\omega 3}P_b - c_{\omega 2}\varepsilon\right), \tag{2}$$

where t is the time variable, z is the vertical coordinate (positive upwards), ν_t is the eddy viscosity, and σ_k^ω and σ_ω are the Schmidt numbers for k and ω, respectively. See Table 1 for values of all the constants in the turbulence model. The coefficient $c_{\omega 3}$ is special, as it is a function rather than a constant; see below.

Further, P_s^{tot} represents total shear production, that is,

$$P_s^{tot} = P_s + P_{LC} + P_{IW}, \tag{3}$$

where P_s is the production due to resolved shear according to

$$P_s = \nu_t\left[\left(\frac{\partial u}{\partial z}\right)^2 + \left(\frac{\partial v}{\partial z}\right)^2\right], \tag{4}$$

where u and v are the eastward and northward velocity components, respectively, and P_{LC} and P_{IW} represent parameterized shear due to Langmuir Circulation (LC) and Internal Waves (IW), respectively; see below. Further, P_b in (1) and (2) represents buoyancy production of TKE according to

$$P_b = \nu_t'\frac{g}{\rho_0}\frac{\partial \rho}{\partial z}, \tag{5}$$

where ν_t' is eddy diffusivity, g is the acceleration of gravity, ρ is the density of seawater and ρ_0 is a reference density. Finally, ε in (1) and (2) is the dissipation rate of TKE, calculated as

$$\varepsilon = (c_\mu^0)^4 k\omega, \tag{6}$$

where c_μ^0 is a constant; see Table 1.

Following Axell [2002], the shear production of TKE due to Langmuir Circulation was parameterized as

$$P_{LC}(z) = \frac{w_{LC}^3(z)}{H_{LC}}. \tag{7}$$

Here w_{LC} is the vertical velocity component due to LC, which is assumed to be zero at the surface ($z = 0$) as well at a finite depth H_{LC} ($z = -H_{LC}$), which is close to the mixed layer depth. Hence, w_{LC} is parameterized as

$$w_{LC} = \begin{cases} c_{LC} U_s \sin(-\frac{\pi z}{H_{LC}}) & \text{if } -z \le H_{LC}, \\ 0 & \text{otherwise.} \end{cases} \tag{8}$$

In (8), U_s is the magnitude of the Stokes drift at the surface, estimated as proportional to the wind speed U_w as

$$U_s = c_s U_w. \tag{9}$$

The coefficient c_{LC} was tuned by Axell [2002] using the Large Eddy Simulation data of Skyllingstad and Denbo [1995], and the value of c_s was given by Li and Garrett [1993]. For numerical values, see Table 1. The depth H_{LC} at which w_{LC} vanishes was assumed to be the depth to which a water parcel with the kinetic energy $U_s^2/2$ can reach on its own by converting its kinetic energy into potential energy, and was estimated by integrating the following integral from the surface downward:

$$\int_{-H_{LC}}^{0} \frac{g}{\rho_0} \frac{\partial \rho(z)}{\partial z} z \; dz = \frac{1}{2} U_s^2. \tag{10}$$

In addition, we have also included an extra source term for turbulence due to breaking internal waves, P_{IW}, based on the work by Axell [2002] with $\delta = 1$ in that paper. It represents small-scale shear due to unresolved internal waves. It is parameterized as

$$P_{IW}(z) = \frac{F_{ml}}{H \rho_0} \frac{N(z)}{\overline{N}}, \tag{11}$$

where F_{ml} is the energy flux from the mixed layer to the interior ocean [assumed constant and equal to 0.9×10^{-3} W m^{-2}], and H is the local depth. In (11), N is the buoyancy frequency calculated from

$$N^2(z) = -\frac{g}{\rho_0} \frac{\partial \rho}{\partial z}, \tag{12}$$

and

$$N(z) = [\max(N^2(z), 0)]^{1/2}, \tag{13}$$

and $\overline{N}$ in (11) is the vertical mean value of $N(z)$.

Finally, we need expressions for the eddy viscosity ν_t and the eddy diffusivity ν_t':

$$\nu_t = c_\mu (c_\mu^0)^3 \frac{k^2}{\varepsilon}, \tag{14}$$

$$\nu_t' = c_\mu' (c_\mu^0)^3 \frac{k^2}{\varepsilon}. \tag{15}$$

As for the stability functions c_μ and c_μ', we use those suggested by Axell and Liungman [2001]:

$$c_\mu = \frac{c_\mu^0 + c_1 R_t}{1 + c_2 R_t + c_3 R_t^2}, \tag{16}$$

$$c_\mu' = \frac{c_\mu^0}{1 + c_4 R_t}; \tag{17}$$

see Table 1 for numerical values. The variable R_t is a turbulent Richardson number, defined as

$$R_t = \frac{k^2 N^2}{\varepsilon^2}. \tag{18}$$

See Axell and Liungman [2001] for further details of the stability functions.

2.3 Ice model

The ice model in HIROMB consists of one ice dynamics part, which controls the movements of the ice, and one thermodynamic part, which controls ice growth and melting. These equations are described in detail by Kleine and Sklyar [1996] and Wilhelmsson [2002] and will not be repeated here. In addition there are budget equations needed to close the set of equations. These were recently extended [Axell, 2006; Kotovirta et al., 2009], based on the work by Lensu [2003], to include ridging variables in addition to the classical variables Sea Ice Concentration (SIC) and total Sea Ice Thickness (SIT). The new implementation permits the calculation of the following ice variables:

- ice concentration,
- level ice thickness h_l,
- ridged ice thickness h_r (volume of ridged ice per unit area),
- total ice thickness $h_{tot} = h_l + h_r$,
- ridge density D (number of ridges per km), and
- ridge sail height H (mean height of the ridges relative to the surrounding ice.

The ice concentration C is solved according to

$$\frac{\partial C}{\partial t} + \nabla \cdot (\overline{u} C) = R, \tag{19}$$

where $\overline{u}$ is the ice drift vector and R is a so-called ridging function which here is parameterized as

$$R = \begin{cases} \nabla \cdot \overline{u} & ; \nabla \cdot \overline{u} < 0 \& C \geq C_r, \\ 0 & ; \text{otherwise}, \end{cases} \tag{20}$$

where $C_r = 1.0$ is the limit for the ice concentration at which ridging starts. Hence, R is always zero except when the ice concentration is already 100 % and there is convergence of ice. Further, it should be noted that terms representing thermodynamic effects are included in the model but have been left out in equation (19).

The total ice thickness h_{tot} is calculated according to

$$\frac{\partial (C h_{tot})}{\partial t} + \nabla \cdot (\overline{u} C h_{tot}) = 0, \tag{21}$$

where h_{tot} is the total ice thickness in the part of the grid cell which has ice. Hence, Ch_{tot} can be interpreted as the mean total ice thickness in the whole grid cell, or total cubic meter ice per square meter.

In adition, there are some ridging equations which are due to Lensu [2003], later modified by Lensu (2004, pers. comm.), and applied by Axell [2006] and Kotovirta et al. [2009]. The ridge density D is calculated as

$$\frac{\partial (CD)}{\partial t} + \nabla \cdot (\overline{u} C D) = \frac{\beta R}{\varphi}, \tag{22}$$

cf Lensu [2003, Eqs. 133-134]. In equation (22), β is the fraction of deformation events that is due to ridging, the remaining part $(1 - \beta)$ being due to rafting which is not included in the model. β is parameterized as

$$\beta = \begin{cases} 1 & ; h_l \geq h_c, \\ 0 & ; h_l < h_c, \end{cases} \tag{23}$$

where $h_c = 0.1$ m.

The function φ in equation (22) is the relative change in ice area per unit change in ridge density. It is parametrized as

$$\varphi = \begin{cases} -\frac{315}{315CD+1000} & ; p = 1, \\ -\frac{315p(1-0.081\sqrt{CDH})}{315CDp+1000} & ; \text{otherwise}. \end{cases} \tag{24}$$

Equation (24) above is based on equation (166) in Lensu [2003], but was later modified to avoid a singularity and non-negative values for φ for large values of D (Lensu, 2004, pers. comm.). Further, p in equation (24) is a variable related to a clustering effect of ridges, and parameterized as

$$p = \min[1.28 \exp(-0.16\sqrt{CDH}), 1.0]. \tag{25}$$

However, if $CDH \geq 68$, then p is limited to

$$p = \frac{1}{3} \tag{26}$$

and

$$\varphi = -\frac{105}{315CD + 3000}. \tag{27}$$

The ridge sail heigh H is calculated with a prognostic equation as

$$\frac{\partial(CDH)}{\partial t} + \nabla \cdot (\overline{u} CDH) = \beta[\alpha_0 \langle H|h_l \rangle + (\alpha - \alpha_0)H], \tag{28}$$

where

$$\langle H|h_l \rangle = 3\sqrt{h_l}, \tag{29}$$

which is the mean ridge sail height formed from level ice thickness h_l.

α in equation (29) is related to the ridging function R as

$$\alpha = \frac{R}{C\varphi} \tag{30}$$

[cf. our equation (19) with equations (131) and (136) in Lensu [2003]], which can be interpreted as the appearing rate of ridge sails per distance unit. Further, α_0 in (28) is given by

$$\alpha_0 = -\frac{3.17R}{p}. \tag{31}$$

We also need a prognostic equation for level ice thickness, h_l, which is calculated as

$$\frac{\partial(Ch_l)}{\partial t} + \nabla \cdot (\overline{u} Ch_l) = Ch_l R. \tag{32}$$

Hence, during a ridging event, when R becomes non-zero and negative, the right-hand-side of (32) also becomes negative. A corresponding equation for ridged ice thickness h_r (or rather, Ch_r) would look exactly the same, but the term on the right-hand-side would be positive instead and work as a source term for mechanical growth of ice thickness. Adding that equation with (32), the positive and negative source terms on the right-hand-side would cancel exactly and result in a zero source term and give us equation (21). However, in the ice model in HIROMB there is no need for a corresponding prognostic equation for Ch_r, as it can be calculated diagnostically as $Ch_r = Ch_{tot} - Ch_l$. Finally, it should be stated once more that all ridging equations above are due to Lensu [2003] and later unpublished work by him (Lensu, 2004, pers. comm.).

2.4 Initial conditions

When determining the initial condition for January 1, 1990, the model field from January 1, 2004, from the operational HIROMB was used as a first guess. This field was then corrected using all available observations (sea ice, salinity, temperature) around the start date January 1, 1990, and the data assimilation method described below. Thus, currents and sea levels were not set to zero in the initial condition.

2.5 Atmospheric forcing

HIROMB has a built-in flux module which calculates fluxes of heat and momentum from atmospheric standard variables; see Wilhelmsson [2002]. These are wind speed (two components), 2-m air temperature, 2-m specific humidity, air pressure, and total cloudiness. Precipitation and evaporation are assumed to balance each other.

At the time of this project, the best available forcing for the earlier years, 1990–1996, was reanalysed atmospheric data from the ERA-40 project [Uppala et al., 2005] with a horizontal resolution of 1.125° (125 km). For the years 1997–2002, operational fields from the ECMWF (European Centre for Medium-Range Weather Forecasting) were used, with a horizontal resolution of 0.5° (55 km). For the remaining years, the Swedish operational version of HIRLAM (High-Resolution Limited-Area Model) was used as forcing, with a horizontal resolution of 0.2° (22 km). Hence, the quality of the atmospheric forcing varies during the reanalysis period.

3 Data assimilation method

Generally, to make good ice-ocean forecasts we need three things: (1) good initial conditions, (2) good boundary conditions, and (3) a model to integrate prognostic equations forward in time. To make ice forecasts, initial fields of Sea Surface Temperature (SST) are preferably required, as well as ice variables (ice concentration, thickness, ridging variables, etc.). To make forecasts of the salinity and temperature structure, vertical profiles of these variables are needed as well. The boundary conditions include both the lateral boundary conditions mentioned above, as well as meteorological forcing on the sea surface. Item (3) above is of course the ice-ocean model HIROMB, in our case.

The concept of data assimilation is all about improving item (1) above, i.e. the initial condition. The general idea is to use observations to slightly correct the model, thus preventing it from straying too far away from reality. In theory, it is possible to include observations into a forecast model in an objective way. Unfortunately, the errors of many of the observed variables are often poorly determined, which implies that in practice there is still some room for subjectivity.

The assimilation scheme used in the operational HIROMB at the time of this reanalysis was the Method of Successive Corrections [Daley, 1991, p. 66]. Today, however, the slightly more advanced OI (Optimal Interpolation) method is used operationally, but it was not implemented yet at the time of this reanalysis. Hence, salinity and temperature were analysed using the old Successive Corrections method. For the ice variables, however, it was decided to simply interpolate the operational ice charts when these were available as this gave better results.

According to the Successive Corrections method, the analysed value f_A (for example temperature) at point r_i is given by

$$f_A(r_i) = f_B(r_i) + \frac{\sum_k w(r)[f_O(r_k) - f_B(r_k)]}{\sum_k w(r) + \varepsilon_O^2)} \tag{33}$$

where f_B is the best-guess background field. Further, r_i represents the model grid point, r_k represents the location of observation k, and ε_O^2 is the constant expected observation error variance normalized by the constant expected background error variance. The value used here was 10^{-4} for both salinity and temperature, which means the observations are assumed to be much more accurate than the background estimates.

The a posteriori weights $w(r)$ in (33) are given by

$$w(r) = \begin{cases} \exp(-\frac{r^2}{2L^2}) & \text{if } r \le 3L, \\ 0 & \text{if } r > 3L. \end{cases} \tag{34}$$

and

$$r = [(x_k - x_i)^2 + (y_k - y_i)^2]^{1/2}$$

is the distance between the model grid point and the observation. Finally, L in (34) is the characteristic length scale over which the observation is assumed to be valid. Here we have used constant values of L equal to 50 km for salinity and temperature.

In general, the correction algorithm in equation (33) is iterated a few times to improve the result, according to

$$f_A^{j+1} = f_B^j + W_i^T[f_O - f_A^j]. \tag{35}$$

Two iterations were used in this study. In equation (35), j is the number of the iteration, W_i^T is the transpose of the column vector of a posteriori weights as in (33), and f_O and f_A^j are the vectors of observations and corresponding grid point values at the observation points, respectively. See Daley [1991, ch. 3] for more details.

4 Observations

4.1 Sea levels

Sea levels cannot be assimilated into the HIROMB model presently. Nevertheless, as they respond to weather forcing and bathymetry, they can be well predicted even without the use of data assimilation. One exception is a very low-frequency change in mean sea level which is not always simulated well by the model. Hence, for operational purposes a bias correction must be applied based on the data from the last month or so. In this report, such a bias correction will be applied before comparing with observations. Figure 2 shows the locations of four sea level stations that will be used for the comparison.

4.2 Salinity and temperature profiles

All salinity and temperature (S/T) profiles used in the data assimilation were extracted from the Swedish Oceanographic Data Centre database called SHARK (Svenskt Havsarkiv). It contains data from SMHI as well as other Swedish and international institutes. SHARK mainly contains low-resolution CTD data from the Baltic Sea as well as Kattegat and Skagerrak; see Figure 2, which shows the locations of S/T profiles used in the data assimilation. A gross error check is made before storage in the SHARK data base.

The observation frequency varies from station to station, but many stations are visited every month or so. See Figure 3 for a time series of the total number of S/T profiles.

4.3 Sea surface temperature and sea ice variables

Since many years, the Swedish Ice Service, located at SMHI, produces gridded maps of sea surface temperature and ice variables such as sea-ice concentration C, level-ice thickness h_l, as well as degree of ridging. The system to produce these SST and ice charts is called IceMap and is used both by the Swedish and the Finnish Ice Service since many years.

The SST maps, available about twice a week, rely on reported in-situ observations as well as satellite imagery, and are gridded with a horizontal resolution of 0.1° (about 11 km). The ice charts are also available about twice a week during the analysis period and rely on satellite imagery as well as reports from ice breakers, and are gridded with a horizontal resolution of 0.04° (about 4.4 km).

The availability of the IceMap charts varies during the 15-year period. During 1990–1998, SST and ice were only analysed during the winter months (about twice a week, usually on Mondays and Thursdays), whereas during 1999–2004 they were both analysed the whole year (but still usually on Mondays and Thursdays). Figure 3 shows the availability of SST and ice charts for each year.

The ice charts also contain information about degree of ridging of the ice. The information partly relies on reports from icebreakers and is subjective to a great extent. During the analysis period the degree of ridging was either "no ridges", "few ridges" or "many ridges". This information was translated into quantitative information by assuming these reports mean $D = 0$, $D = 2$ and $D = 4$ ridges per km, respectively. There is no information about ridge sail height H in the ice charts, so it is assumed that all ridges have sail heights of $H = 1.4$ m, which is close to the observed mean value for the Baltic Sea.

To be able to assimilate also the ridged ice thickness h_r, a statistical relationship is needed to relate h_r to other ridging parameters. Using mean observed relationships given by Lensu [2003], the following relationship was obtained and used:

$$h_r = 0.129 D H^2. \tag{36}$$

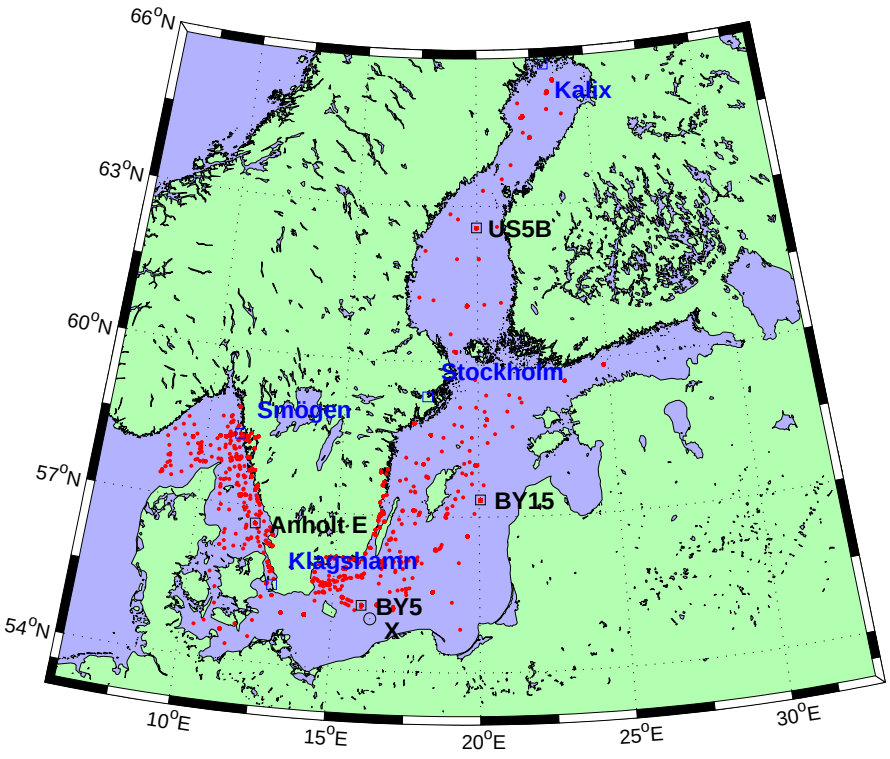

Figure 2: Locations of the salinity and temperature profiles used in the data assimilation (red dots). Also shown are four standard T/S stations (black squares), a validation T/S station (Station "X", black circle), and stations used in the sea level verification (blue squares).

As stated previously, ridged ice thickness is not a prognostic model variable, but level ice thickness and total ice thickness are. The sum of level and ridged ice thickness is therefore used in the data assimilation for the total ice thickness, according to

$$h_{tot} = h_l + h_r. \tag{37}$$

5 Results

A reanalysis data set contains a huge amount of information, and only a fraction of it can be analysed and discussed in this report. We will start by first checking the SST and SIC data assimilation performance for a sample date, as well as time series of salinity and temperature for a sample measuring station, by comparing with observations. Then we will analyse sea level data, S/T profiles, mean salinity and temperature time series, and then finally the Baltic Sea ice extent.

5.1 Assimilation of sea ice concentration and sea surface temperature

The assimilation of sea ice went well, as can be seen in Figure 4 which shows the observed ice situation for a sample date (March 11, 2004) according to the IceMap system to the left and the analysis to the right. Most features in the observations are present in the analysis. However, it is clear by studying e.g. the ice edge that the analysed field is somewhat smoothed. The original data in the ice chart has well-defined ice edges. The interpolation being done to produce the analysis involves a certain horizontal length scale, here set to 10 km, which results in a rather smooth transition from ice covered areas to open water. This is a difficult problem in ice data assimilation which will have to be addressed in the future. Apart from the somewhat smoothed ice fields, the result looks good.

The analysis in Figure 4 (b) also shows SST, which also looks good compared to the SST from the IceMap system in Figure 4 (a). In this case we see that the SST from the IceMap system is

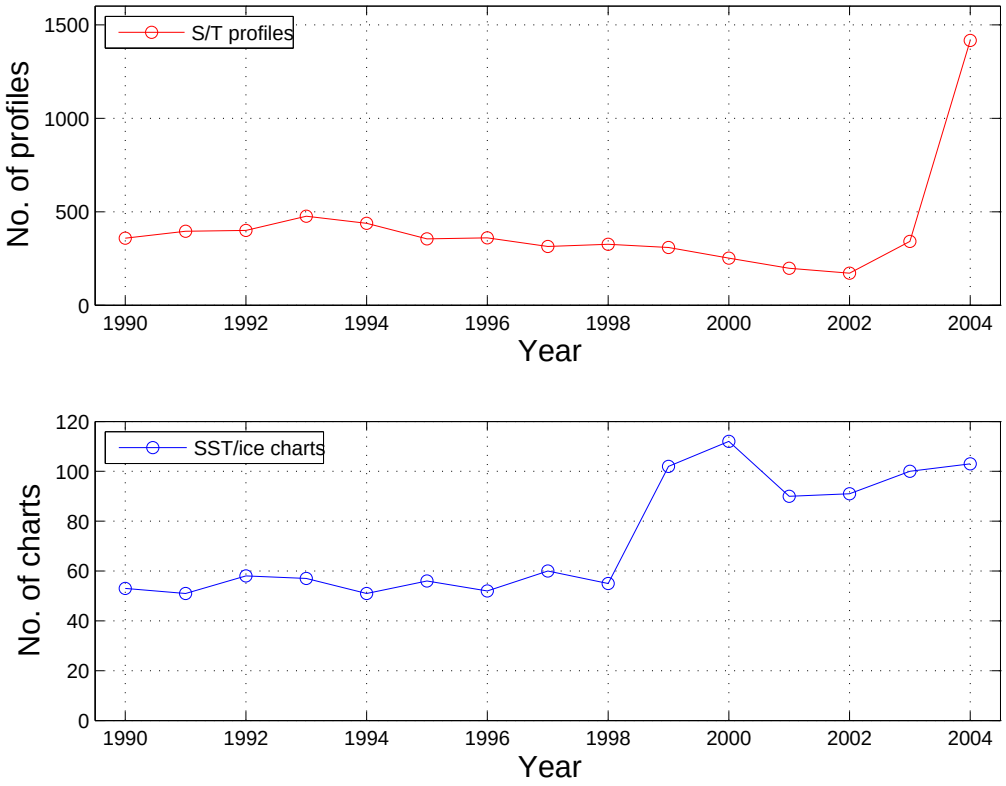

Figure 3: Observation statistics for the data assimilation, in terms of number of S/T profiles and SST/ice charts.

rather smooth, whereas the analysed field is not. The reason why the SST from IceMap is rather smooth is because the product involves hand drawn isolines based on available observations. Using a data assimilation method such as the Successive Corrections method implies that mostly the large-scale features are changed. Hence, small-scale features often survive during assimilation of salinity or temperature. Whether a certain feature is "small-scale" or not depends on the assimilation length scale. As stated above, here we have used a constant of 50 km in the horizontal. This is in contrast with the assimilation of ice variables, which was done using simple interpolation.

5.2 Assimilation of in situ measurements of salinity and temperature

To check the assimilation of salinity and temperature profiles, salinity and temperature have been extracted from the reanalysis data set for the location latitude 55.0° N 16.3° E, called *Station X* in Figure 2. These observation data are from the ICES data base and not included in the SHARK data base. Hence, they are independent data as they were not used in the data assimilation. Two depth levels were chosen: 0 m and 40 m depth. The result for salinity is shown in Figure 5. It is clear that the data assimilation has worked as intended in both depth levels, bringing the reanalysed data close to the observed values in most cases. The corresponding results for temperature is shown in Figure 6. It is clear that the data assimilation works well also for this variable.

5.3 Sea levels

All sea level data, observations as well as model data, were bias corrected before any comparisons were made. The bias correction was made by calculating a mean value of the last 30 days which was then subtracted from the current value. Hence, the bias correction, or offset, changed with time. The sea level stations chosen for analysis were *Kalix*, *Stockholm*, *Klagshamn*, and *Smögen*; see their locations in Figure 2 . All sea level stations have their own references, which are usually not related to each other. For the four stations, the long-term means are about 140, 280, 200, and

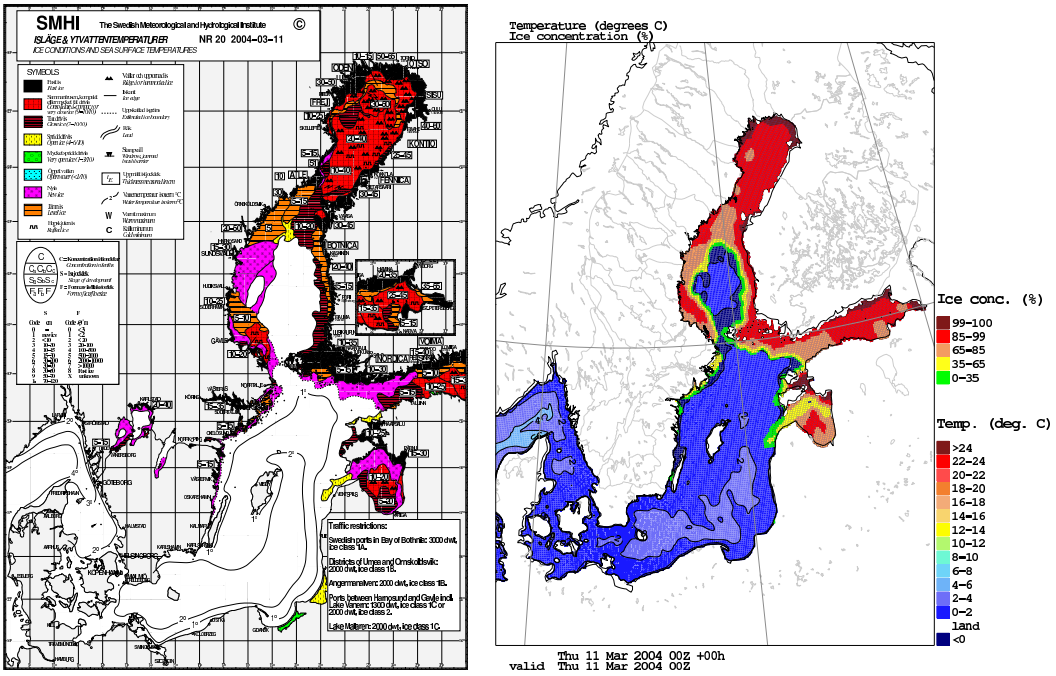

(a) (b)

Figure 4: (a) Operational ice chart from SMHI including Sea Surface Temperature and Sea Ice Concentration for the date 2004-03-11. (b) Corresponding Sea Surface Temperature and Sea Ice Concentration from the reanalysis (NB03).

220 cm, respectively. The 15-year mean values for the NS12 model grid is 34 cm for Kalix, 28 cm for Stockholm, 17 cm for Klagshamn, and 8 cm for Smögen. The corresponding mean values for the NB03 model grid are 36, 29, 19, and 11 cm, respectively. The reason for the lateral difference is mainly due to generally higher sea levels in the brackish Baltic Sea to compensate for its lower salinity compared to *Smögen*, which is located in Skagerrak where the salinity is higher.

Figure 7 shows a comparison of bias-corrected sea level data from the model (both NS12 and NB03 grids) with corresponding bias-corrected observations for a short sample period, January 1996. It is clear that the low-frequency variability is modelled nicely, and for the most part also the high-frequency variability. However, model data are only saved every 6 hours, which is not so good for comparisons of the semidiurnal tide in the Skagerrak and Kattegat area (which has a main period of about 12 hours). Nevertheless, the results are satisfactory.

Figure 8 shows time series of monthly correlations for the whole analysed period. The results are best at *Stockholm*, with typical correlations of about 0.9, and slightly less at the other stations. It is interesting to see that the coarser grid, NS12, is about as good as the fine grid, NB03, in most cases, except at the Skagerrak station *Smögen*. The reason for the latter discrepancy is unknown. Finally, Figure 9 shows the corresponding rms (root-mean-square) error of the model for NS12 and NB03. Also here we see that NS12 is worse than NB03 at *Smögen*.

5.4 Salinity and temperature profiles

Salinity and temperature profiles were extracted (NB03 only) for each day during the 15-year period for a few observation stations; see Figures 10 and 11. These are locations where observed profiles are available approximately once a month. This means that the model is close to observations at these locations at least every month or so (not shown). These figures are for NB03 data only, but NS12 data are very similar except that the total depth differs somewhat.

Figure 10 (b) shows a sharp increase in bottom salinity at *BY5* in early 1993. This is the well-known, strong saltwater inflow into the Baltic Sea, and another strong one in 2003. According to the data it takes about a year before the saltwater reaches the Eastern Gotland Basin at *BY15*; see Figure 10 (c). The surface salinity at *Anholt E* has a high-frequency variability between

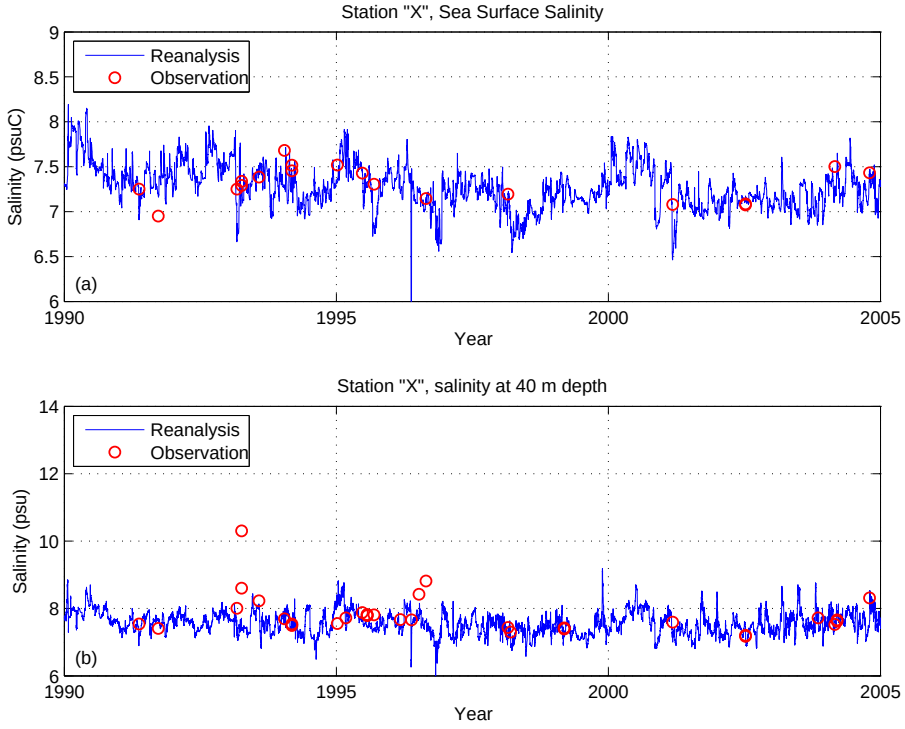

Figure 5: Validation of data assimilation of salinity at *Station X*, at (a) the surface and (b) 40 m depth. The observed data are independent data from the ICES data base and not used in the data assimilation. The reanalysis data are interpolated from the NB03 grid.

approximately 15 and 25 psu; see Figure 10 (a). This is partly due to movements of the lateral salinity front in the Kattegat area, and partly due to strong vertical mixing events. In early 1993, i.e. at the time of the strong Baltic inflow, the surface salinity in Kattegat (*Anholt E)*) is very high, which is probably connected with the strong inflow.

As for the temperature profiles in Figure 11, the seasonal thermocline is well reproduced with depths reaching about 20-30 meters. The seasonal variability reaches about 100 m depth in some locations; see Figures 11 (b) and (c), and even deeper in the less stratified Bothnian Sea (*US5B*); see Figure 11 (d). Further, the particularly cold winters in 1996 and 2003 are clearly visible in all locations; see also Section "Sea ice" below.

5.5 Mean salinity and temperature

As mentioned in the introduction, it is interesting to study mean values of salinity and temperature, to see how they change on longer time scales. This was done by first calculating volume mean values of both salinity and temperature (correcting for changes in sea levels). Then 15-year climatologies were calculated for salinity and temperature for each day of the calendar year. This allows us to calculate anomalies from the climatology for each day of the year.

Figure 12 (a) shows the mean salinity as a function of time for both NS12 and NB03. The reason why NS12 has higher mean salinity is that a greater portion of that grid covers the North Sea, where the salinity is higher. Figure 12 (b) shows the same data, except as anomalies relative to the 1990–2004 climate. The first couple of years seem inconclusive, but the last 13 years or so show a slow increase in salinity in both model grids.

The corresponding results for the mean temperature are shown in Figure 13 (a) and (b). The top panel (a) shows the mean temperature as a function of time for both grids, and the seasonal cycle is clearly present. The bottom panel (b) shows the mean temperature anomalies relative to the 1990–2004 climate. Both grids seem to agree on large interannual variations, where certain years are cooler and other years are warmer than normal. It is clear that the winters 1996 and 2003 were rather cold, and to some extent also 1994. Finally, it is interesting to note that there is

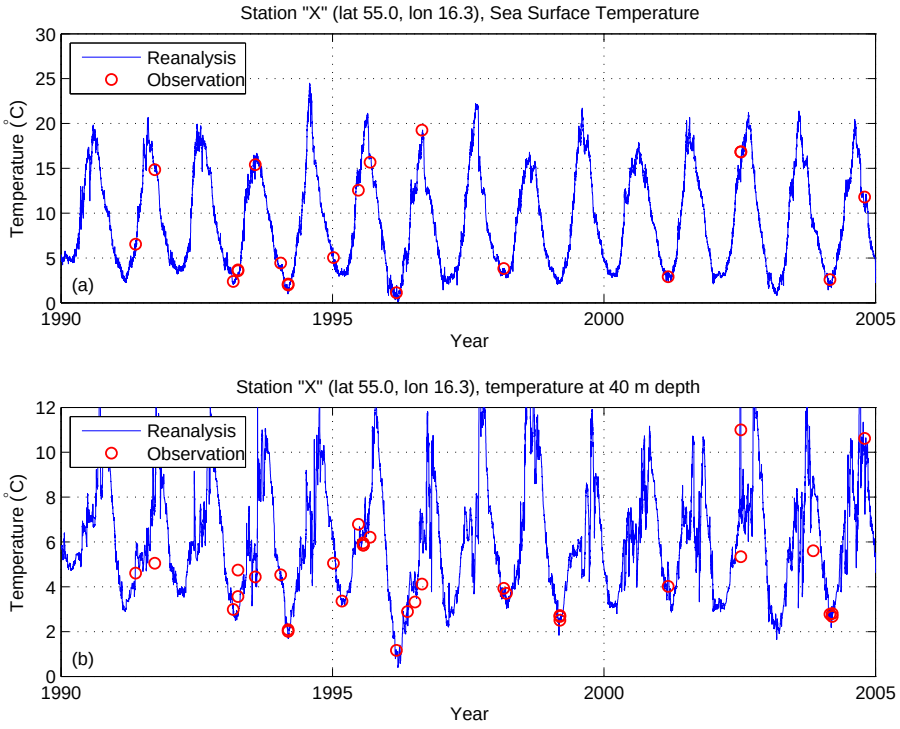

Figure 6: Validation of data assimilation of temperature at *Station X*, at (a) the surface and (b) 40 m depth. The observed data are independent data from the ICES data base and not used in the data assimilation. The reanalysis data are interpolated from the NB03 grid.

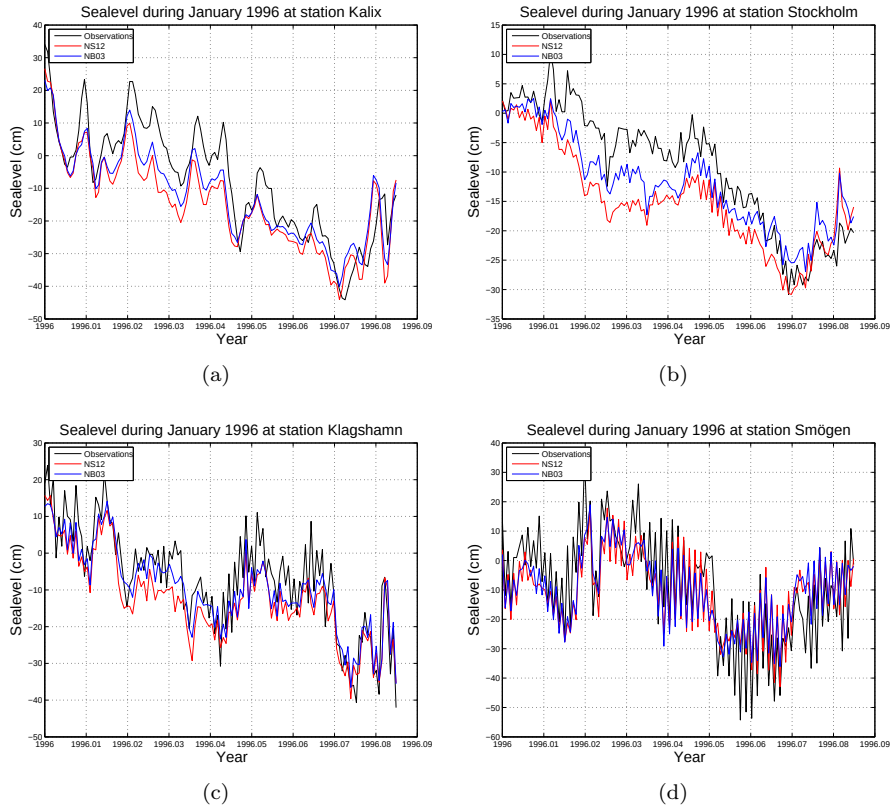

Figure 7: Time series of observed and simulated bias-corrected sea levels for the sample month January 1996 at the sea level stations (a) Kalix, (b) Stockholm, (c) Klagshamn, and (d) Smögen.

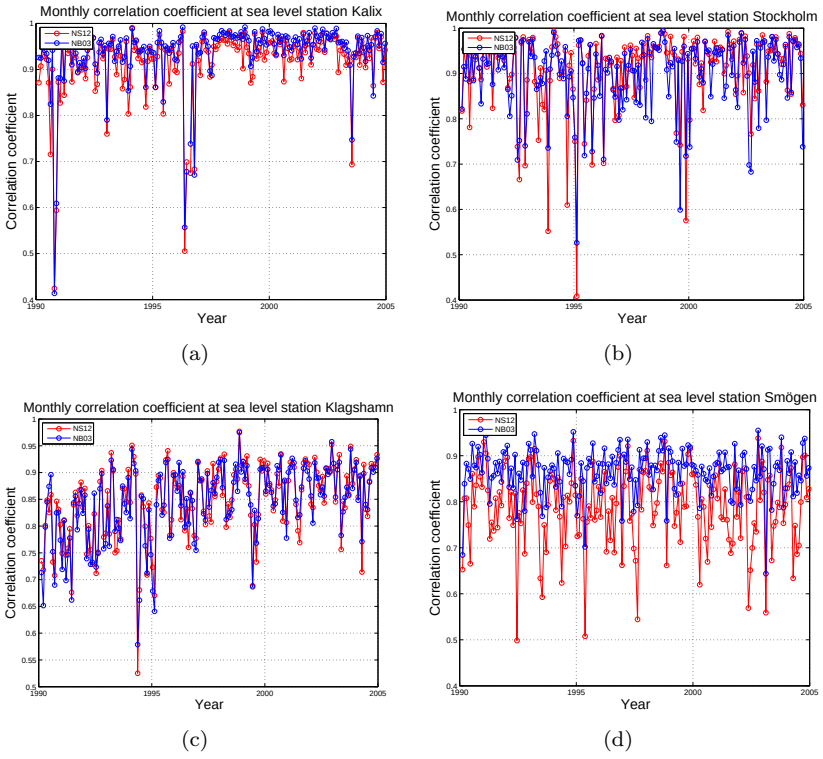

Figure 8: Time series of monthly correlations of bias-corrected sea levels for the whole 15-year period except January 1990 at the sea level stations (a) Kalix, (b) Stockholm, (c) Klagshamn, and (d) Smögen.

no clear trend during this short 15-year period.

5.6 Sea ice

Figure 14 shows the ice extent in the model area, defined as the total area of grid cells with at least 15% ice concentration. The peaks of the reanalysis time series (both NS12 and NB03) follow the annual maximum ice extent according to the ice charts (IceMap) rather well. In some years the reanalysis overpredicts the ice extent. This may have two different reasons.

First, observations were not available every day during the reanalysis, which means the data gap is filled in by the model. This is as it should be, but if there is a cold bias in the model there may be a too large ice extent. If this occurs near the date of the annual maximum ice extent, the analysed maximum ice extent may be overestimated. In the case 1996, which was the year of largest difference between analysed and observed maximum ice extent, the date of largest observed extent, according the ice charts, was February 22 with an extent of 237 000 square kilometers. The analysed value on this date was 250 000 square km, i.e. a slight overestimate. On February 8 and 12, the observed values were 230 000 and 212 000 square kilometers, respectively, whereas the analysed values were 269 000 and 242 000, respectively. However, on February 11 the analysed value was 320 000 square kilometers, which is due to freezing in the model which may be overestimated. This may be due to a cold bias in the model system, particularly near the coast due to too much land influence in the air temperature in the meteorological forcing. This is particularly a problem during the years 1990–1996 as we used ERA-40 data as forcing, with a coarse horizontal resolution (125 km), but also during the years 1997–2002 when the operational meteorological fields from ECMWF were used (resolution about 50 km). The last two years (2003–2004) we used meteorological forcing from HIRLAM with 22 km resolution, which should be OK. Inspection of the data shows that this effect, of overestimation due to a cold bias in the model, seems to be the main reason for the large overestimate of the analysed ice extent also in the year 1991, which was the second largest difference.

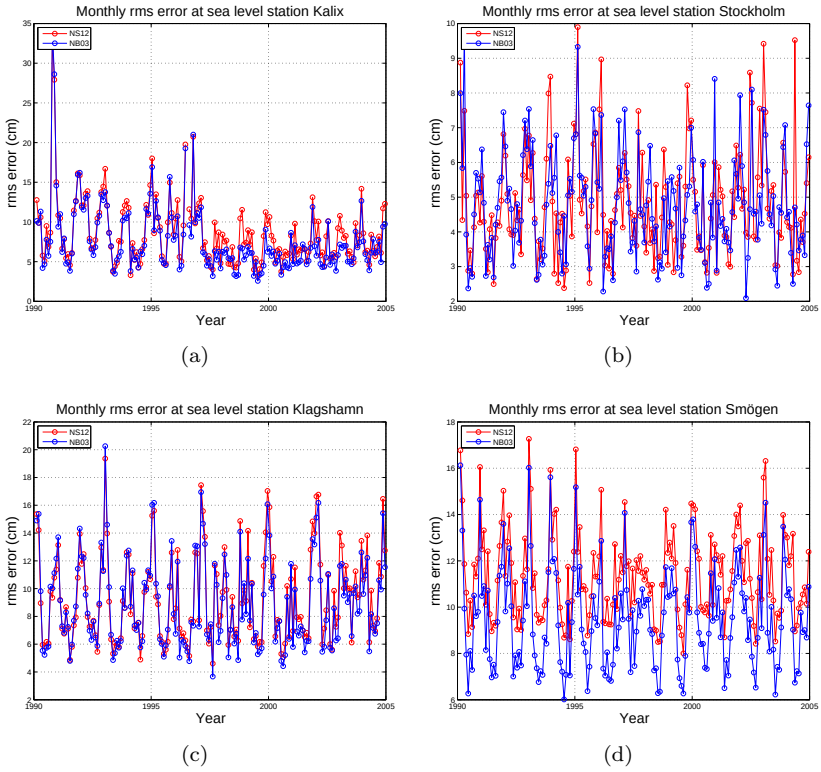

Figure 9: Time series of monthly rms errors of bias-corrected sea levels for the whole 15-year period except January 1990 at the sea level stations (a) Kalix, (b) Stockholm, (c) Klagshamn, and (d) Smögen.

The second reason why the analyses may overestimate ice extent is due to the horizontal resolution of the model grid itself, being 5.5 and 22 km for NB03 and NS12, respectively. In contrast, the ice charts from the IceMap system are gridded with 4.4 km resolution. The reason is that in a large grid cell with, say, 50 % ice concentration, the area of the whole grid cell contributes to the total ice extent (see definition above). If the same ice had been present in a grid with four times as high resolution (as in the case of NB03 relative to NS12), the same area would be covered by 16 smaller cells. Now, of these 16 cells, perhaps only half of these are covered by ice with more that 15% ice concentration, which means that this same total area (the 16 smaller cells) only contribute with half the area to the total sum of ice extent, compared with the case of lower resolution. This effect is largest near the ice edge (and near the coast for similar reasons), so the total difference in ice extent is normally not that large, however.

6 Summary and discussion

A 15-year reanalysis data set for the period 1990–2004 has been created, which consists of two nested model grids. The coarse grid has a horizontal resolution of 12 nm (22 km) and covers the North Sea and the Baltic Sea, whereas the fine grid has a horizontal resolution of 3 nm (5.5 km). A simple data assimilation method has been used (Successive Corrections), but the results look promising. The data assimilated include analysed SST and ice variables from the IceMap system (used by the Ice Service at SMHI) as well as salinity and temperature profiles from research ships.

When choosing the atmospheric forcing in a reanalysis, we generally want the forcing to be (a) as good as possible, and (b) be as consistent as possible during the reanalysis period. These two requirements are sometimes in conflict with each other, however. For this project, the best available forcing for the latter years was simply not available for the earlier years of the reanalysed period which of course is a drawback. For climate studies with long time series of reanalysed data, it would have been better to retain the same atmospheric forcing during the whole reanalysed period. In

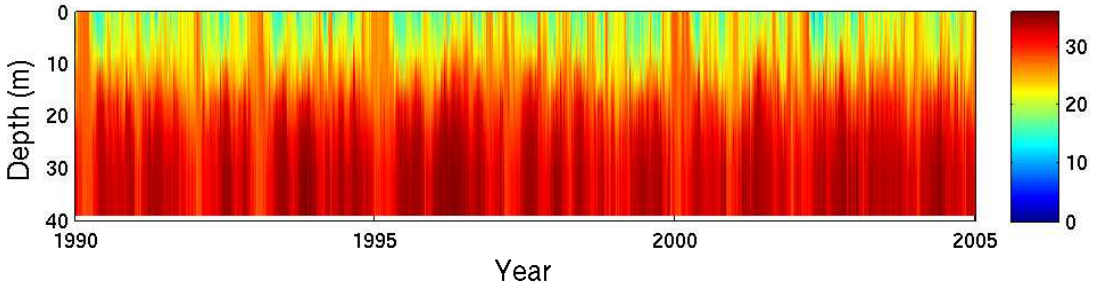

(a)

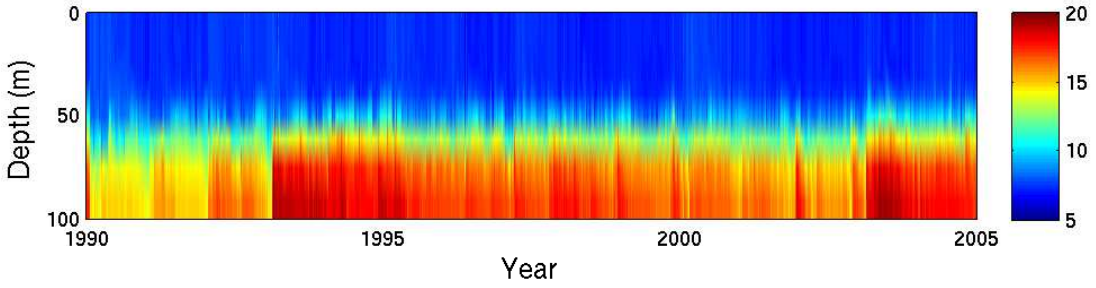

(b)

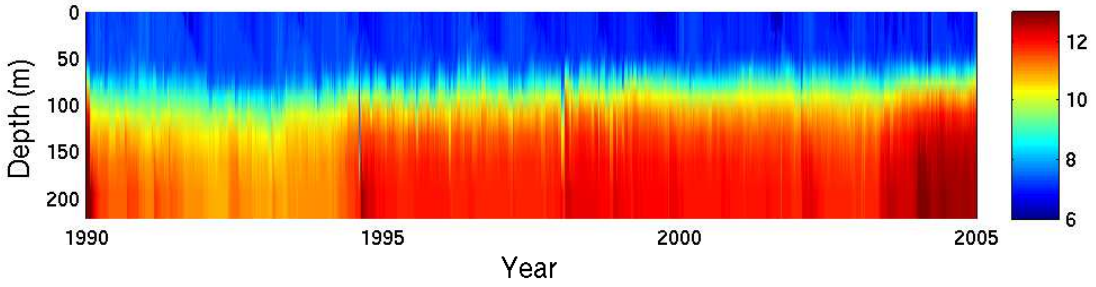

(c)

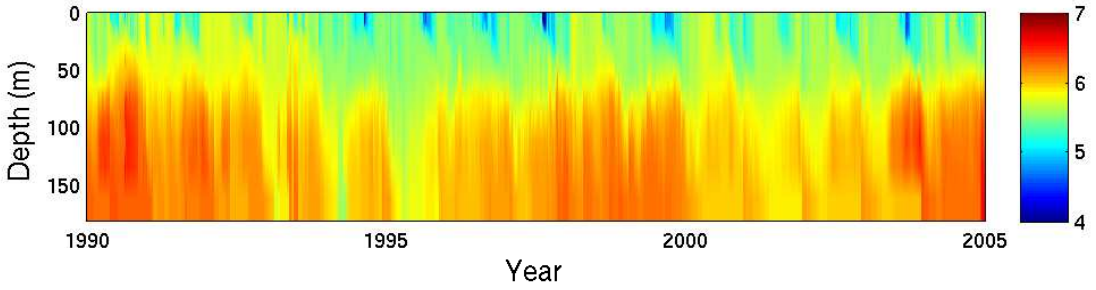

(d)

Figure 10: Time series of daily salinity profiles for the whole 15-year period at the stations (a) *Anholt E*, (b) *BY5*, (c) *BY15*, and (d) *US5B*.

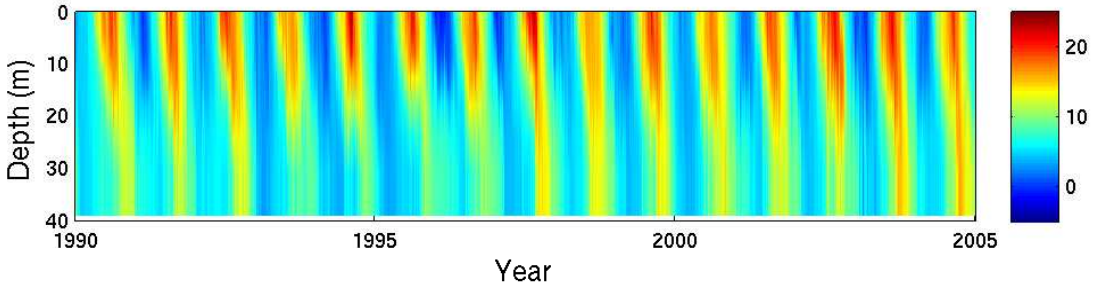

(a)

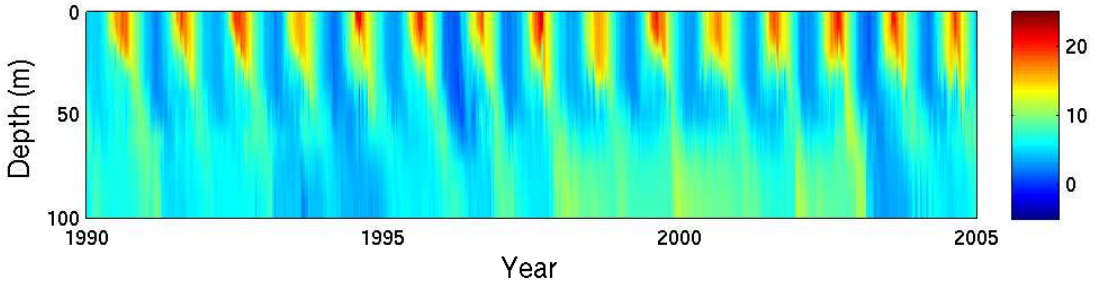

(b)

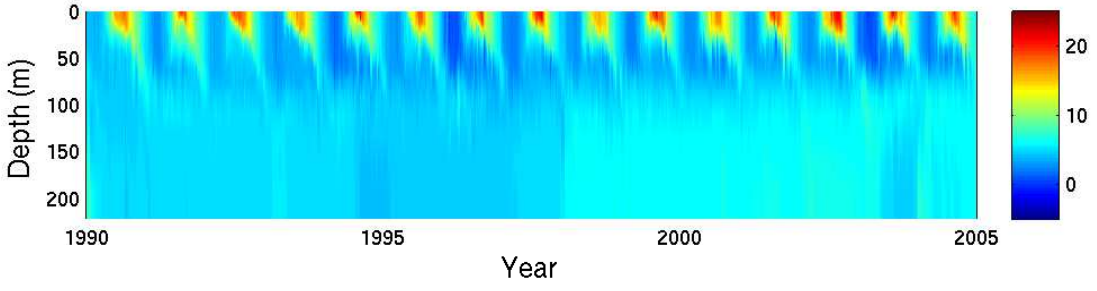

(c)

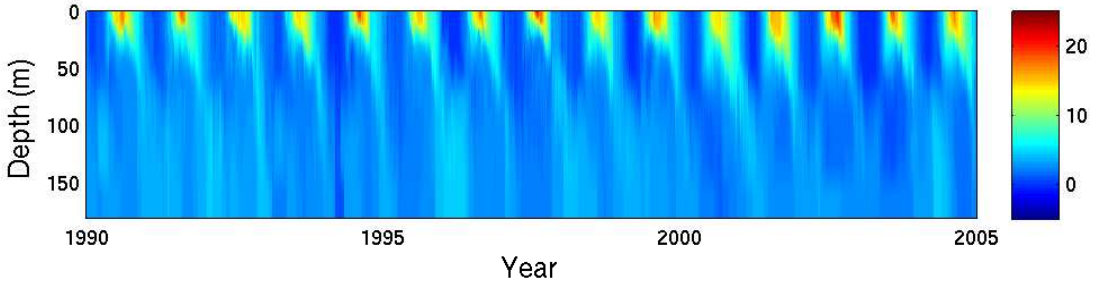

(d)

Figure 11: Time series of daily temperature profiles for the whole 15-year period at the stations *Anholt E*, (b) *BY5*, (c) *BY15*, and (d) *US5B*.

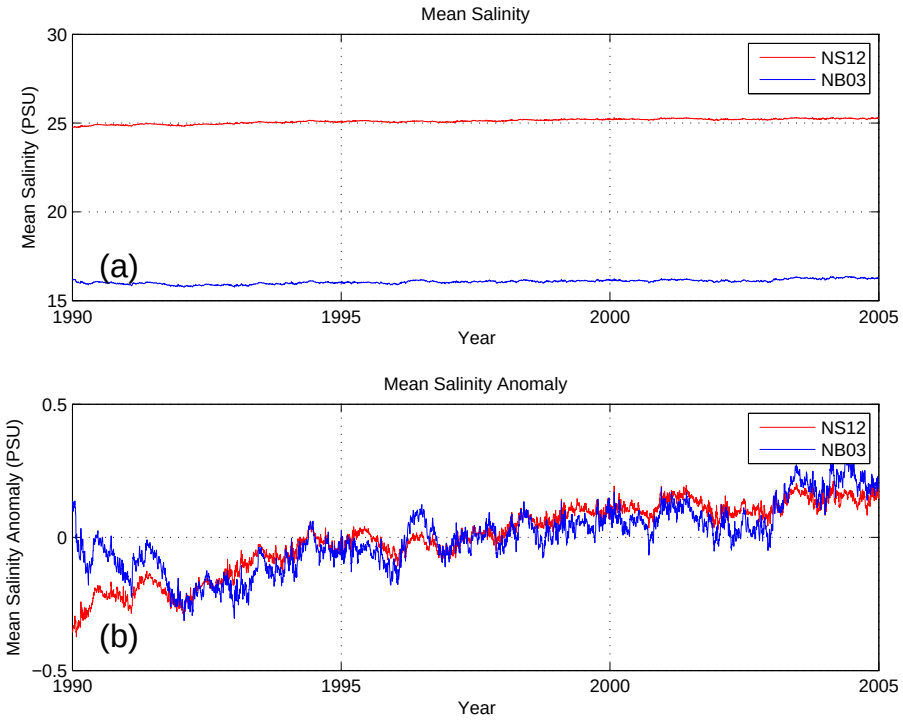

Figure 12: Mean salinity in terms of (a) absolute values and (b) relative to the 1990–2004 mean. Results are shown for both NS12 and NB03.

this case, however, the time period was only 15 years and thus not of sufficient length for climate studies. Therefore, here we instead prioritized (a) above, i.e. to have as good atmospheric forcing as possible, even though the forcing became slightly inconsistent. In future reanalysis projects, which will cover longer time periods, better atmospheric forcing will be used.

Sea levels were not assimilated, but validation against coastal observations gave mostly satisfactory results. One problem with the validation is that model data have only been saved every six hours, which is half the semi-diurnal period of the tides in the North Sea-Skagerrak area. A higher time resolution for the sea level data would have been preferred, especially for that area but also for the Baltic Sea.

Further, the results for temperature and salinity were mainly good, despite the simple data assimilation method. However, there is much room for improvements. First, the screening of observations must be improved to avoid assimilating profiles of bad quality. This happened for example at station *BY15* in the Eastern Gotland Basin in the Baltic Sea on several occasions, though the stratification recovered fast due to model dynamics as well as new observations.

Finally, the ice variables in the reanalysis data set are mostly very similar to the original IceMap data, but the model contributed with data between the times of observations, which was only twice a week for the reanalysis period. This gave some problems during the early part of the analysed period, as too much land influence in the coarse meteorological forcing data (ERA-40) resulted in too low air temperatures during winter. Similarly, a warm bias is expected near the coasts during summer but this has not been confirmed.

This reanalysis was completed in 2005 and was probably the first reanalysis of the Baltic Sea covering more than ten years. It has been used from time to time at SMHI in smaller projects when reliable salinity, temperature or current fields have been needed. Perhaps of greater value is the experience gained which will serve to improve future reanalyses of the Baltic Sea.

There is much room for improvements. First, the data assimilation system must be improved. Today's operational data assimilation system at SMHI is based on univariate Optimal Interpolation with correlation functions depending on the vicinity of coastlines and local stratification. Further, tests are currently being made using multivariate Optimal Interpolation using ensemble statistics to generate realistic correlation functions, so-called Ensemble Optimal Interpolation (EnOI). In

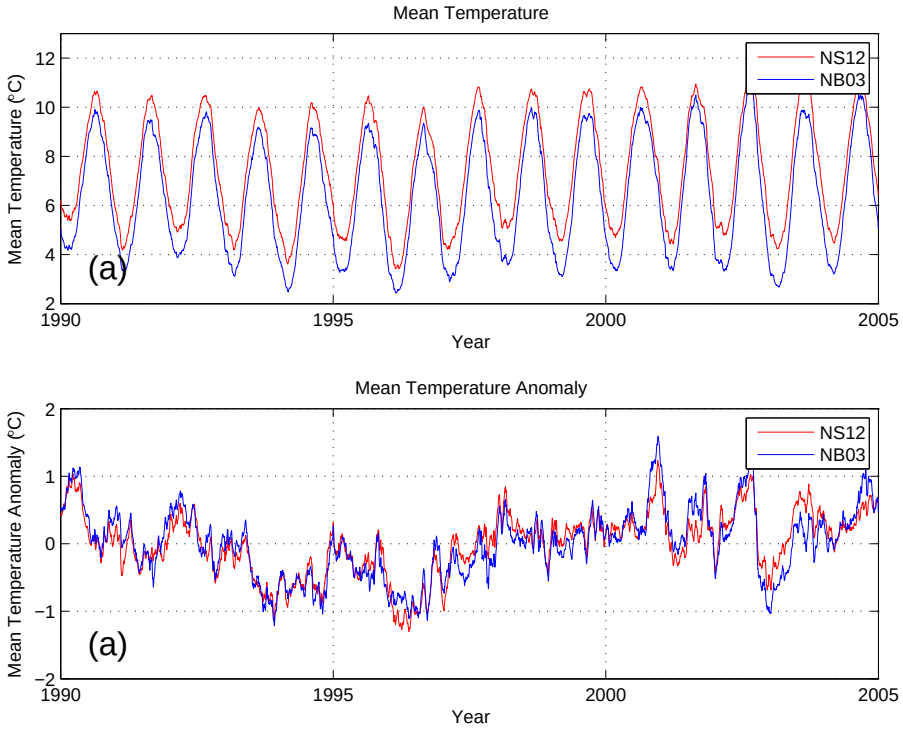

Figure 13: Mean temperature in terms of (a) absolute values and (b) relative to the 1990–2004 mean. Results are shown for both NS12 and NB03.

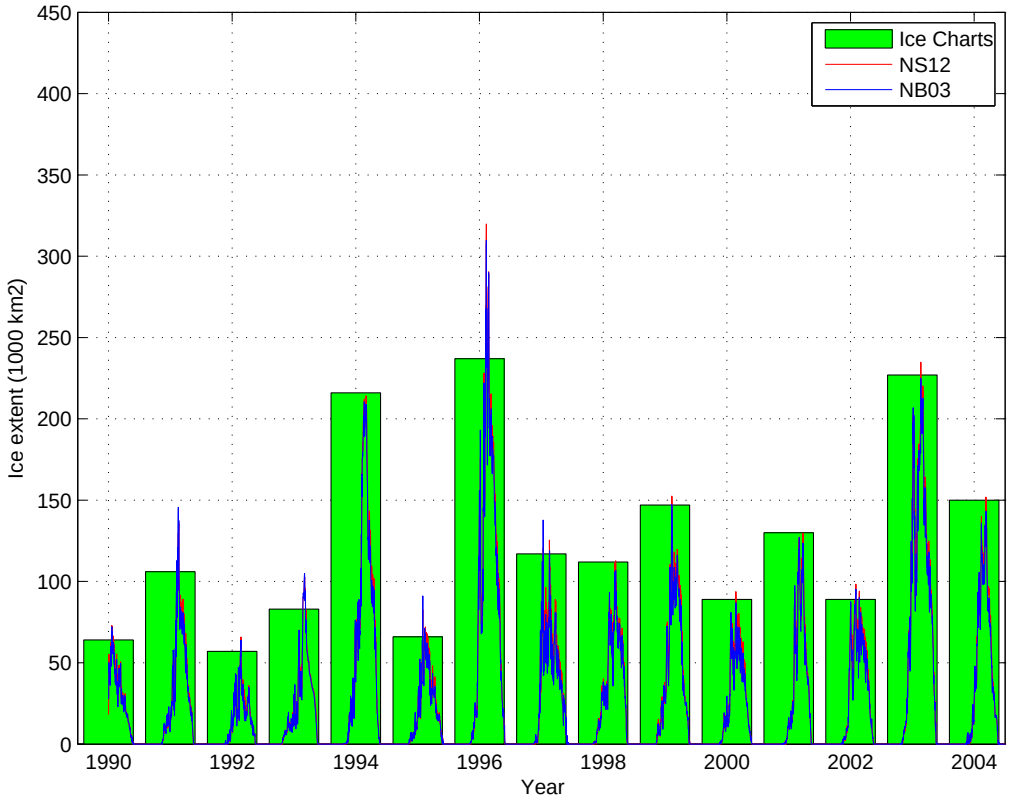

Figure 14: Baltic Sea ice extent for the NS12 and NB03 grids. The results are compared with annual maximum sea ice extent using ice charts only.

addition, experiments are being made with a new multivariate Ensemble 3D-Var system (En3D-Var). Other obvious improvements include using more observations, extending the time period and using improved, homogeneous atmospheric forcing.

Acknowledgments

This ice ridging equations in HIROMB and the Successive Correction data assimilation method were implemented and tested during the EU funded project IRIS (Ice Ridging Information for Decision Making in Shipping Operations), 2003–2005, under the Fifth Framework Programme. Project Reference: EVK3-CT-2002-00083. The actual reanalysis work was funded by SMHI. Thanks also to Markus Meier for reading the manuscript.

Appendix A: Derivation of the coefficients in the k-ω turbulence model

The two differential equations in the k-ω turbulence model are

$$\frac{\partial k}{\partial t} = \frac{\partial}{\partial z}\left(\frac{\nu_t}{\sigma_k^\omega}\frac{\partial k}{\partial z}\right) + P_s + P_b - \varepsilon, \tag{38}$$

$$\frac{\partial \omega}{\partial t} = \frac{\partial}{\partial z}\left(\frac{\nu_t}{\sigma_\omega}\frac{\partial \omega}{\partial z}\right) + \frac{\omega}{k}\left(c_{\omega 1}P_s + c_{\omega 3}P_b - c_{\omega 2}\varepsilon\right), \tag{39}$$

where the independent variables t and z are the time variable and the vertical coordinate (positive upwards), respectively. To solve the equation system we need, in addition to the equations given in Section 2.2, the values of five coefficients, whose values can be determined with the help of observations. The unknown parameters are (1) c_μ^0, (2) $c_{\omega 1}$, (3) $c_{\omega 2}$, (4) $c_{\omega 3}$, (5) σ_k^ω, and (6) σ_ω. The main reference for the following derivations (except $c_{\omega 3}$) is Umlauf and Burchard [2003]; see that paper for more details.

The *first* constraint is that in the logarithmic boundary layer, k is approximately constant and given by

$$k = \frac{u_*^2}{(c_\mu^o)^2}$$

and observations indicate that $(c_\mu^o)^2 \approx 0.3$ [e.g. Mellor and Yamada, 1982]. With an accuracy of, say, 10 %, this implies $0.52 \leq c_\mu^o \leq 0.57$. For historical reasons we follow Mellor and Yamada [1982] and set $c_\mu^o = 0.5562$.

The *second* constraint follows from the special case of homogeneous turbulence. Then eqs. (38) and (39) may be written

$$\frac{dk}{dt} = P_s + P_b - \varepsilon, \tag{40}$$

and

$$\frac{d\omega}{dt} = \frac{\omega}{k}(c_{\omega 1}P_s + c_{\omega 3}P_b - c_{\omega 2}\varepsilon), \tag{41}$$

respectively, since in homogeneous flow all transports are zero. Further, using (6) and the relation between turbulent length scale l and k and ε,

$$\varepsilon = \frac{(c_{\mu^0})^3 k^{3/2}}{l},$$

we obtain

$$l = \frac{1}{c_\mu^0}\frac{k^{1/2}}{\omega}. \tag{42}$$

Using the chain rule of derivation on (42) we arrive at

$$\frac{1}{l}\frac{dl}{dt} = \frac{1}{2}\frac{1}{k}\frac{dk}{dt} - \frac{1}{\omega}\frac{d\omega}{dt}. \tag{43}$$

Inserting (40) and (41) into (43) we obtain

$$\frac{1}{l}\frac{dl}{dt} = \frac{\varepsilon}{k}\left(c_{\omega 2} - \frac{1}{2}\right) + \frac{1}{k}\left(-c_{\omega 1} + \frac{1}{2}\right)P_s + \frac{1}{k}\left(-c_{\omega 3} + \frac{1}{2}\right)P_b. \tag{44}$$

Now, since shear cannot impose a length scale in homogeneous turbulence, the shear term (containing P_s) must be identical to zero. Hence, we must have $c_{\omega 1} = 1/2$ [Tennekes, 1989].

The *third* constraint can be derived by studying the temporal decay of isotropic homogeneous turbulence (in the laboratory approximated by the spatial decay of grid-generated turbulence). It can be shown that the turbulent kinetic energy k decays with time t as

$$k \propto t^d,$$

where $d \approx -1.2$ according to observations. For the k-ω model it can be shown that

$$d = -\frac{1}{c_{\omega 2}}$$

[Umlauf and Burchard, 2003], which in turn implies $c_{\omega 2} \approx 0.833$.

The *fourth* constraint is obtained by applying the law of the wall on eq. (39) which yields

$$\sigma_\omega = \frac{\kappa^2}{(c_\mu^0)^2(c_{\omega 2} - c_{\omega 1})}.$$

After insertion of derived values of c_μ^0, $c_{\omega 1}$ and $c_{\omega 2}$, and using a common literature value of the classical constant $\kappa = 0.40$ (Karman's constant), we find that $\sigma_\omega = 1.552$.

The *fifth* constraint can be obtained from the case of shear-free, unstratified, stationary turbulence, in which there is a balance between turbulent transport terms and dissipation terms in eqs. (38) and (39). Grid stirring experiments show the following decay laws:

$$k \propto (z + z_0)^\alpha, \tag{45}$$

$$l = L(z + z_0), \tag{46}$$

where $-3.0 \leq \alpha \leq -1.7$ and $0.1 \leq L \leq 0.3$. Following Umlauf and Burchard [2003] we find that

$$\alpha = \frac{4(\sigma_k^\omega)^{1/2}}{3(\sigma_k^\omega)^{1/2} - (\sigma_k^\omega + 24\sigma_\omega c_{\omega 2})^{1/2}}, \tag{47}$$

$$L = \frac{(c_\mu^0)^{3/2}}{c_\mu^{1/2}} \left(\frac{5\sigma_k^\omega + 12\sigma_\omega c_{\omega 2} - 3(\sigma_k^\omega(\sigma_k^\omega + 24\sigma_\omega c_{\omega 2}))^{1/2}}{12} \right)^{1/2}. \tag{48}$$

Choosing $\alpha = -2.0$ we find that must have $\sigma_k^\omega = 1.30$, which implies that $L \approx 0.26$ (if we assume $c_\mu \approx c_\mu^0$) which is well within the observed range.

The *sixth* and last constraint is connected with the coefficient $c_{\omega 3}$, which, as it has turned out, is not a constant but a function. Burchard and Baumert [1995] derived a relationship between $c_{\varepsilon 3}$ in the k-ε turbulence model and the steady-state flux Richardson number R_f, in the case of equilibrium between local sources and sinks in the transport equations for k and ε. As the structure of the k-ε turbulence model and the present k-ω turbulence model are identical, the results can be used here too. The following expression is obtained:

$$c_{\omega 3} = c_{\omega 2} - \frac{c_{\omega 2} - c_{\omega 1}}{R_f}. \tag{49}$$

Following the arguments by Arneborg [2000] and Axell [2002] we assume R_f has different values in different situations. R_f is the flux Richardson number, which may be interpreted as an efficiency factor of turbulent mixing in which turbulent kinetic energy is turned into potential energy through mixing. Reported near-surface values are in the range $0.14 \leq R_f \leq 0.20$ [Osborn, 1980; Ivey and Imberger, 1991; Itsweire et al., 1993]. Axell and Liungman [2001] found in their work with a one-equation turbulence model that their tuned value of a certain coefficient, related to mixed layer deepening, corresponds to $R_f = 0.16$, using the same stability functions as we do here. Hence, here we will assume $R_f = 0.16$ during stable situations near the surface (when $P_s > P_{IW}$).

Arneborg [2000] found, however, that in patchy turbulence, found further away from the surface, the large-scale efficiency factor R_f is only half the value within a patch. Hence, in the stably stratified interior, far from the surface layer (when $P_s < P_{IW}$), we instead assume $R_f = 0.08$, i.e. half the near-surface value [Arneborg, 2000]. See also the discussion by Axell [2002]. Inserting these values of R_f into equation (49) gives $c_{\omega 3} = -1.25$ near the surface and $c_{\omega 3} = -3.33$ in the stably stratified interior.

In unstable situations (convection), however, the local closure suggested by Burchard and Baumert [1995] breaks down, as the transport terms cannot be neglected in this case. The value used during convection has tentatively been set to $c_{\omega 3} = +1.0$ which seems to give good results in geophysical situations.

To summarize, all the six unknown parameters in the k-ω turbulence model have now been assigned values. See Table 1.

Appendix B: Monthly mean SST and SIC fields

Monthly mean fields have been calculated for most variables, including sea levels, sea ice concentration, level ice thickness, ridged ice thickness, total ice thickness, ice ridge sail height, ice ridge density, ice drift, currents, salinity, and temperature; hence eleven variables in total. There are 180 months from the 15-year reanalysis, which implies that $11 \times 180 = 1980$ figures may be plotted, if we restrict ourselves to surface variables. In this appendix we will limit ourselves to show two variables, SST and SIC, plotted together which results in 180 figures; see below.

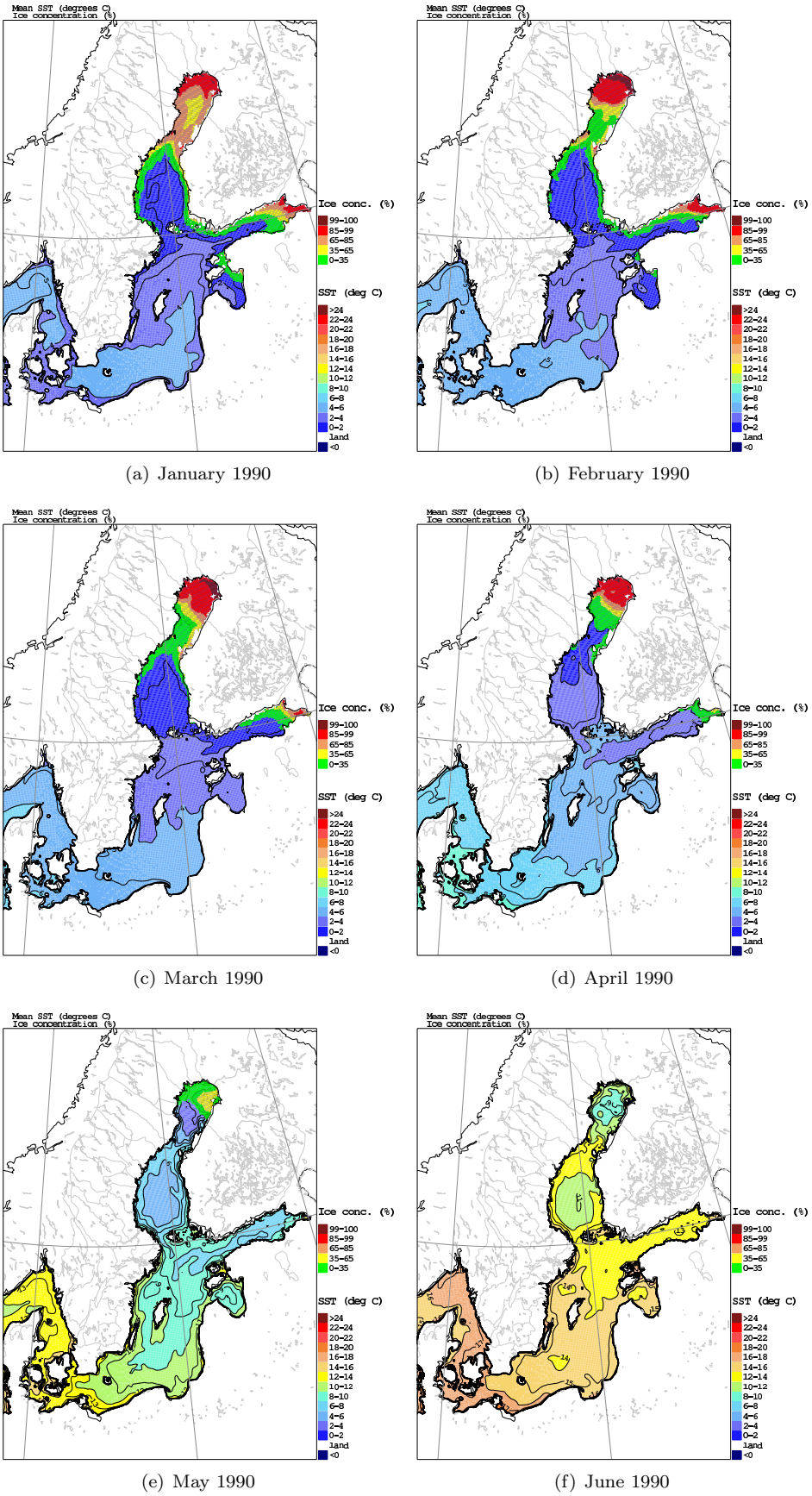

(a) January 1990

(b) February 1990

(c) March 1990

(d) April 1990

(e) May 1990

(f) June 1990

Figure 15: Monthly mean SST and SIC fields for January to June 1990.

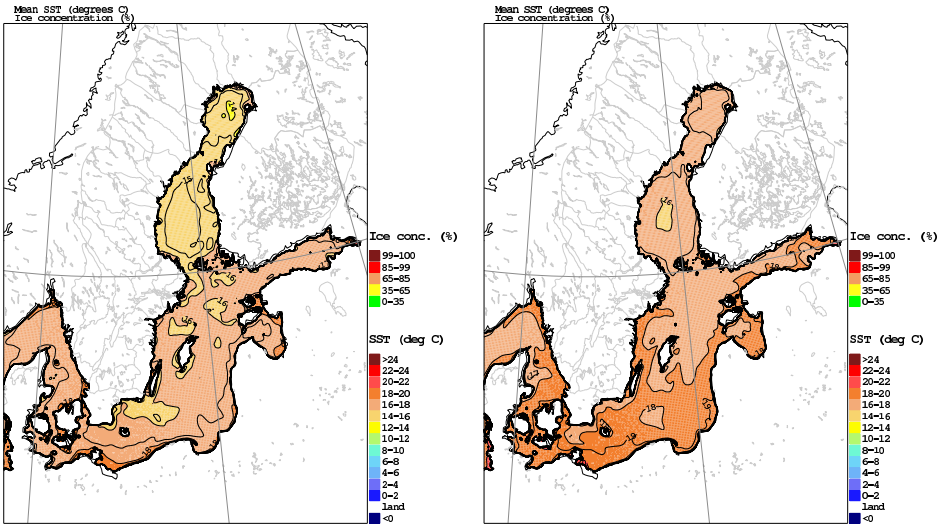

(a) July 1990

(b) August 1990

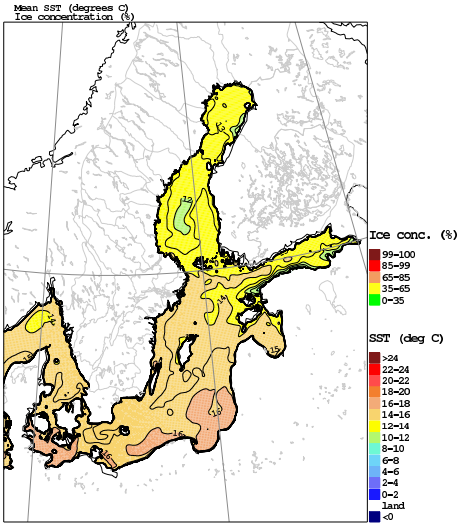

(c) September 1990

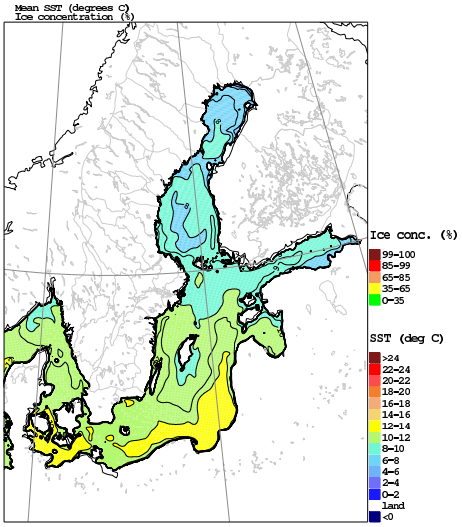

(d) October 1990

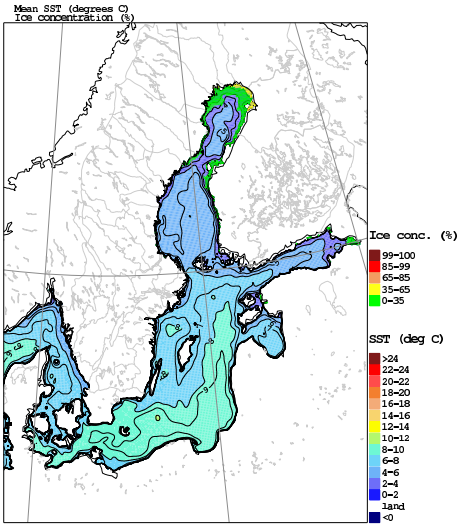

(e) November 1990

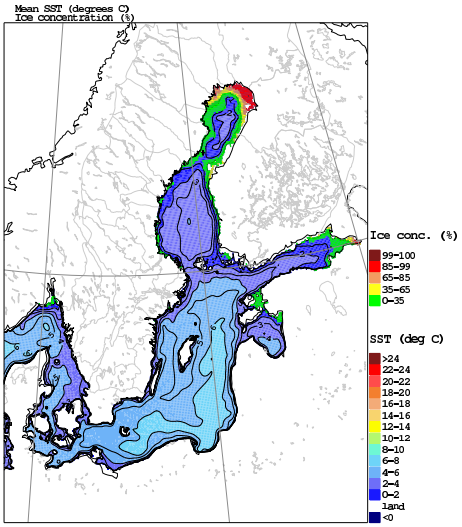

(f) December 1990

Figure 16: Monthly mean SST and SIC fields for July to December 1990.

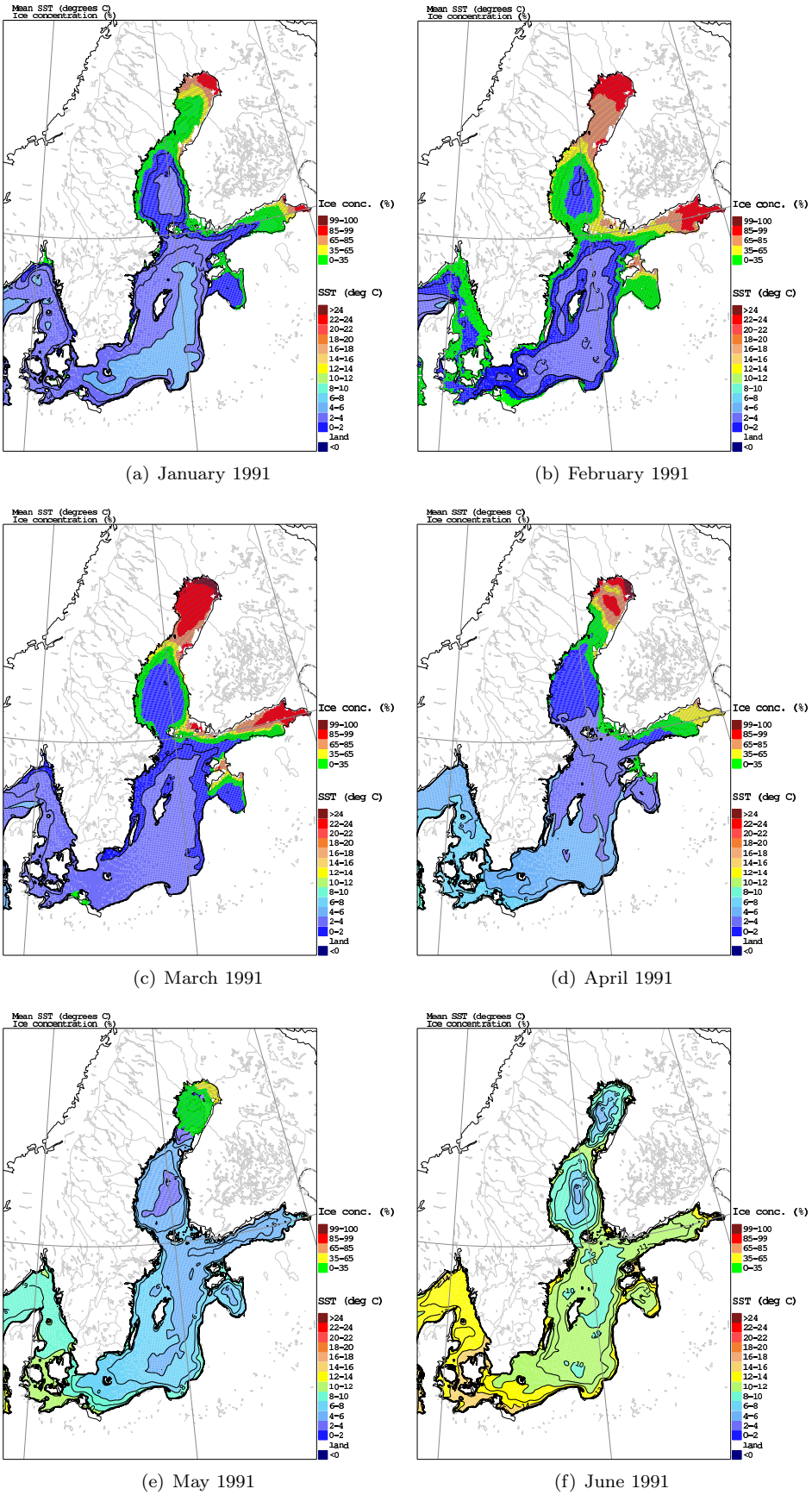

(a) January 1991

(b) February 1991

(c) March 1991

(d) April 1991

(e) May 1991

(f) June 1991

Figure 17: Monthly mean SST and SIC fields for January to June 1991.

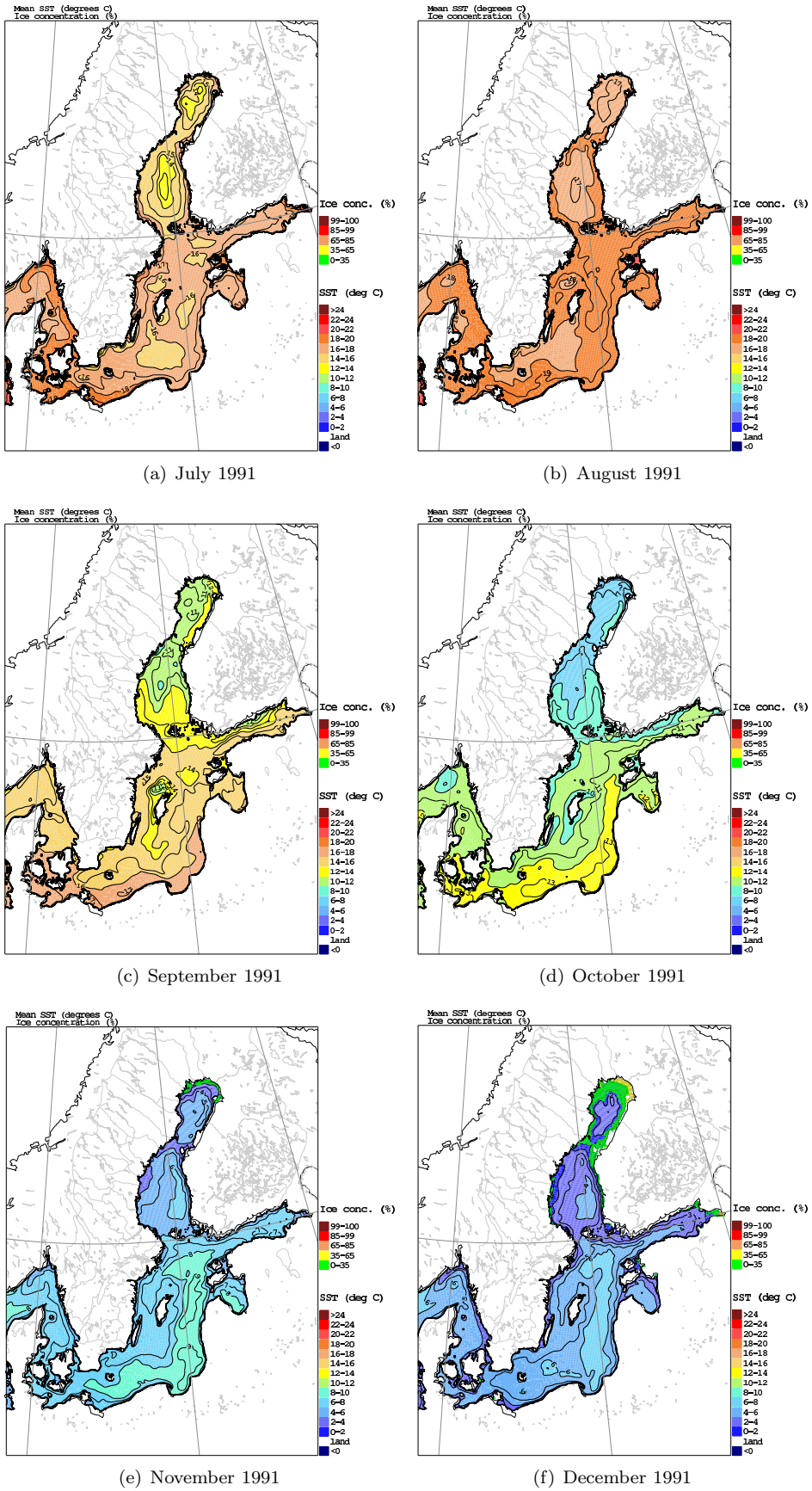

(a) July 1991

(b) August 1991

(c) September 1991

(d) October 1991

(e) November 1991

(f) December 1991

Figure 18: Monthly mean SST and SIC fields for July to December 1991.

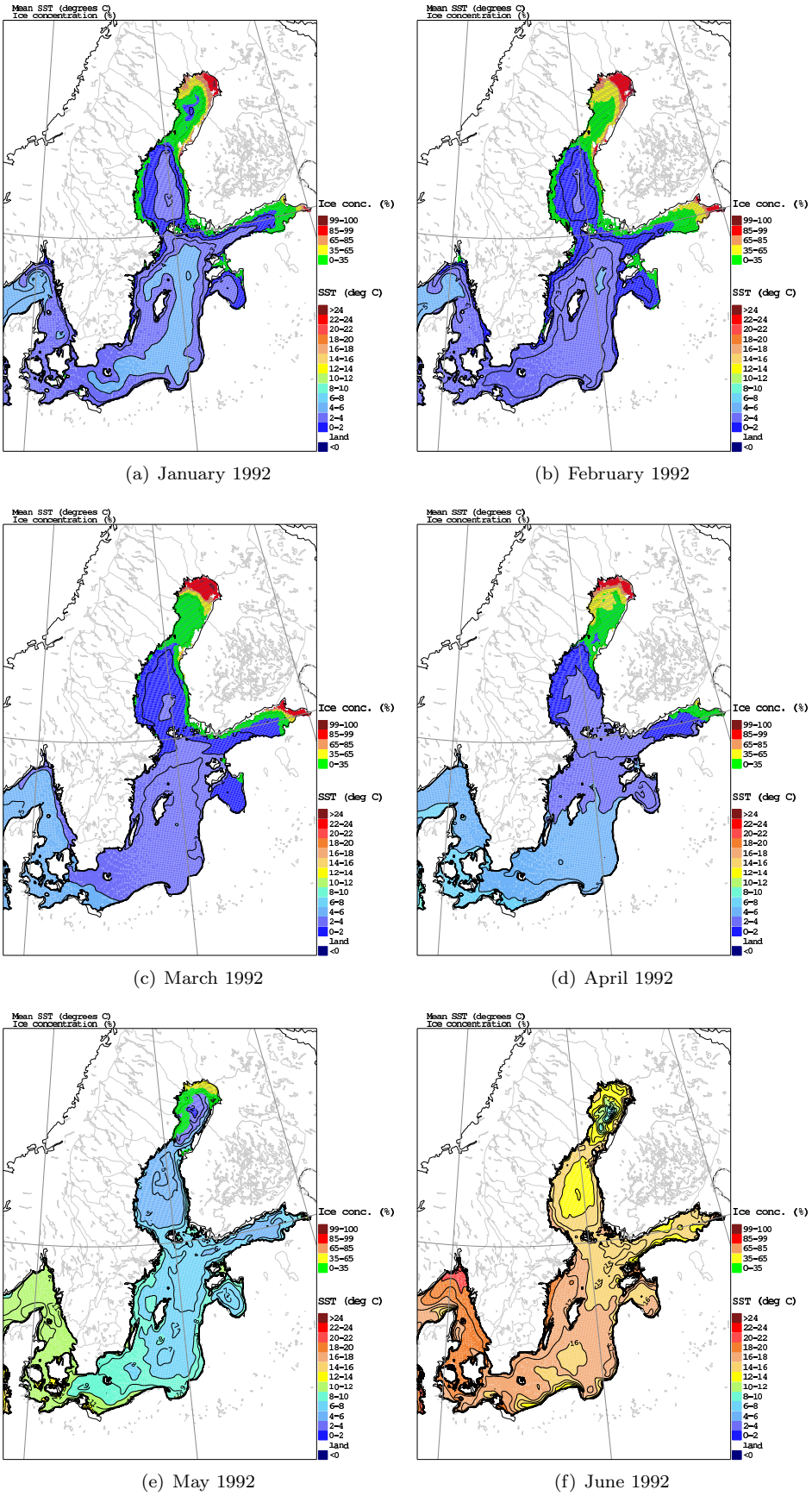

(a) January 1992

(b) February 1992

(c) March 1992

(d) April 1992

(e) May 1992

(f) June 1992

Figure 19: Monthly mean SST and SIC fields for January to June 1992.

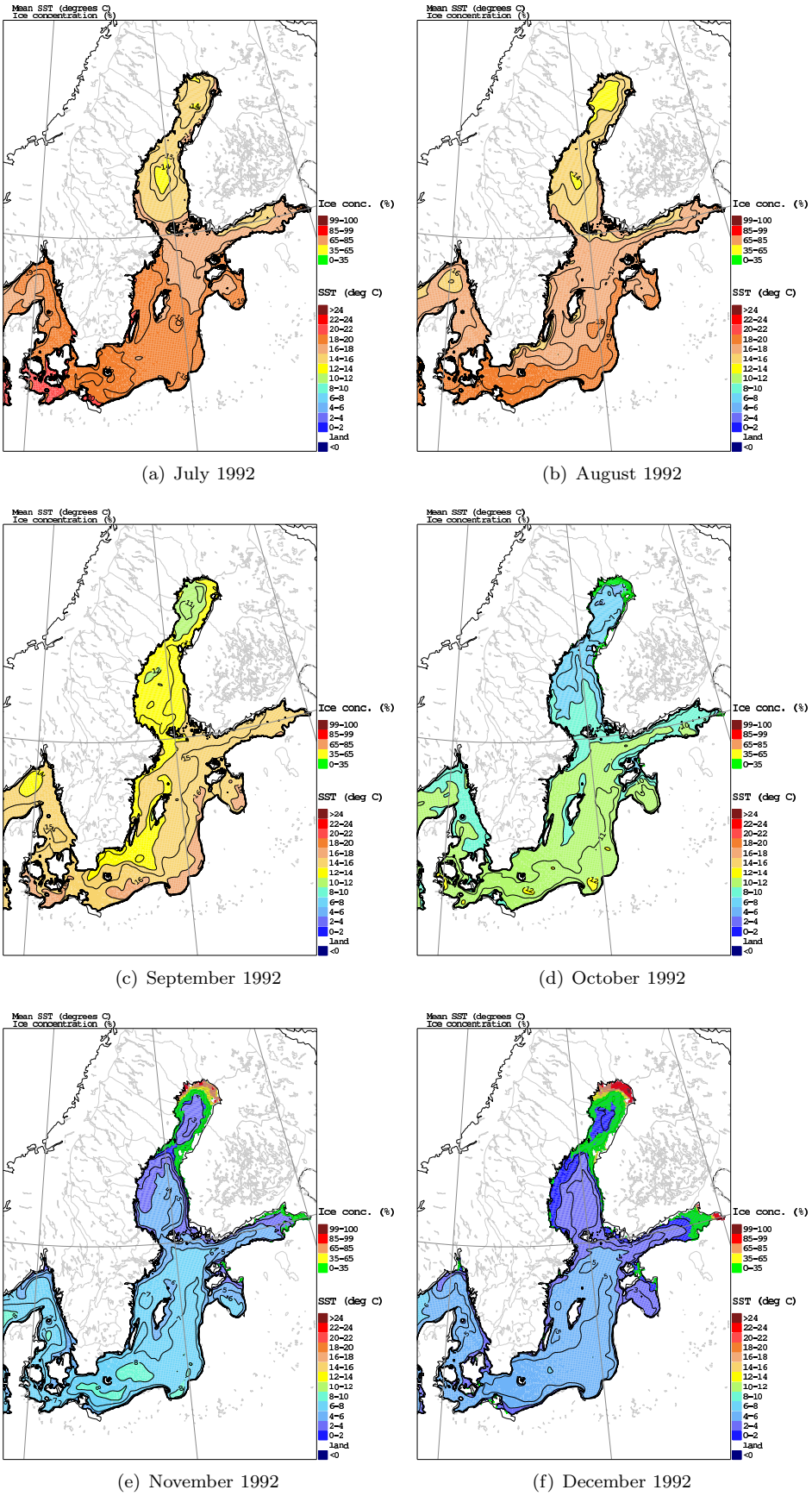

(a) July 1992

(b) August 1992

(c) September 1992

(d) October 1992

(e) November 1992

(f) December 1992

Figure 20: Monthly mean SST and SIC fields for July to December 1992.

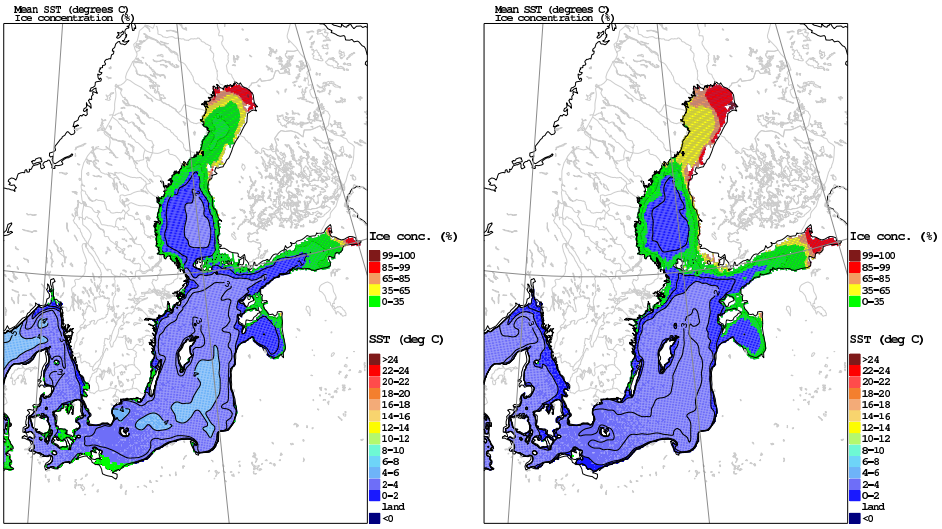

(a) January 1993

(b) February 1993

(c) March 1993

(d) April 1993

(e) May 1993

(f) June 1993

Figure 21: Monthly mean SST and SIC fields for January to June 1993.

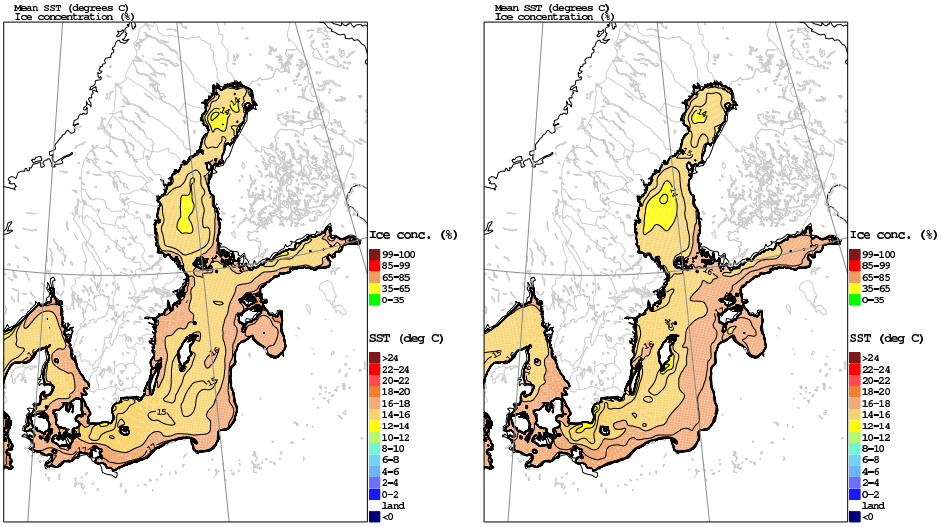

(a) July 1993

(b) August 1993

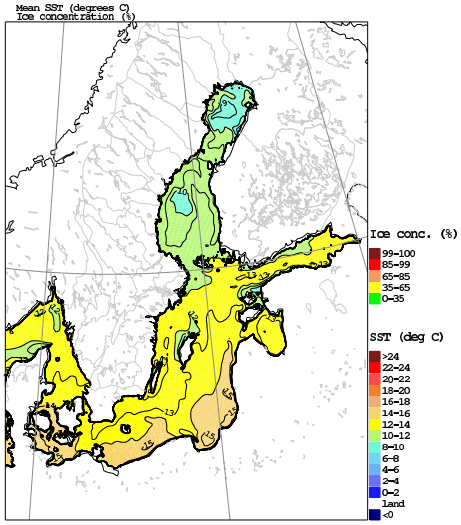

(c) September 1993

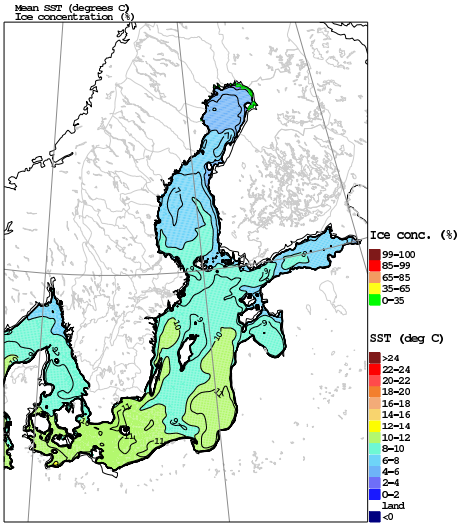

(d) October 1993

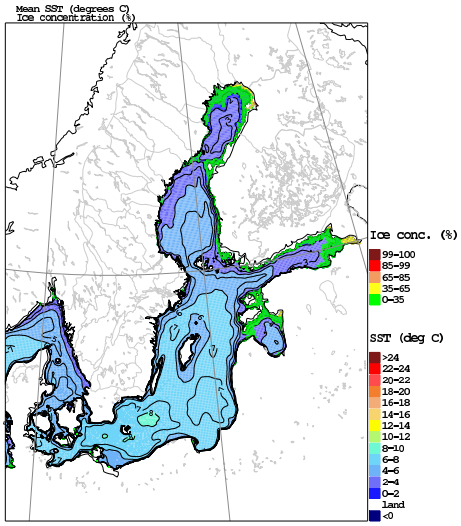

(e) November 1993

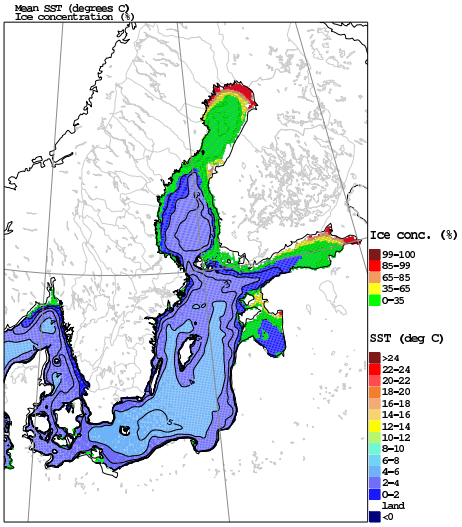

(f) December 1993

Figure 22: Monthly mean SST and SIC fields for July to December 1993.

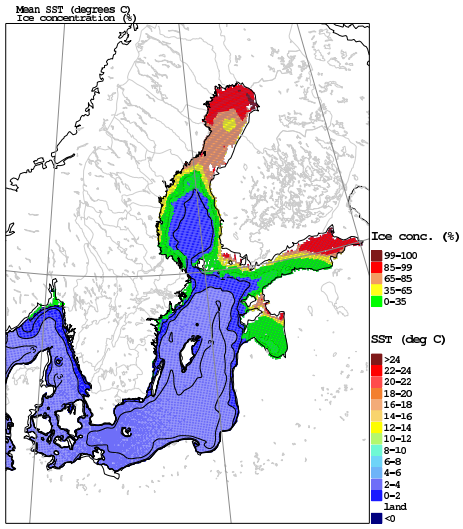

(a) January 1994

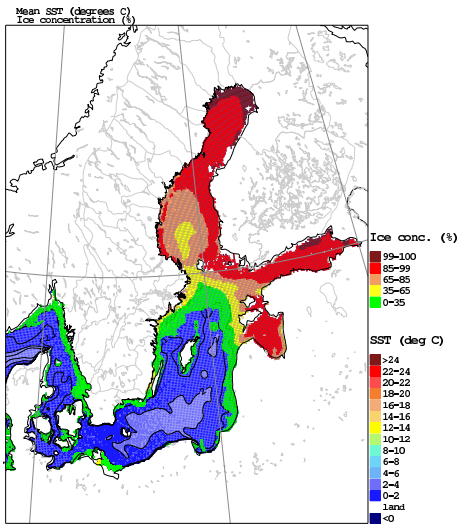

(b) February 1994

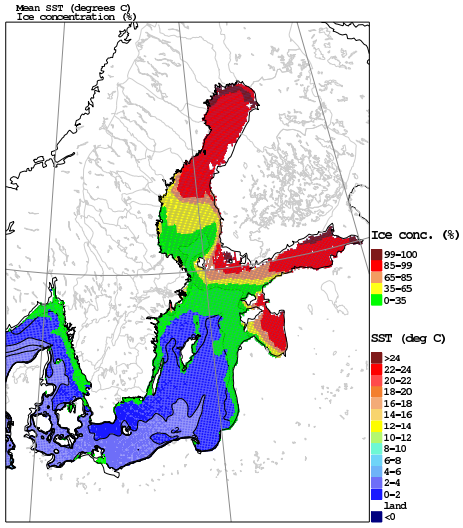

(c) March 1994

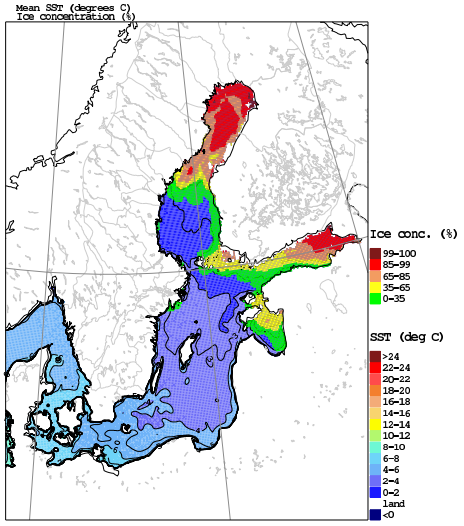

(d) April 1994

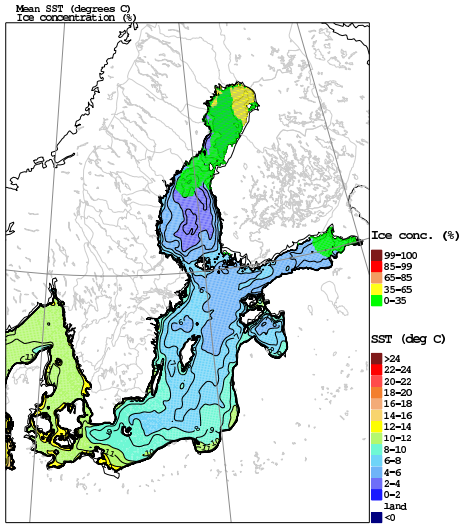

(e) May 1994

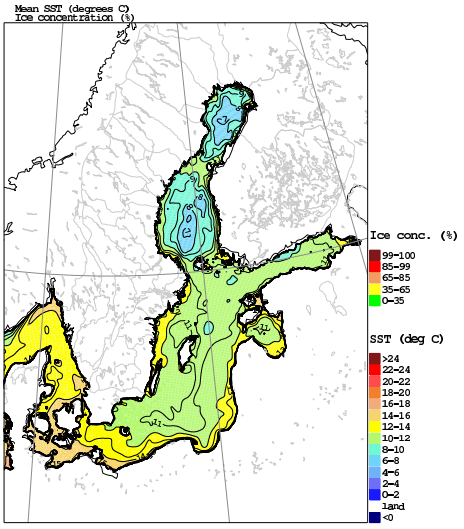

(f) June 1994

Figure 23: Monthly mean SST and SIC fields for January to June 1994.

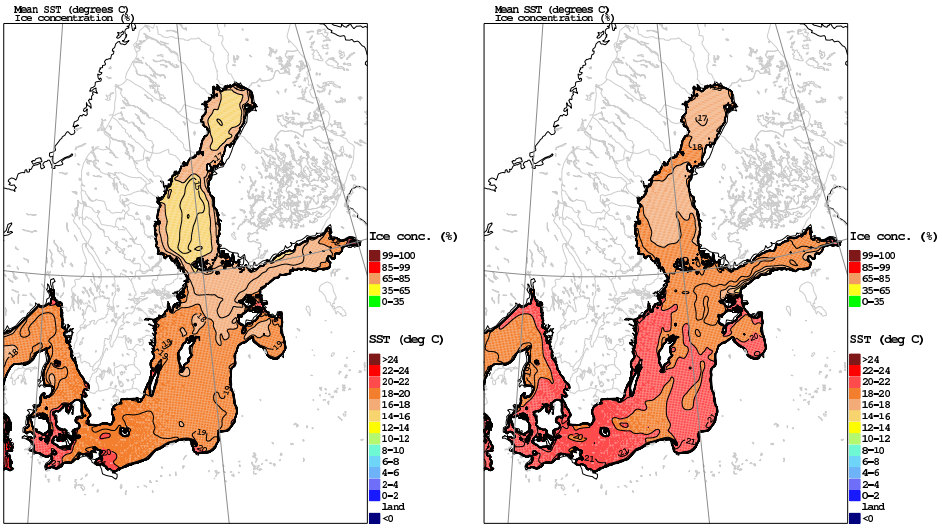

(a) July 1994

(b) August 1994

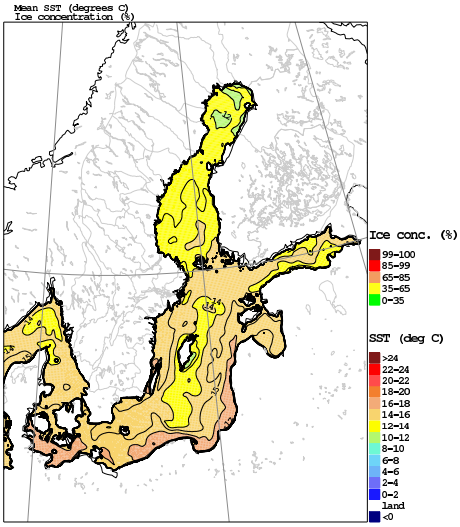

(c) September 1994

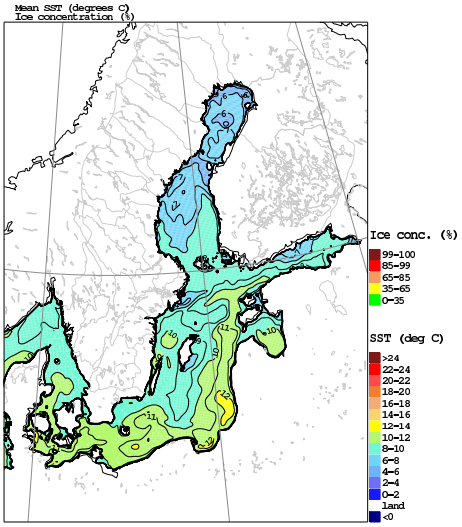

(d) October 1994

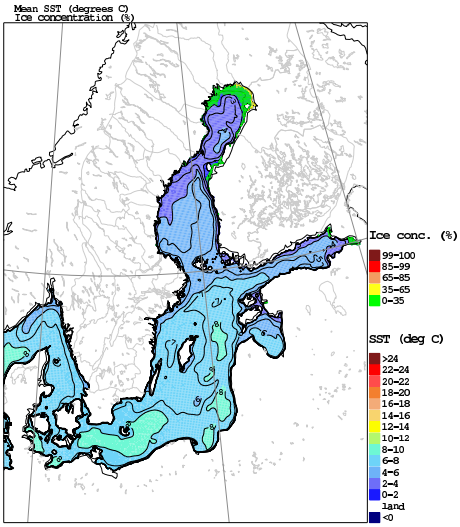

(e) November 1994

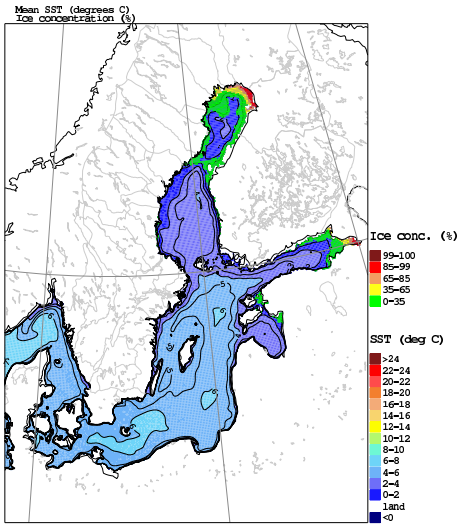

(f) December 1994

Figure 24: Monthly mean SST and SIC fields for July to December 1994.

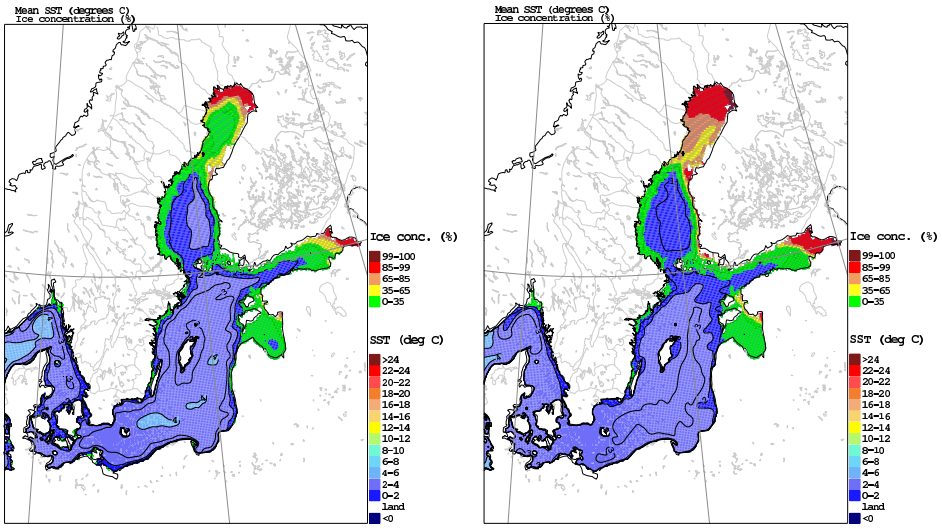

(a) January 1995

(b) February 1995

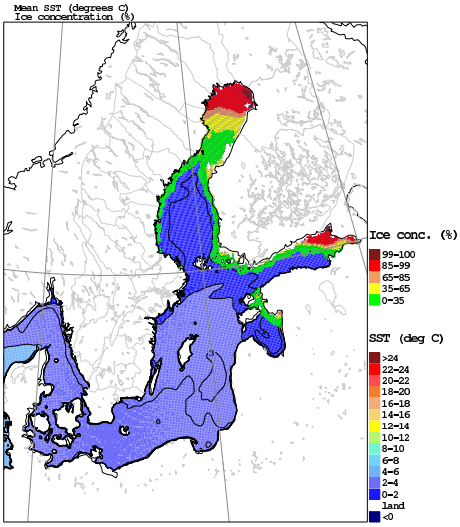

(c) March 1995

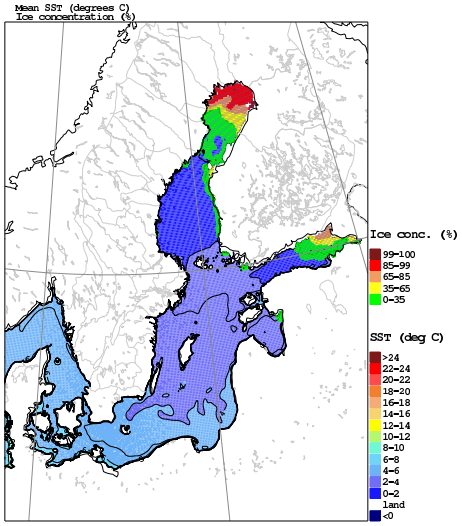

(d) April 1995

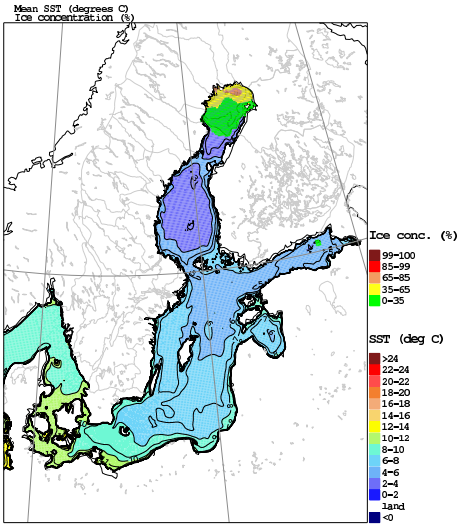

(e) May 1995

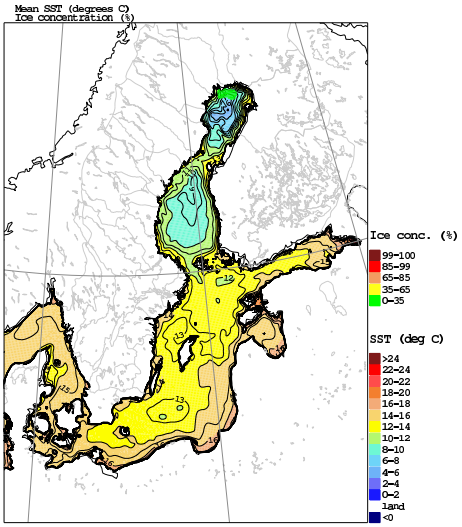

(f) June 1995

Figure 25: Monthly mean SST and SIC fields for January to June 1995.

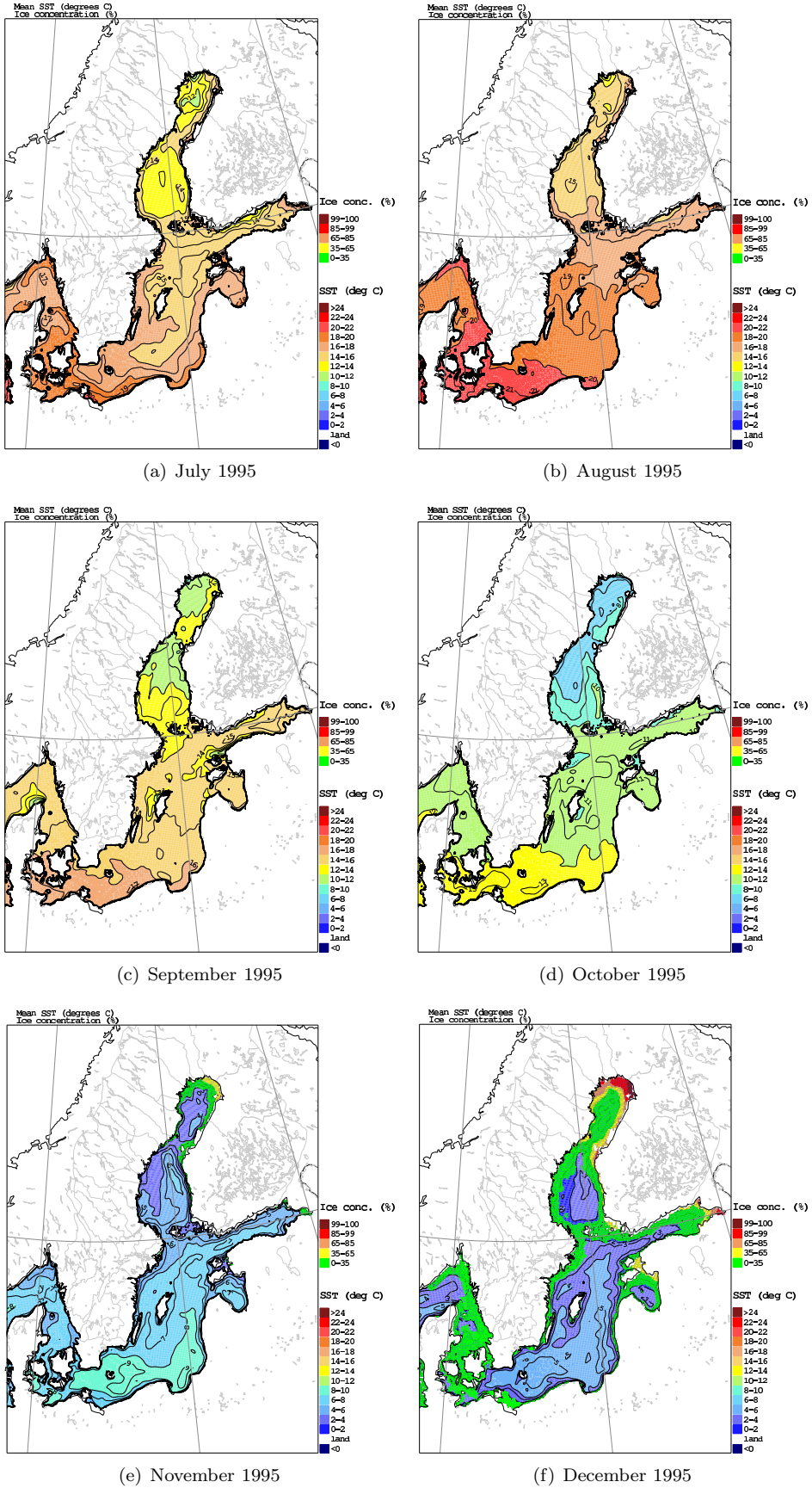

(a) July 1995

(b) August 1995

(c) September 1995

(d) October 1995

(e) November 1995

(f) December 1995

Figure 26: Monthly mean SST and SIC fields for July to December 1995.

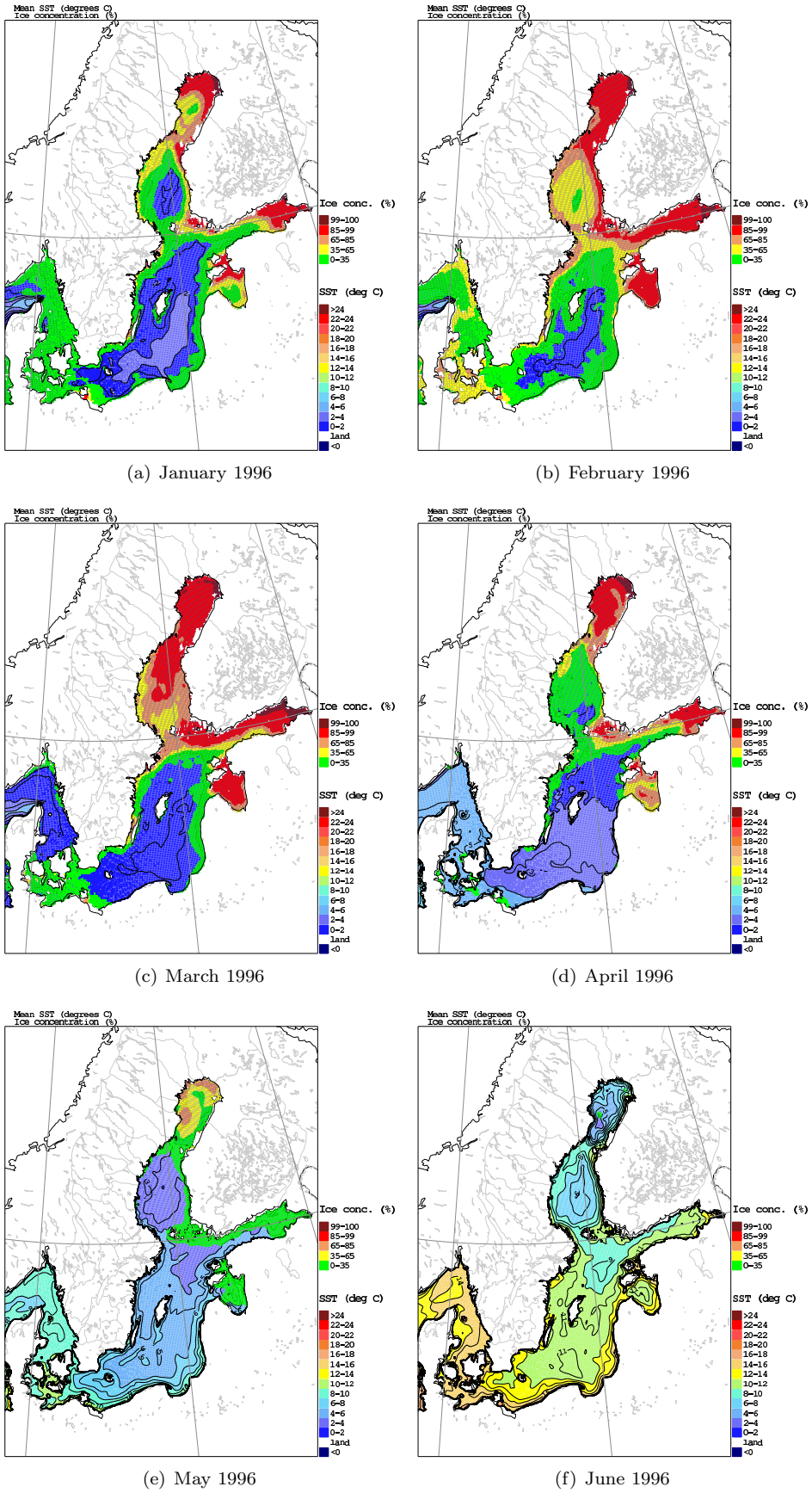

(a) January 1996

(b) February 1996

(c) March 1996

(d) April 1996

(e) May 1996

(f) June 1996

Figure 27: Monthly mean SST and SIC fields for January to June 1996.

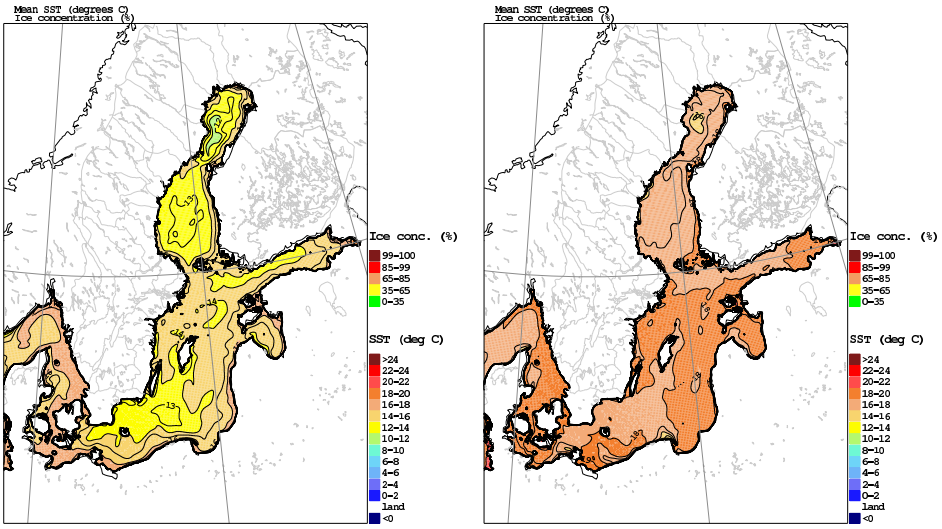

(a) July 1996

(b) August 1996

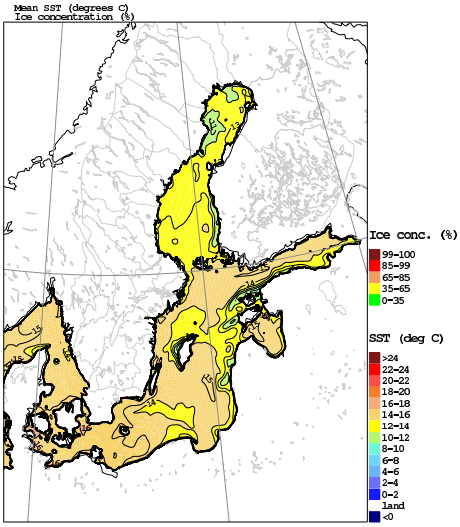

(c) September 1996

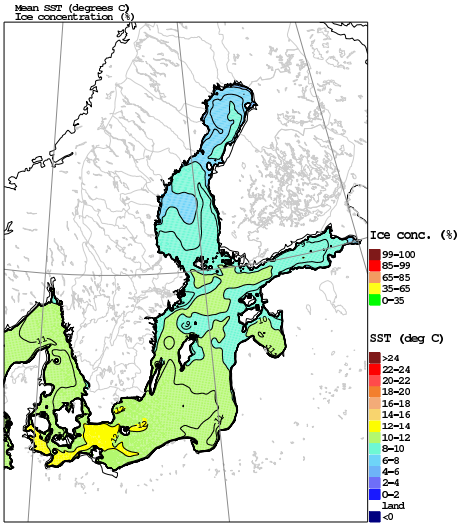

(d) October 1996

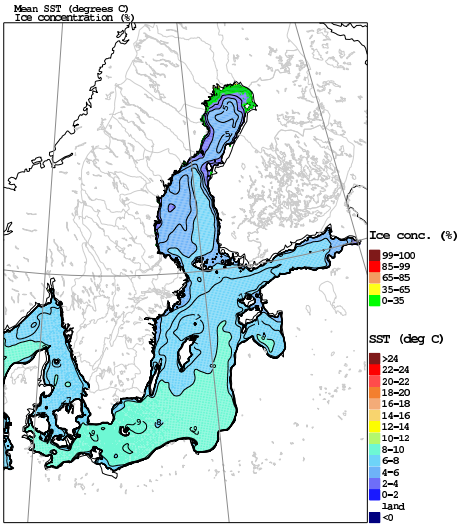

(e) November 1996

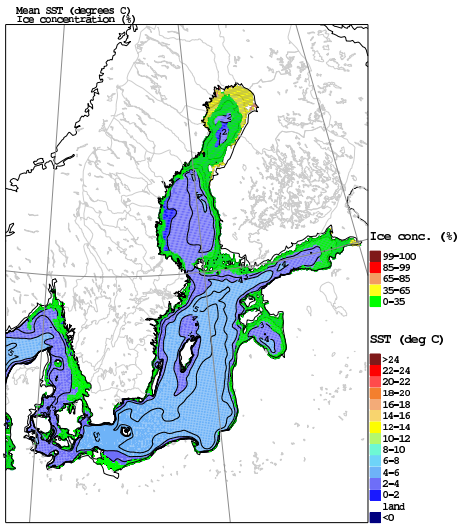

(f) December 1996

Figure 28: Monthly mean SST and SIC fields for July to December 1996.

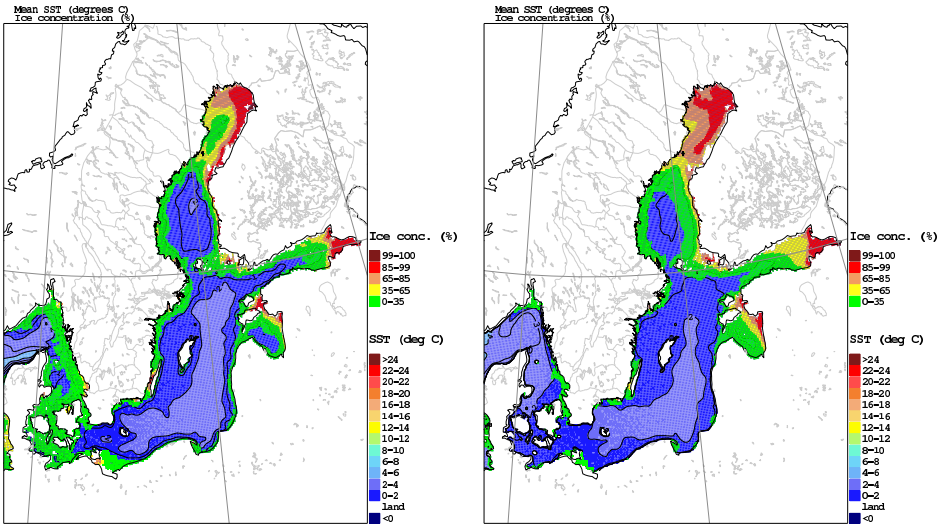

(a) January 1997

(b) February 1997

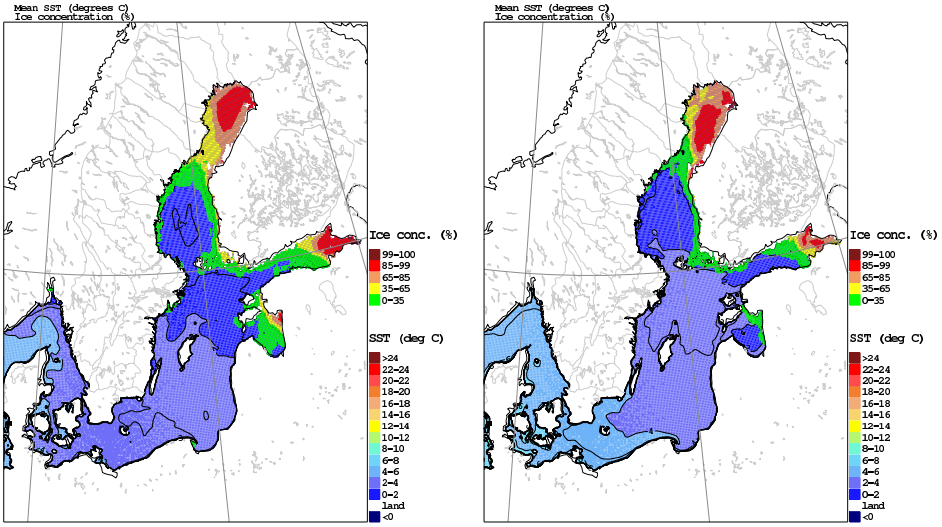

(c) March 1997

(d) April 1997

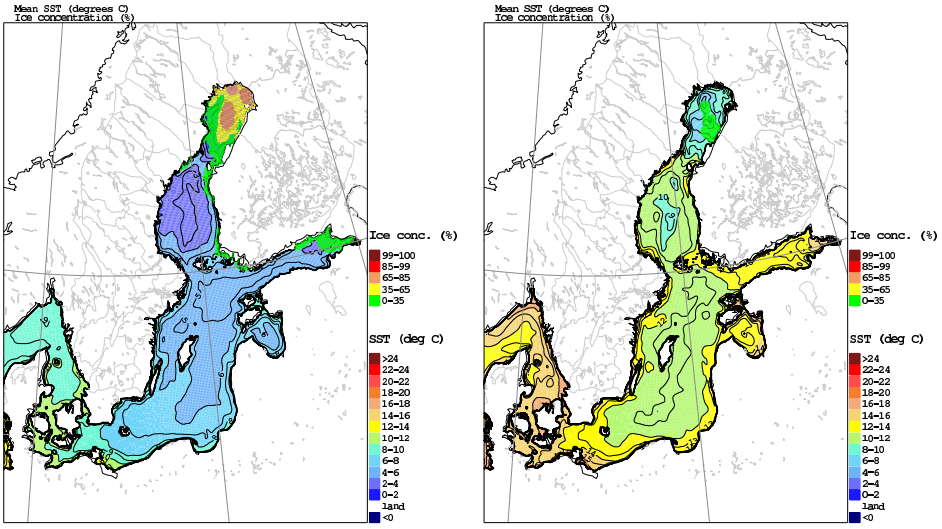

(e) May 1997

(f) June 1997

Figure 29: Monthly mean SST and SIC fields for January to June 1997.

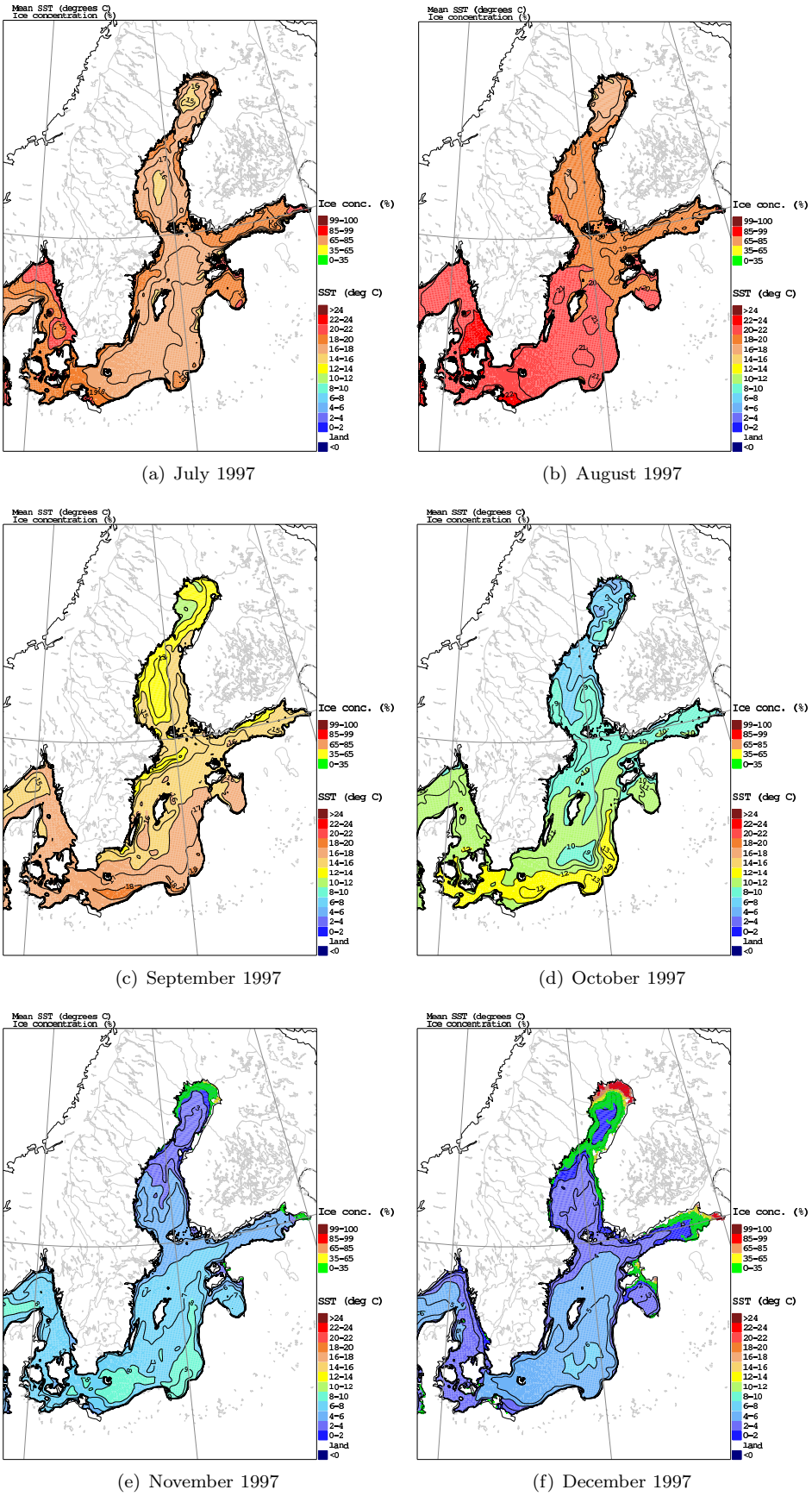

(a) July 1997

(b) August 1997

(c) September 1997

(d) October 1997

(e) November 1997

(f) December 1997

Figure 30: Monthly mean SST and SIC fields for July to December 1997.

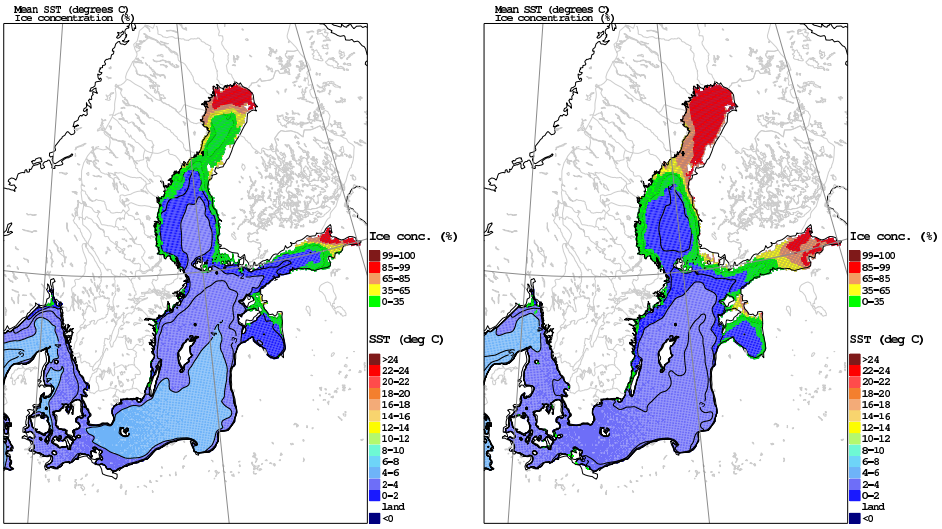

(a) January 1998

(b) February 1998

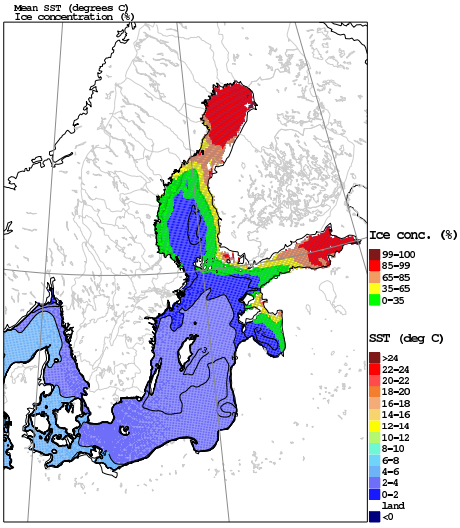

(c) March 1998

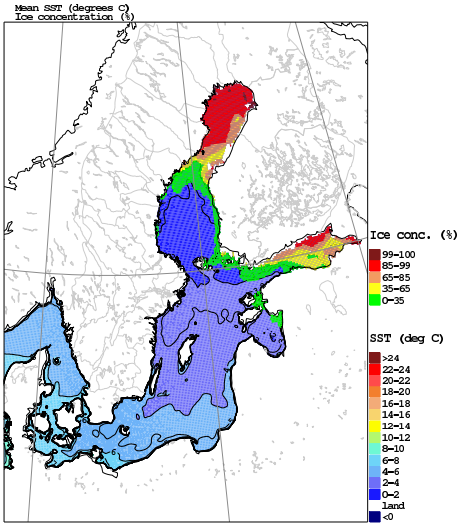

(d) April 1998

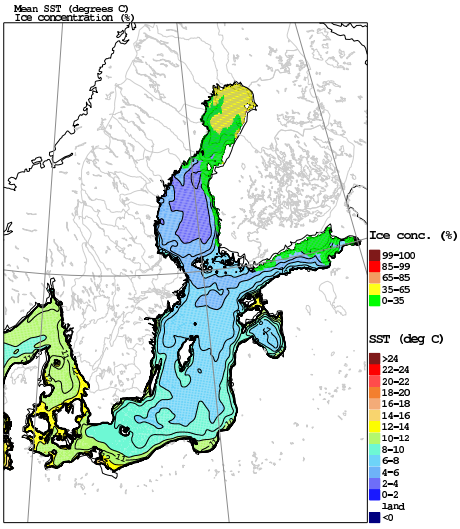

(e) May 1998

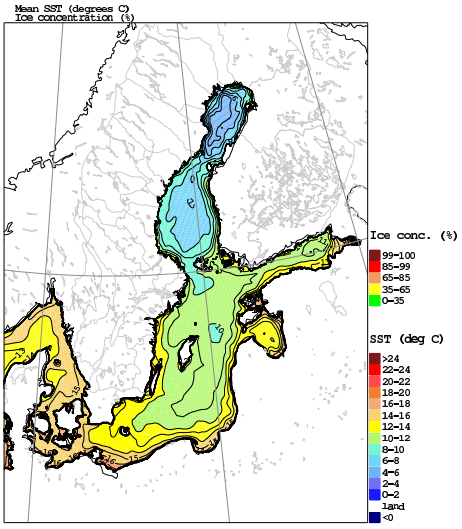

(f) June 1998

Figure 31: Monthly mean SST and SIC fields for January to June 1998.

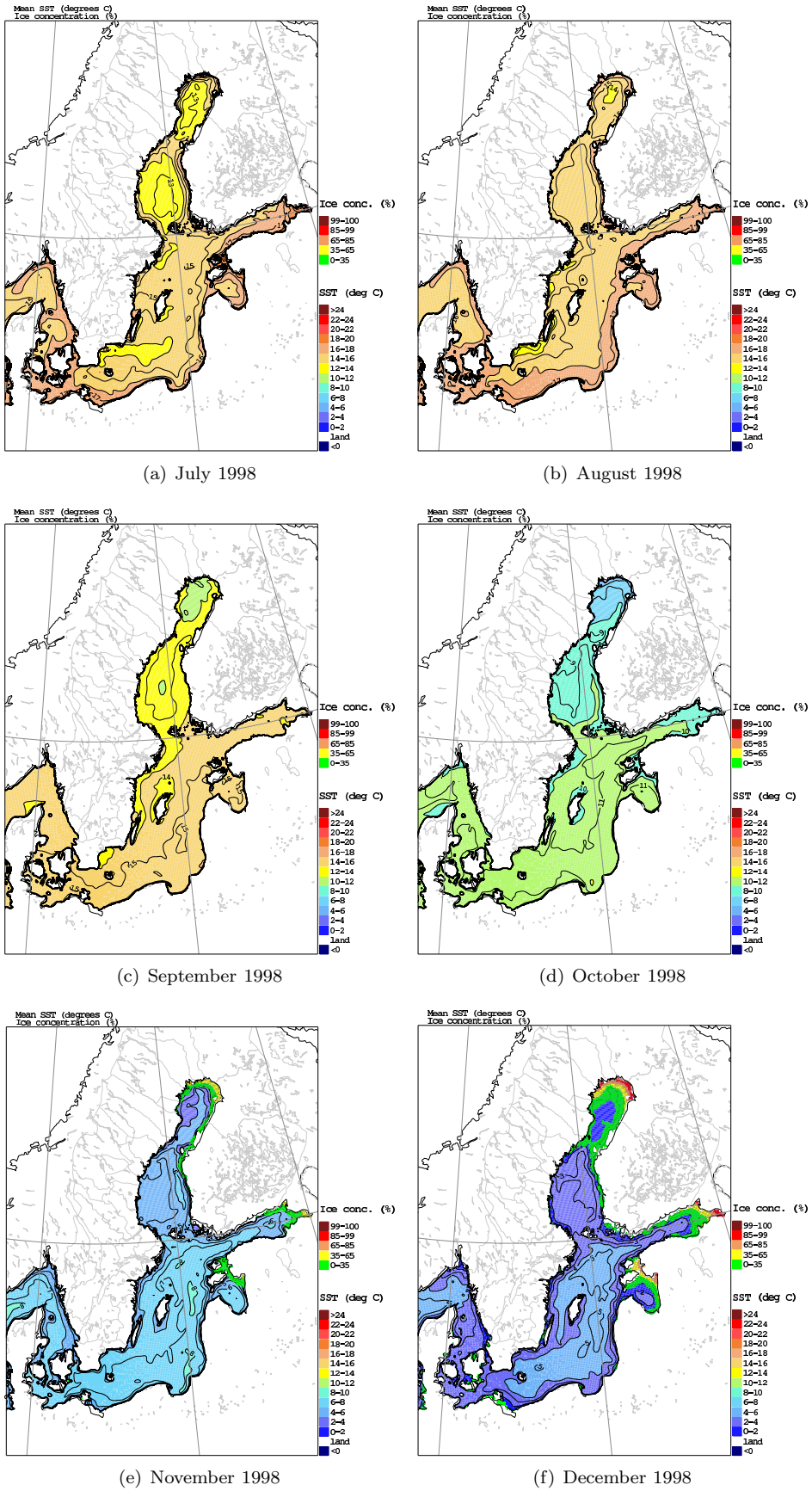

(a) July 1998

(b) August 1998

(c) September 1998

(d) October 1998

(e) November 1998

(f) December 1998

Figure 32: Monthly mean SST and SIC fields for July to December 1998.

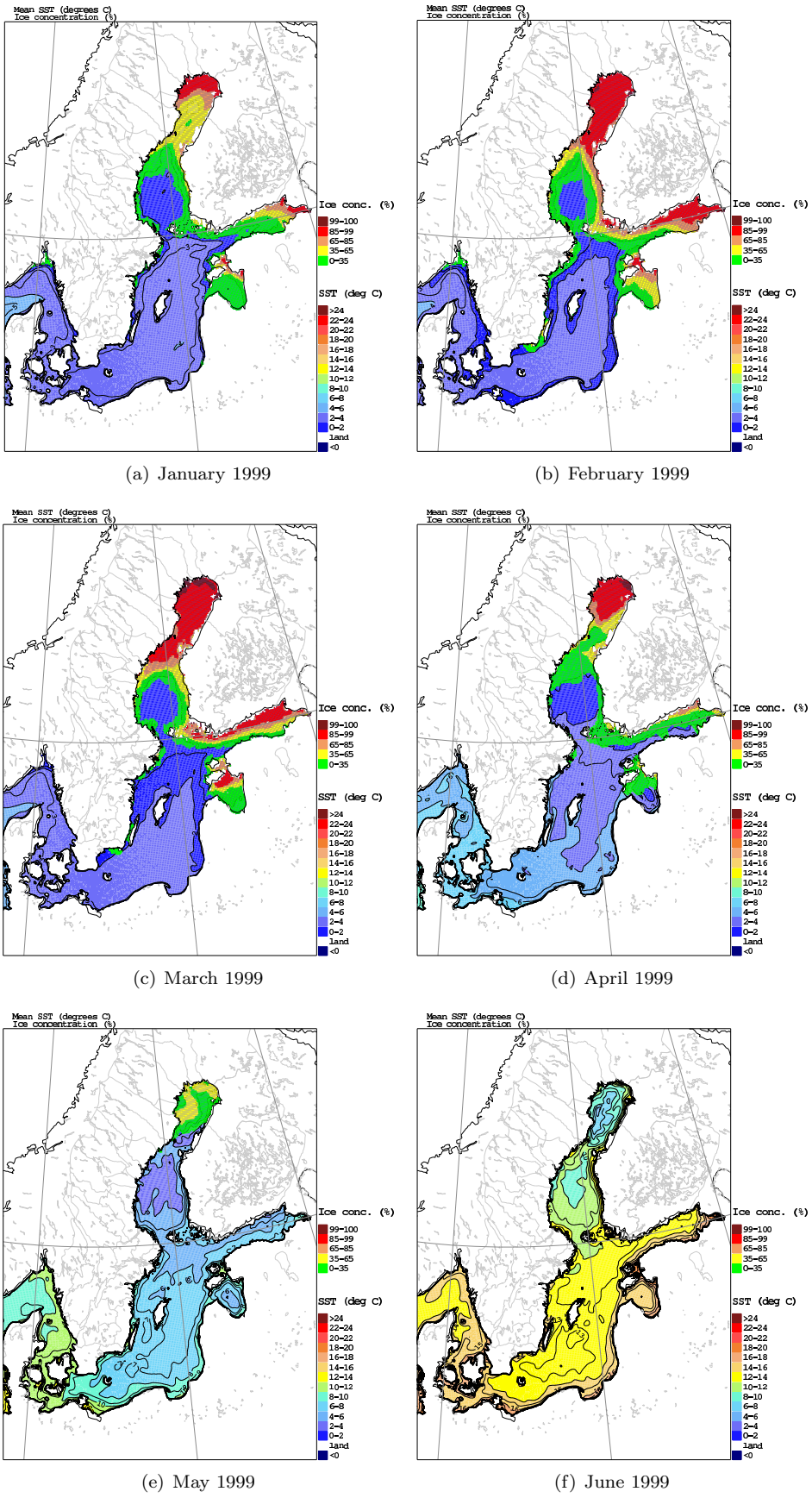

(a) January 1999

(b) February 1999

(c) March 1999

(d) April 1999

(e) May 1999

(f) June 1999

Figure 33: Monthly mean SST and SIC fields for January to June 1999.

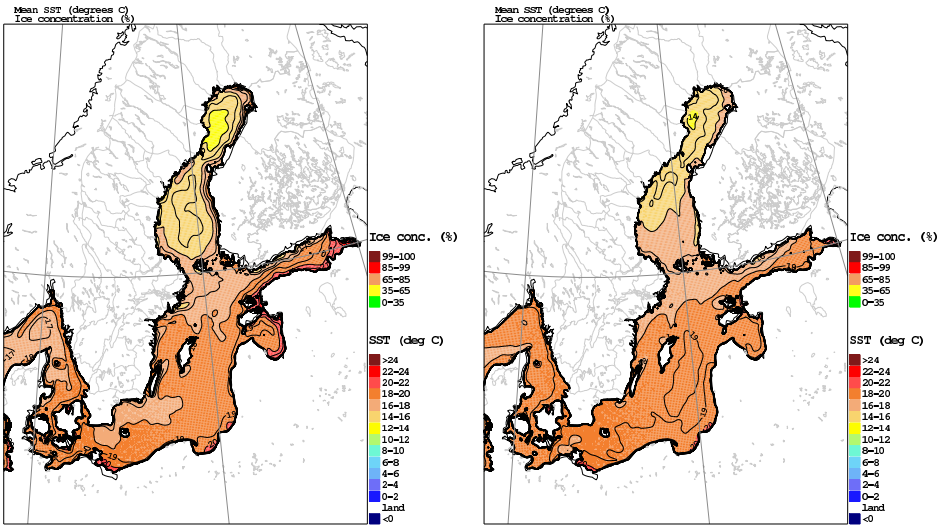

(a) July 1999

(b) August 1999

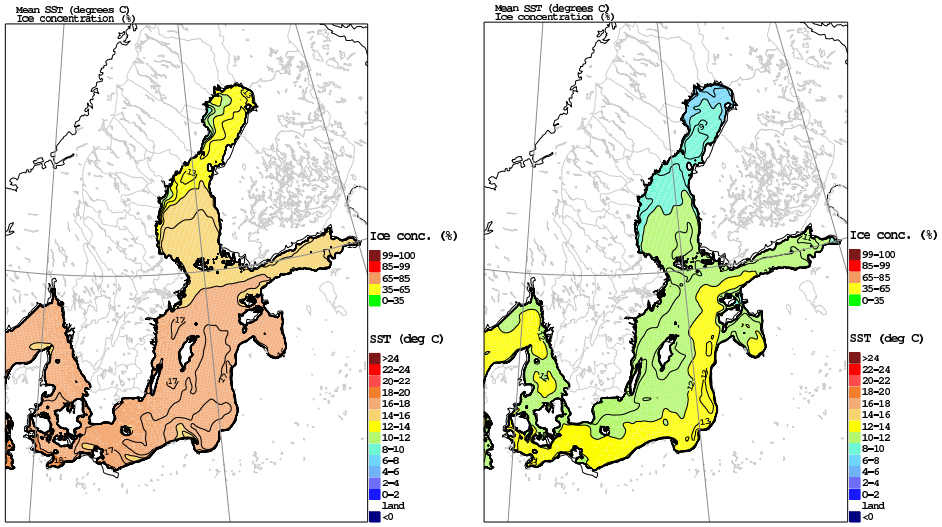

(c) September 1999

(d) October 1999

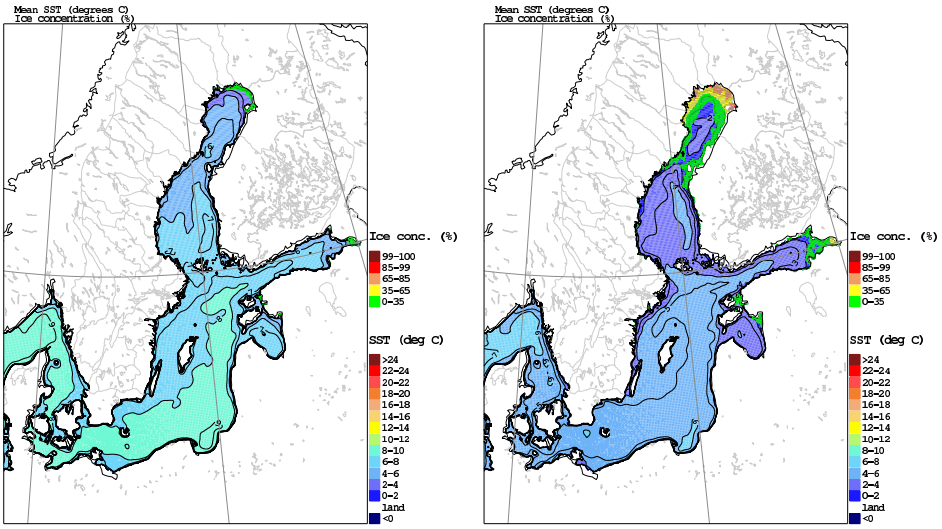

(e) November 1999

(f) December 1999

Figure 34: Monthly mean SST and SIC fields for July to December 1999.

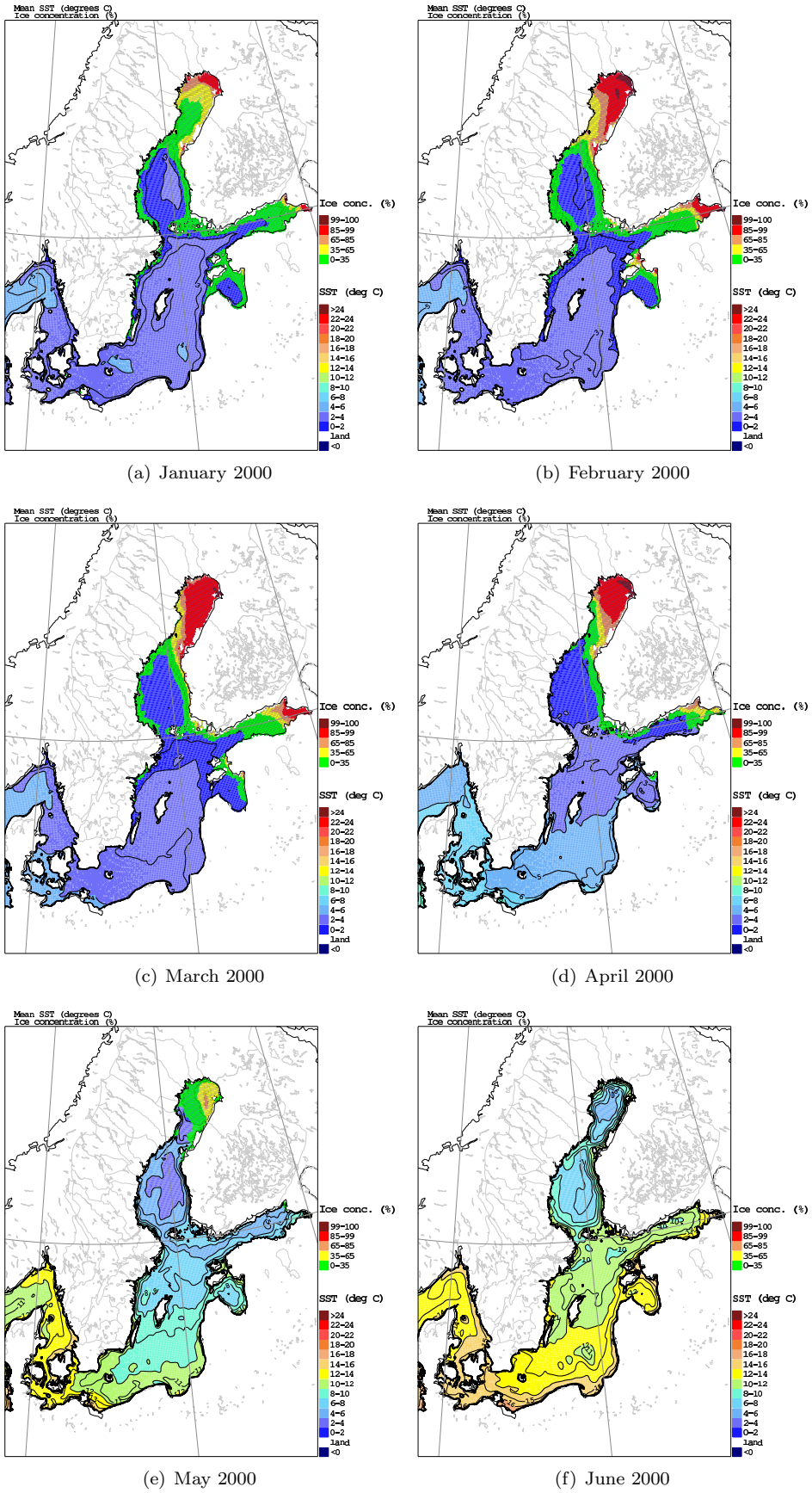

(a) January 2000

(b) February 2000

(c) March 2000

(d) April 2000

(e) May 2000

(f) June 2000

Figure 35: Monthly mean SST and SIC fields for January to June 2000.

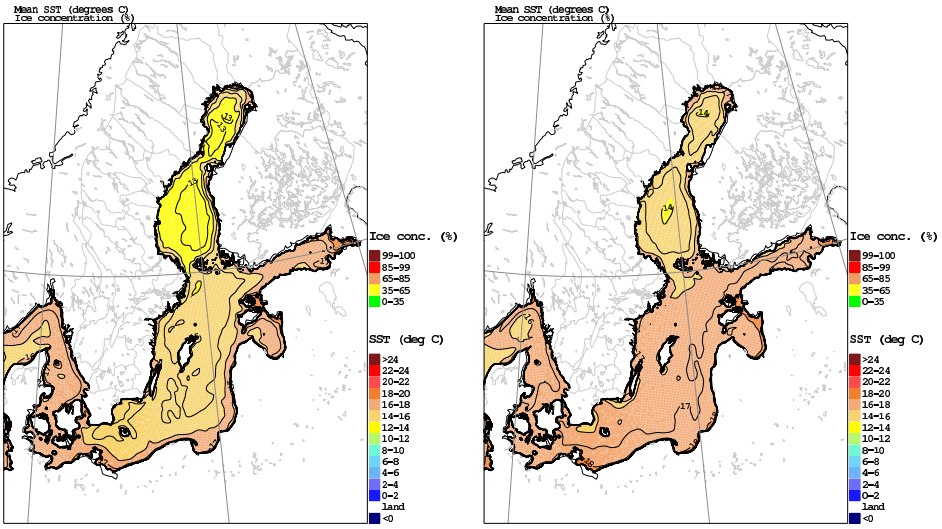

(a) July 2000

(b) August 2000

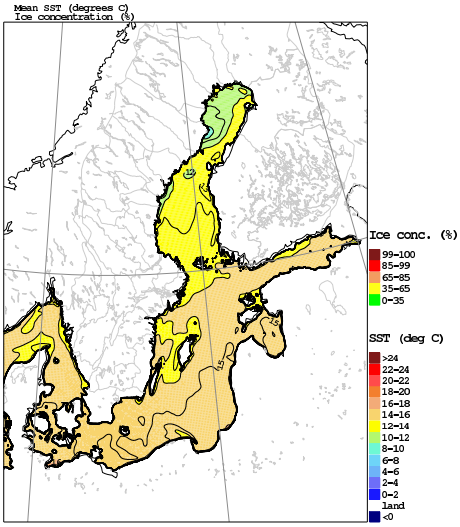

(c) September 2000

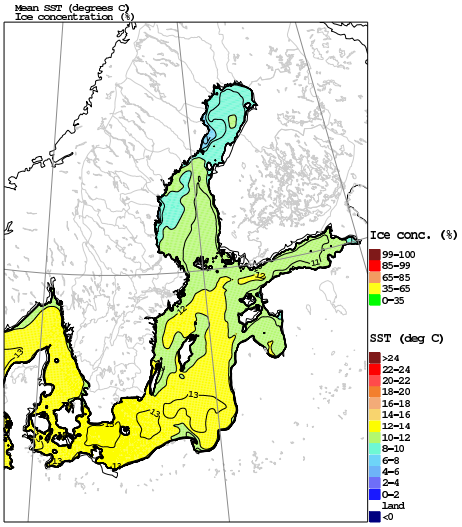

(d) October 2000

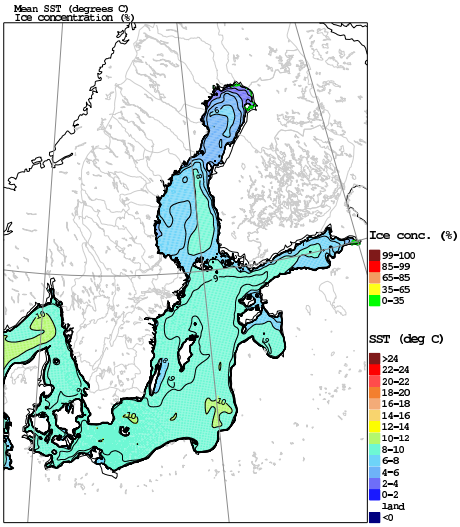

(e) November 2000

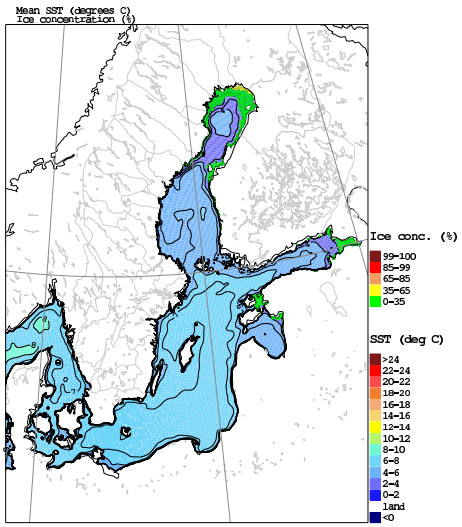

(f) December 2000

Figure 36: Monthly mean SST and SIC fields for July to December 2000.

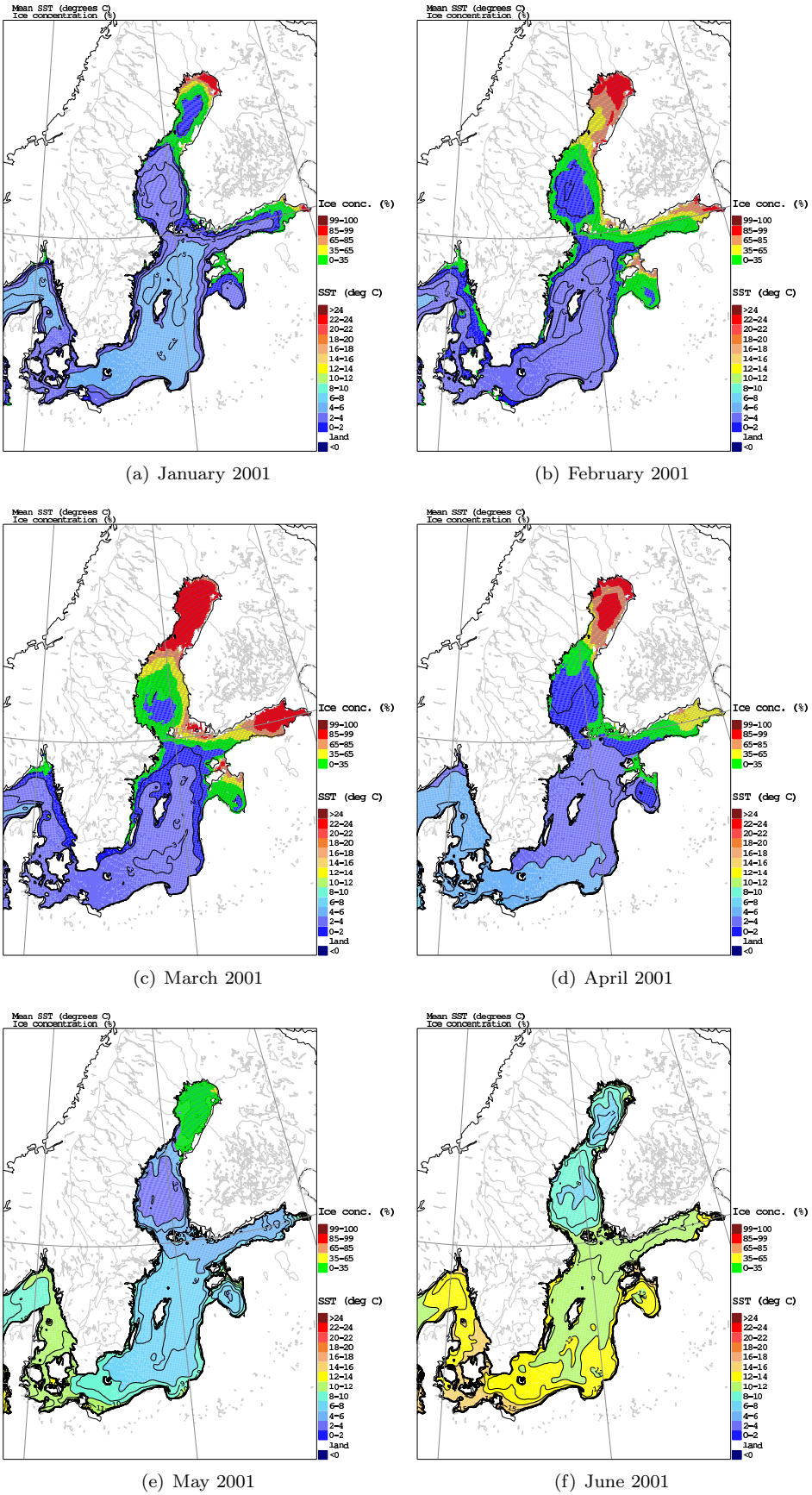

(a) January 2001

(b) February 2001

(c) March 2001

(d) April 2001

(e) May 2001

(f) June 2001

Figure 37: Monthly mean SST and SIC fields for January to June 2001.

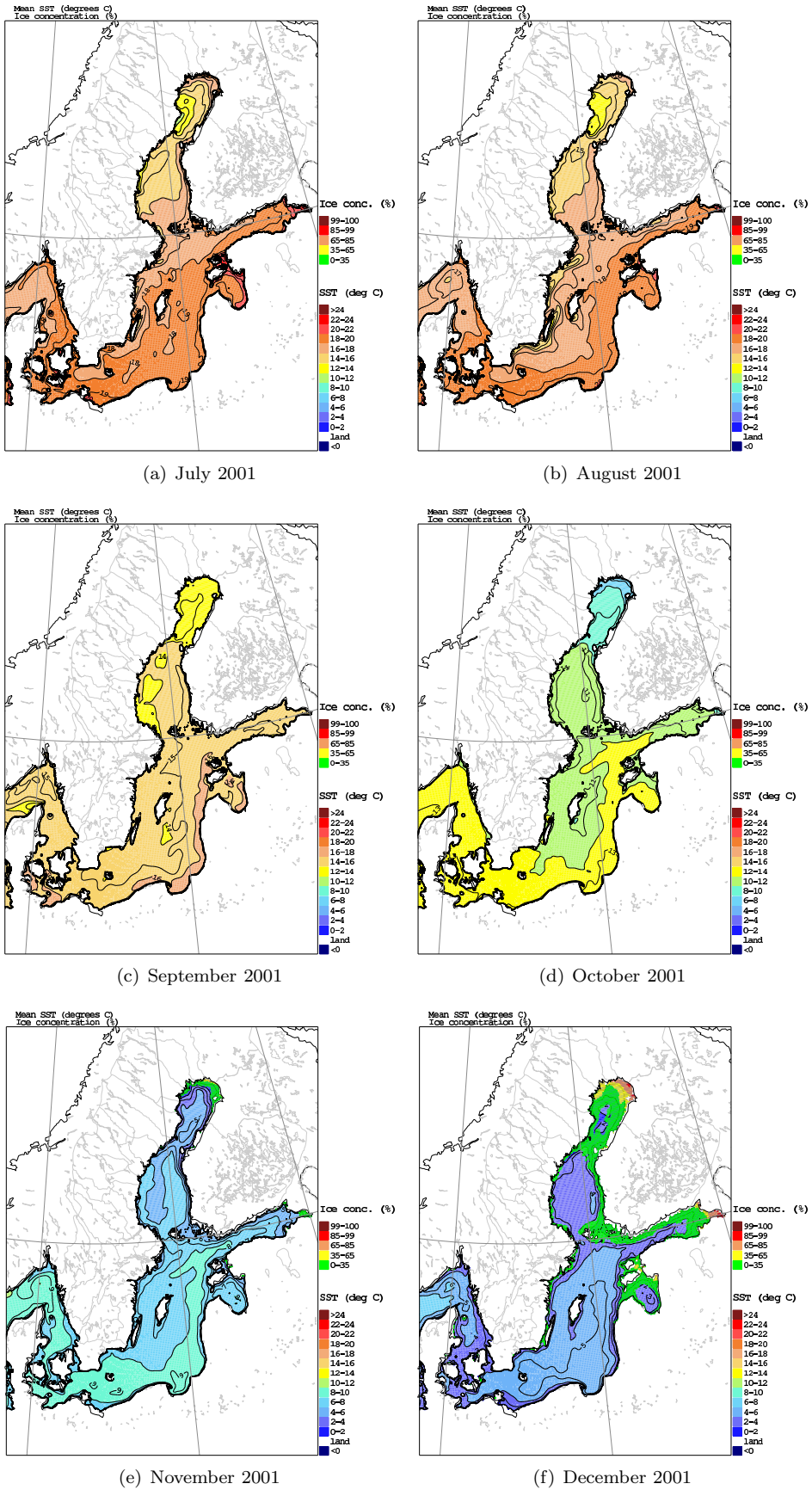

(a) July 2001

(b) August 2001

(c) September 2001

(d) October 2001

(e) November 2001

(f) December 2001

Figure 38: Monthly mean SST and SIC fields for July to December 2001.

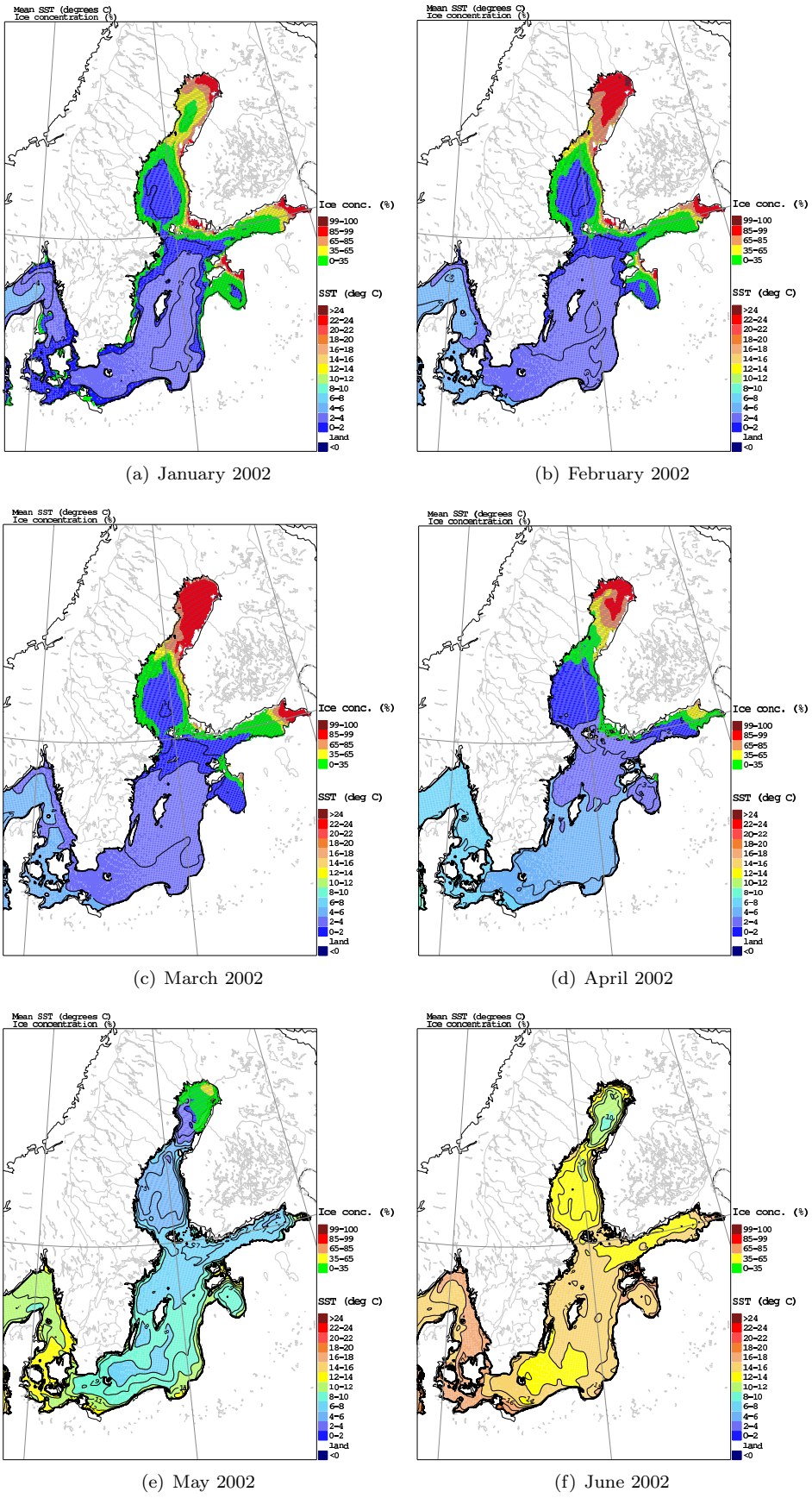

(a) January 2002

(b) February 2002

(c) March 2002

(d) April 2002

(e) May 2002

(f) June 2002

Figure 39: Monthly mean SST and SIC fields for January to June 2002.

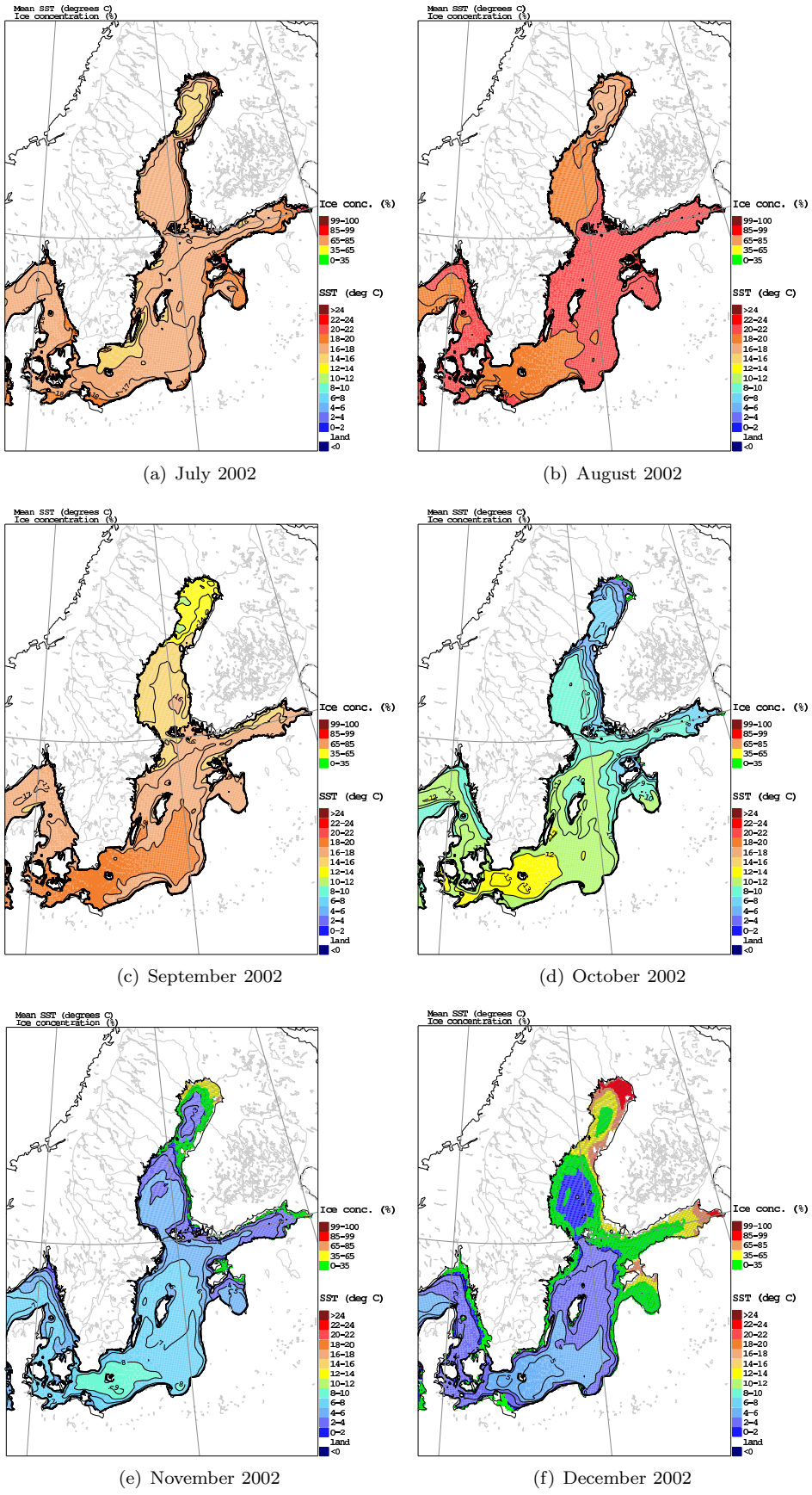

(a) July 2002

(b) August 2002

(c) September 2002

(d) October 2002

(e) November 2002

(f) December 2002

Figure 40: Monthly mean SST and SIC fields for July to December 2002.

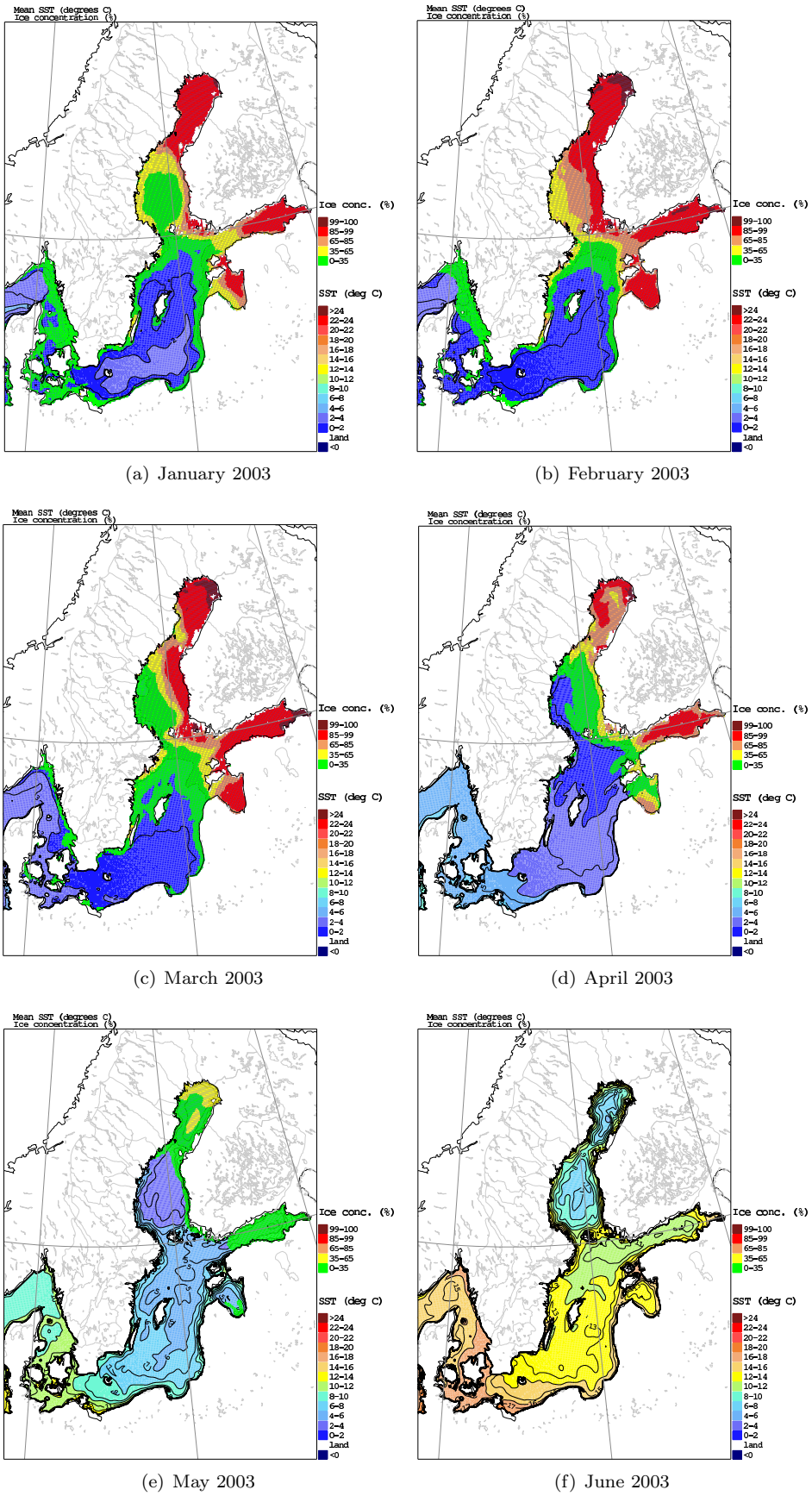

(a) January 2003

(b) February 2003

(c) March 2003

(d) April 2003

(e) May 2003

(f) June 2003

Figure 41: Monthly mean SST and SIC fields for January to June 2003.

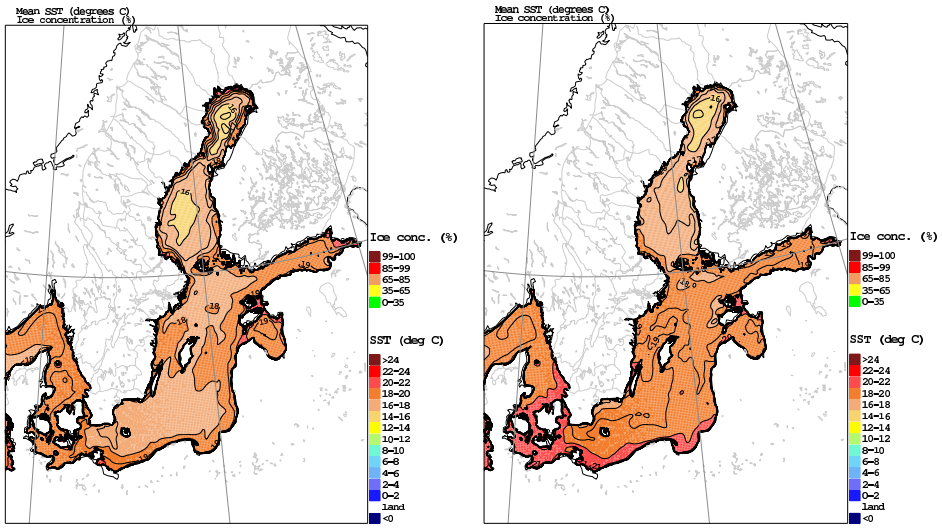

(a) July 2003

(b) August 2003

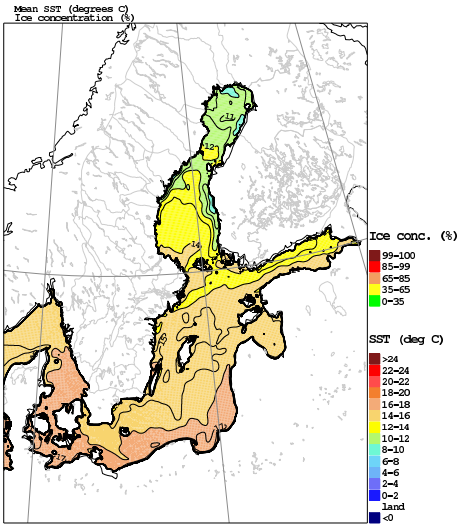

(c) September 2003

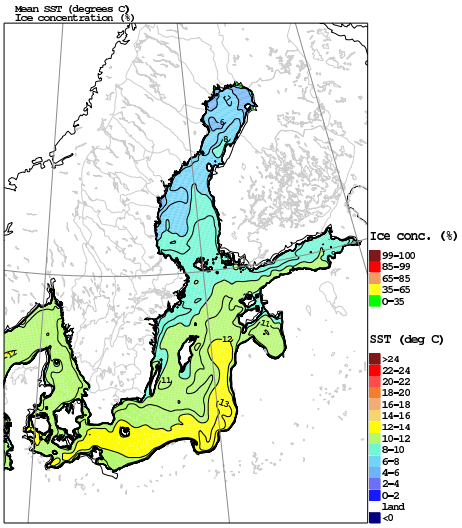

(d) October 2003

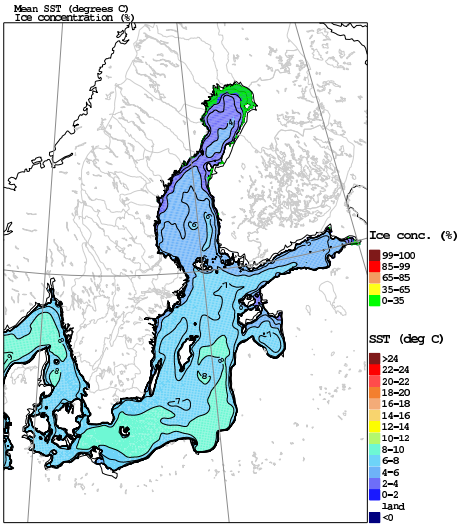

(e) November 2003

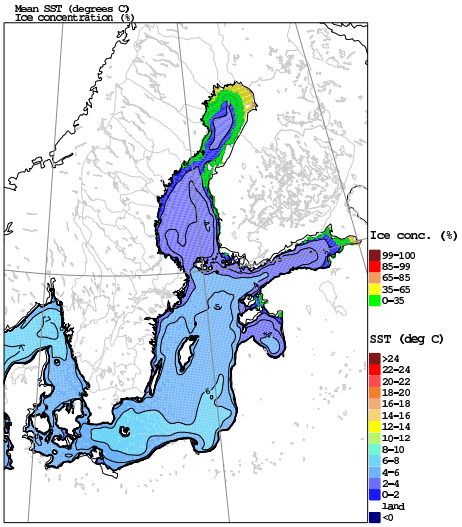

(f) December 2003

Figure 42: Monthly mean SST and SIC fields for July to December 2003.

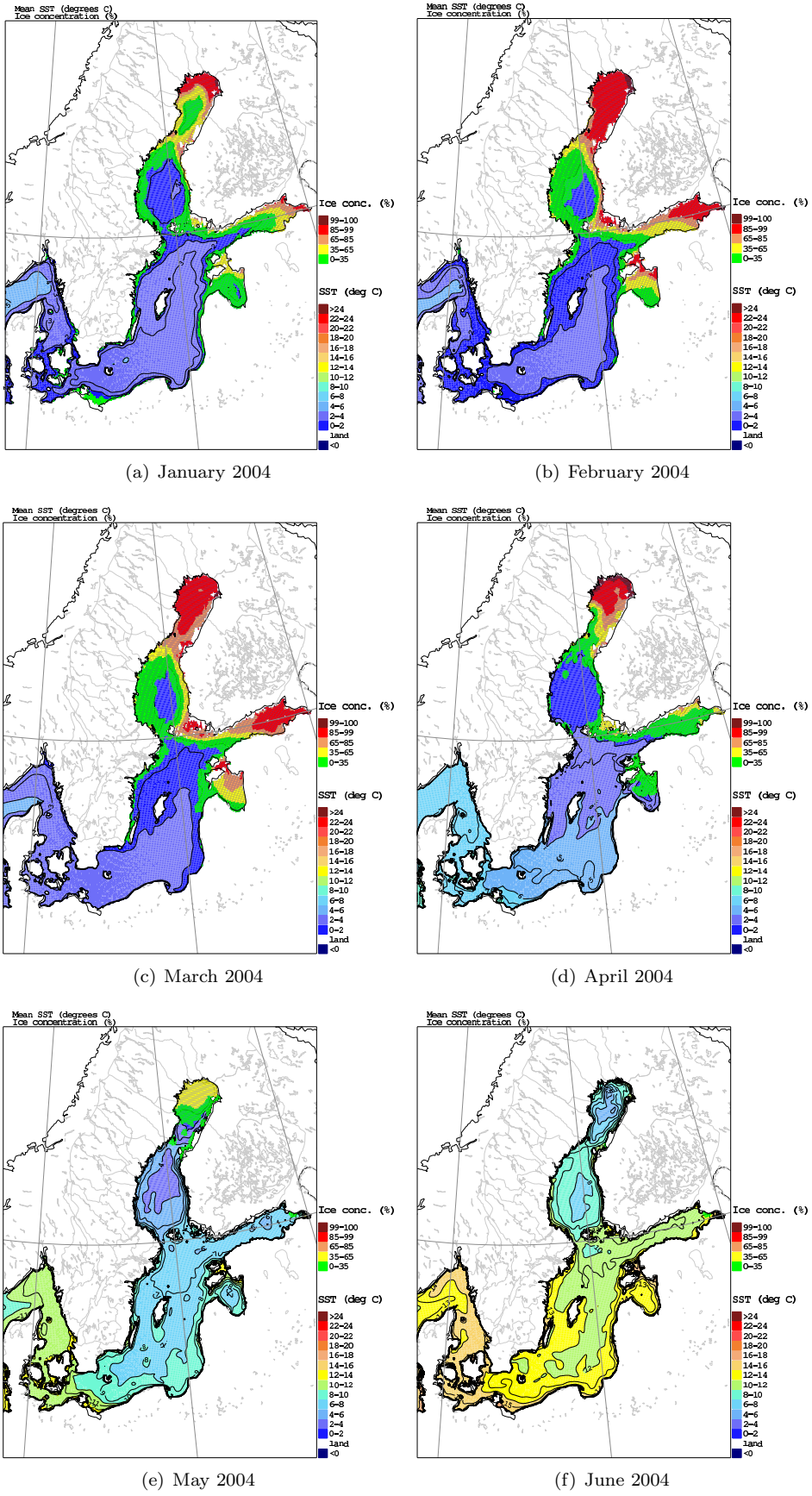

(a) January 2004

(b) February 2004

(c) March 2004

(d) April 2004

(e) May 2004

(f) June 2004

Figure 43: Monthly mean SST and SIC fields for January to June 2004.

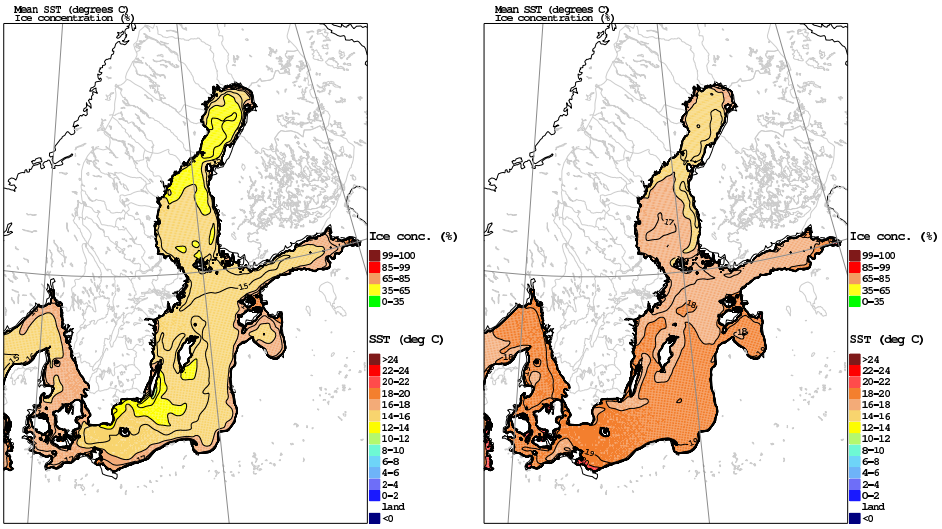

(a) July 2004

(b) August 2004

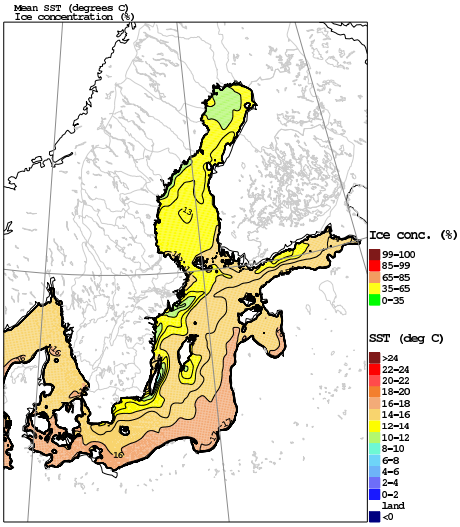

(c) September 2004

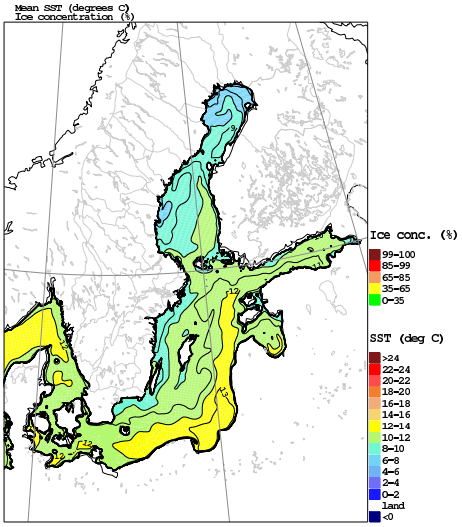

(d) October 2004

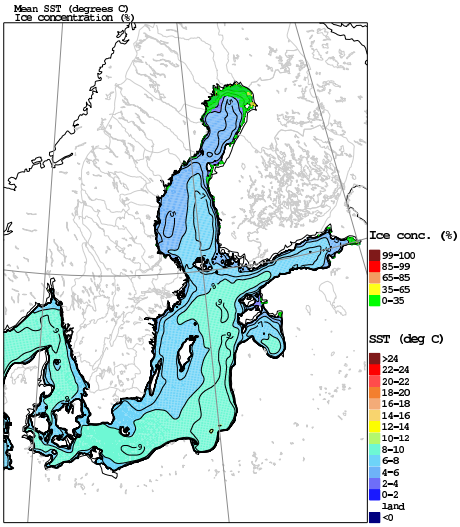

(e) November 2004

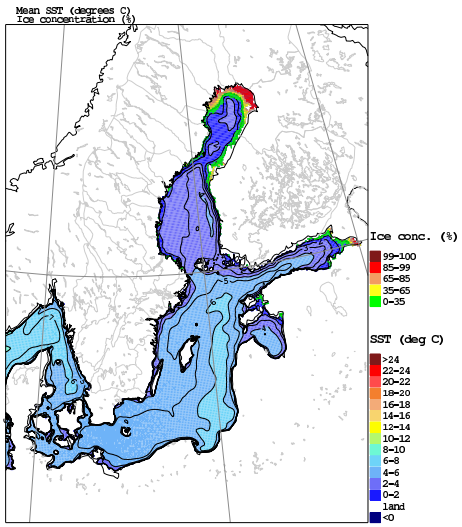

(f) December 2004

Figure 44: Monthly mean SST and SIC fields for July to December 2004.

References

Arneborg, L. 2000. Oceanographic studies of internal waves and diapycnal mixing. Ph.D. thesis, Department of Oceanography, Earth Sciences Centre, Göteborg University, Sweden.

Axell, L. 2002. Wind-driven internal waves and Langmuir circulations in a numerical ocean model of the southern Baltic Sea. J. Geophys. Res. 107(C11), doi:10.1029/2001JC000922.

Axell, L. 2006. Extended ice forecast modelling for the Baltic Sea. In: H. Dahlin, N. C. Flemming, P. Marchand, and S. E. Petersson (Eds.), European operational oceanography: Present and future, Proceedings of the Fourth International Conference on EuroGOOS, pp. 531–534.

Axell, L. B. and Liungman, O. 2001. A one-equation turbulence model for geophysical application: Comparison with data and the k-ε model. Env. Fluid Mech. 1, 71–106.

Burchard, H. and Baumert, H. 1995. On the performance of a mixed-layer model based on the k-ε turbulence closure. J. Geophys. Res. 100, 8523–8540.

Daley, R. 1991. Atmospheric data analysis, Chapt. 3. Cambridge Atmospheric and Space Sciences Series, Cambridge University Press.

Fransson, L. 2005. A comparison of two turbulence models in HIROMB. Report B457, Earth Sciences Centre, Göteborg University, Göteborg, Sweden.

Funkquist, L. and Kleine, E. 2007. HIROMB: An introduction to HIROMB, an operational baroclinic model for the Baltic Sea. Report Oceanography, 37, Swedish Meteorological and Hydrological Institute, SE–601 76 Norrköping, Sweden.

Funkquist, L. and Ljungemyr, P. 1997. Validation of HIROMB during 1995-96. Oceanografi, 67, Swedish Meteorological and Hydrological Institute, SE–601 76 Norrköping, Sweden.

Itsweire, E., Koseff, J., Briggs, D., and Ferziger, J. 1993. Turbulence in stratified shear flows: Implications for interpreting shear-induced mixing in the ocean. J. Phys. Oceanogr.

Ivey, G. and Imberger, J. 1991. On the nature of turbulence in a stratified fluid. Part I: The energetics of mixing. J. Phys.Oceanogr.

Kleine, E. and Sklyar, S. 1996. Mathematical features of Hibler's model of large-scale sea-ice dynamics. D. Hydrogr. Z. 47, 179–230.

Kotovirta, V., Jalonen, R., Axell, L., Riska, K., and Berglund, R. 2009. A system for route optimization in ice-covered waters. Cold Regions Science and Technology 55(doi: 10.1016/j.coldregions.2008.07.003).

Lensu, M. 2003. The evolution of ridged ice fields. Ph.D. thesis, Helsinki University of Technology, Ship Laboratory, Finland.

Li, M. and Garrett, C. 1993. Cell merging and the jet/downwelling ratio in Langmuir circulation. J. Mar. Res.

Mellor, G. L. and Yamada, T. 1982. Development of a turbulence closure model for geophysical fluid problems. Reviews of Geophysics and Space Physics.

Omstedt, A. and Hansson, D. 2006. The Baltic Sea ocean climate system memory and response to changes in the water and heat balance components. Cont. Shelf Res. 26, 236–251.

Omstedt, A. and Nohr, C. 2004. Calculating the water and heat balances of the Baltic Sea using ocean modelling and available meteorological, hydrological and ocean data. Tellus 56A, 400–414.

Osborn, T. R. 1980. Estimates of the local rate of vertical diffusion from dissipation measurements. J. Phys. Oceanogr. 10, 83–89.

Skyllingstad, E. and Denbo, D. W. 1995. An ocean large-eddy simulation of Langmuir circulations and convection in the surface mixed layer. J. Geophys. Res.

Tennekes, H. 1989. The decay of turbulence in plane homogeneous shear flow. In: J. R. Herring and J. C. McWilliams (Eds.), Lecture notes on turbulence, World Scientific, pp. 32–35.

Umlauf, L. and Burchard, H. 2003. A generic length-scale equation for geophysical turbulence models. J. Mar. Syst. 61, 235–265.

Umlauf, L., Burchard, H., and Hutter, K. 2003. Extending the k-ω turbulence model towards oceanic applications. Oc. Mod. 5, 195–218.

Uppala, S. M., Kållberg, P. W., Simmons, A. J., Andrae, U., Bechtold, V. D. C., Fiorino, M., Gibson, J. K., Haseler, J., Hernandez, A., Kelly, G. A., Li, X., Onogi, K., Saarinen, S., Sokka, N., Allan, R. P., Andersson, E., Arpe, K., Balmaseda, M. A., Beljaars, A. C. M., van de Berg, L., Bidlot, J., Bormann, N., Caires, S., Chevallier, F., Dethof, A., Dragosavac, M., Fisher, M., Fuentes, M., HÃ^{3}lm, E., Hoskins, B. J., Isaksen, L., Janssen, P. A. E., Jenne, R., McNally, A. P., Mahfouf, J.-F., Morcrette, J.-J., Rayner, N. A., Saunders, R. W., Simon, P., Sterl, A., e. Trenberth, K., Untch, A., Vasiljevic, D., Viterbo, P., and Woollen, J. 2005. The ERA-40 re-analysis. Q. J. R. Meteorol. Soc. 131(612), 2961–3012. doi: 10.1256/qj.04.176.

Wilhelmsson, T. 2002. Parallellization of the HIROMB ocean model. Licentiate Thesis, Royal Institute of Technology, Department of Numerical and Computer Science, Stockholm, Sweden.

Winsor, P., Rodhe, J., and Omstedt, A. 2001. Baltic Sea ocean climate: an analysis of 100 yr of hydrographic data with focus on the freshwater budget. Clim. Res. 18, 5–15.

Winsor, P., Rodhe, J., and Omstedt, A. 2003. Erratum. Baltic Sea ocean climate: an analysis of 100 yr of hydrographic data with focus on the frewshwater budget.. Clim. Res. 25, 183.

Earlier issues published in RO

1 Lars Gidhagen, Lennart Funkquist and Ray Murthy (1986)
Calculations of horizontal exchange coefficients using Eulerian time series current meter data from the Baltic Sea.

2 Thomas Thompson (1986)
Ymer-80, satellites, arctic sea ice and weather.

3 Stig Carlberg et al (1986)
Program för miljökvalitetsövervakning - PMK.

4 Jan-Erik Lundqvist och Anders Omstedt (1987)
Isförhållandena i Sveriges södra och västra farvatten.

5 Stig Carlberg, Sven Engström, Stig Fonselius, Håkan Palmén, Eva-Gun Thelén, Lotta Fyrberg och Bengt Yhlen (1987)
Program för miljökvalitetsövervakning - PMK. Utsjöprogram under 1986.

6 Jorge C. Valderama (1987)
Results of a five year survey of the distribution of UREA in the Baltic sea.

7 Stig Carlberg, Sven Engström, Stig Fonselius, Håkan Palmén, Eva-Gun Thelén, Lotta Fyrberg, Bengt Yhlen och Danuta Zagradkin (1988).
Program för miljökvalitetsövervakning - PMK. Utsjöprogram under 1987

8 Bertil Håkansson (1988)
Ice reconnaissance and forecasts in Storfjorden, Svalbard.

9 Stig Carlberg, Sven Engström, Stig Fonselius, Håkan Palmén, Eva-Gun Thelén, Lotta Fyrberg, Bengt Yhlen, Danuta Zagradkin, Bo Juhlin och Jan Szaron (1989)
Program för miljökvalitetsövervakning - PMK. Utsjöprogram under 1988.

10 L. Fransson, B. Håkansson, A. Omstedt och L. Stehn (1989)
Sea ice properties studied from the ice-breaker Tor during BEPERS-88.

11 Stig Carlberg, Sven Engström, Stig Fonselius, Håkan Palmén, Lotta Fyrberg, Bengt Yhlen, Bo Juhlin och Jan Szaron (1990)
Program för miljökvalitetsövervakning - PMK. Utsjöprogram under 1989.

12 Anders Omstedt (1990)
Real-time modelling and forecasting of temperatures in the Baltic Sea.

13 Lars Andersson, Stig Carlberg, Elisabet Fogelqvist, Stig Fonselius, Håkan Palmén, Eva-Gun Thelén, Lotta Fyrberg, Bengt Yhlen och Danuta Zagradkin (1991)
Program för miljökvalitetsövervakning – PMK. Utsjöprogram under 1989.

14 Lars Andersson, Stig Carlberg, Lars Edler, Elisabet Fogelqvist, Stig Fonselius, Lotta Fyrberg, Marie Larsson, Håkan Palmén, Björn Sjöberg, Danuta Zagradkin, och Bengt Yhlen (1992)
Haven runt Sverige 1991. Rapport från SMHI, Oceanografiska Laboratoriet, inklusive PMK - utsjöprogrammet. (The conditions of the seas around Sweden. Report from the activities in 1991, including PMK - The National Swedish Programme for Monitoring of Environmental Quality Open Sea Programme.)

15 Ray Murthy, Bertil Håkansson and Pekka Alenius (ed.) (1993)
The Gulf of Bothnia Year-1991 - Physical transport experiments.

16 Lars Andersson, Lars Edler and Björn Sjöberg (1993)
The conditions of the seas around Sweden. Report from activities in 1992.

17 Anders Omstedt, Leif Nyberg and Matti Leppäranta (1994)
A coupled ice-ocean model supporting winter navigation in the Baltic Sea.
Part 1. Ice dynamics and water levels.

18 Lennart Funkquist (1993)
An operational Baltic Sea circulation model. Part 1. Barotropic version.

19 Eleonor Marmefelt (1994)
Currents in the Gulf of Bothnia. During the Field Year of 1991.

20 Lars Andersson, Björn Sjöberg and Mikaell Krysell (1994)
The conditions of the seas around Sweden.
Report from the activities in 1993.

21 Anders Omstedt and Leif Nyberg (1995)
A coupled ice-ocean model supporting winter navigation in the Baltic Sea.
Part 2. Thermodynamics and meteorological coupling.

22 Lennart Funkquist and Eckhard Kleine (1995)
Application of the BSH model to Kattegat and Skagerrak.

23 Tarmo Köuts and Bertil Håkansson (1995)
Observations of water exchange, currents, sea levels and nutrients in the Gulf of Riga.

24 Urban Svensson (1998)
PROBE An Instruction Manual.

25 Maria Lundin (1999)
Time Series Analysis of SAR Sea Ice Backscatter Variability and its Dependence on Weather Conditions.

26 Markus Meier[1], Ralf Döscher[1], Andrew, C. Coward[2], Jonas Nycander[3] and Kristofer Döös[3] (1999). RCO – Rossby Centre regional Ocean climate model: model description (version 1.0) and first results from the hindcast period 1992/93.

[1] Rossby Centre, SMHI [2] James Rennell Division, Southampton Oceanography Centre, [3] Department of Meteorology, Stockholm University

27 H. E. Markus Meier (1999)
First results of multi-year simulations using a 3D Baltic Sea model.

28 H. E. Markus Meier (2000)
The use of the $k - \varepsilon$ turbulence model within the Rossby Centre regional ocean climate model: parameterization development and results.

29 Eleonor Marmefelt, Bertil Håkansson, Anders Christian Erichsen and Ian Sehested Hansen (2000)
Development of an Ecological Model System for the Kattegat and the Southern Baltic. Final Report to the Nordic Councils of Ministers.

30 H.E Markus Meier and Frank Kauker (2002).
Simulating Baltic Sea climate for the period 1902-1998 with the Rossby Centre coupled ice-ocean model.

31 Bertil Håkansson (2003)
Swedish National Report on Eutrophication Status in the Kattegat and the Skagerrak OSPAR ASSESSMENT 2002

32 Bengt Karlson & Lars Andersson (2003)
The Chattonella-bloom in year 2001 and effects of high freshwater input from river Göta Älv to the Kattegat-Skagerrak area

33 Philip Axe and Helma Lindow (2005)
Hydrographic Conditions Around Offshore Banks

34 Pia M Andersson, Lars S Andersson (2006)
Long term trends in the seas surrounding Sweden. Part one - Nutrients

35 Bengt Karlson, Ann-Sofi Rehnstam-Holm & Lars-Ove Loo (2007)
Temporal and spatial distribution of diarrhetic shellfish toxins in blue mussels, Mytilus edulis (L.), at the Swedish West Coast, NE Atlantic, years 1988-2005

36 Bertil Håkansson
Co-authors: Odd Lindahl, Rutger Rosenberg, Pilip Axe, Kari Eilola, Bengt Karlson (2007)
Swedish National Report on Eutrophication Status in the Kattegat and the Skagerrak OSPAR ASSESSMENT 2007

37 Lennart Funkquist and Eckhard Kleine (2007)
An introduction to HIROMB, an operational baroclinic model for the Baltic Sea

38 Philip Axe (2008)
Temporal and spatial monitoring of eutrophication variables in CEMP

39 Bengt Karlson, Philip Axe, Lennart Funkquist, Seppo Kaitala, Kai Sørensen (2009)
Infrastructure for marine monitoring and operational oceanography

40 Marie Johansen, Pia Andersson (2010)
Long term trends in the seas surrounding Sweden
Part two – Pelagic biology

41 Philip Axe, (2012)
Oceanographic Applications of Coastal Radar

42 Martin Hansson, Lars Andersson, Philip Axe (2011)
Areal Extent and Volume of Anoxia and Hypoxia in the Baltic Sea, 1960-2011

43 Philip Axe, Karin Wesslander, Johan Kronsell (2012)
Confidence rating for OSPAR COMP

44 Germo Väli, H.E. Markus Meier, Jüri Elken (2012)
Simulated variations of the Baltic Sea halocline during 1961-2007

SMHI

Swedish Meteorological and Hydrological Institute
SE 601 76 NORRKÖPING
Phone +46 11-495 80 00 Telefax +46 11-495 80 01

ISIISSN 0283-1112